

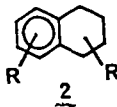
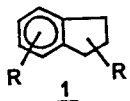
SYNTHESIS OF ALKYLATED INDANES AND TETRALINS  
FOR USE IN FOSSIL FUEL ANALYSIS

By

D. S. Watt, M. Adamczyk, and D. A. Netzel  
Department of Chemistry, University of Wyoming  
and Department of Energy, Laramie Energy Technology Center  
Laramie, Wyoming 82070

ABSTRACT

The availability of authentic hydrocarbon samples in the substituted indane and tetralin families would facilitate the analysis of certain fossil fuel mixtures. We have developed general procedures for the efficient preparation of simple alkylated indanes 1 tetralins 2 from common precursors. We have examined the  $^{13}\text{C}$  NMR and mass spectral fragmentation data for hydrocarbons 1 and 2 in detail.



A TIME-TEMPERATURE-CONCENTRATION MATRIX FOR INDUCED  
SEDIMENT FORMATION IN SHALE DIESEL FUEL

By

J. V. Cooney, E. J. Beal, and R. N. Hazlett  
Naval Research Laboratory, Code 6180, Washington, D.C. 20375

INTRODUCTION

Deterioration in fuel quality with time has been a continuing problem in the utilization of middle distillate fuels. These stability problems will intensify as we develop alternative sources of fuel, such as shale oil and coal. Present knowledge has suggested that for some fuels, nitrogen heterocycles may play a causative role in the formation of insoluble sediments and gums under conditions of ambient and accelerated storage (1). In light of the high costs of fuel processing, substantial savings could be realized if it were possible to identify those nitrogen heterocycles which are most actively involved in the formation of insoluble material. Currently, it appears that relatively non-basic nitrogen heterocycles, particularly those which contain alkyl groups in certain positions, may be the most troublesome (2). However, in other fuels and under different test conditions, basic nitrogen compounds may play a significant role (3).

In addressing this subject, we are defining the stability of shale-derived diesel fuel marine (DFM), stressing the sample under accelerated storage conditions, and determining the amount of total insoluble material produced. This report describes results obtained when 2,5-dimethylpyrrole (DMP) was used as a dopant in a time-temperature-concentration matrix. Results of a survey of other nitrogen compounds as fuel additives are also presented.

EXPERIMENTAL

Storage Test Techniques

The experimental procedures used were developed from reported methods (2). In summary, 300 ml samples of filtered fuel were stressed in the dark in 500 ml screw-cap borosilicate Erlenmeyer flasks (Teflon-lined caps). All samples were run in duplicate. Vented tests were accomplished by using modified screw caps which were drilled to hold 6 mm glass tubing (with glass wool plugs). After stress, test flasks were allowed to cool to room temperature before being filtered under slight vacuum through a double layer of Gelman glass fiber filter paper. Flask contents were then rinsed with several ml of *n*-heptane, with additional sediment being collected on the filter paper. The filter cake was rinsed with *n*-heptane to remove adsorbed fuel. The flasks and filter holders were heated (120°C) under vacuum for twelve hours, allowed to equilibrate on a benchtop (several hours), and accurately weighed several times on an analytical balance. Appropriate blank flask/filter holder corrections were applied. Filtrable sediment values were obtained from the corrected net weight change of the filter holder with adherent gum values determined from the weight change of the test flask (4).

Reagents

The base fuel for the present study is DFM refined from Paraho crude shale oil by SOHIO. This fuel, produced in the U.S. Navy's Shale-II demonstration, is well-characterized (4). It was available with (sample "D-1") and without (sample "D-11") antioxidant added. The antioxidant, 2,4-dimethyl-6-*t*-butylphenol (AO-30), was present at the 24 mg/l level in fuel D-11. No other additives were present in either sample. All nitrogen compounds used as dopants were pure by NMR, capillary GC, and/or mp. Fresh DMP was stored frozen under nitrogen so as to prevent autoxidation and it remained colorless under this storage. The concentration matrix was prepared by appropriate dilution of a quantity of stock-doped fuel solution (typically 450 ppm w/v nitrogen).

RESULTS AND DISCUSSION

Accelerated fuel stability tests are important to the producers of fuels and to those performing research on chemical instability phenomena (5). The majority of these tests measure sediment weight in order to estimate fuel instability, and test temperatures have varied between ambient and

150°C. Although higher temperatures enable storage tests to be completed in minimum time periods, the accompanying uncertainty of the significance of the observed conditions may be dominant. Figure 1 summarizes a time-temperature matrix for several accelerated fuel stability tests which have appeared in the literature. It is noteworthy that a majority of the stability tests depicted fall close to the solid line, which represents a doubling of test time for each 10°C drop in temperature. The line extrapolates to approximately one year of ambient storage. The present study has concentrated on the lower temperature range (43, 65, and 80°C) in an effort to examine the reliability of using such accelerated storage tests as measures of ambient stability. As indicated by Figure 1, stress times were selected to bracket the solid line at each of the three temperatures.

The promotion of sediment formation in fuels by DMP has been reported to be a facile process, characterized by an activation energy of 10-15 kcal/mol (1,2). When subjected to storage at 43°C for periods of time ranging from 52 to 179 days DMP-doped Shale-II DFM formed large amounts of insoluble material. The DMP was added to samples D-1 and D-11 at concentrations of 0, 45, 135, 270 and 450 ppm N (w/v), and vented trials were also conducted at 45 and 450 ppm. The deviation between duplicate stress samples was small and indicated very good reproducibility for the test procedure. In general, the adherent gum comprised only 5-10% of the total insolubles. Venting of test flasks did not affect the amount of insoluble material formed. In a similar manner, the presence of the antioxidant (AO-30) in D-11 was of no consequence.

The DMP test matrix at 80°C (stress lengths 4-28 days) provided results which compared exceptionally well with those obtained at 43°C. In general, results at 65°C (11-50 days) also showed good agreement with the other two temperature regimens, although agreement between duplicates was somewhat less satisfactory at this temperature. The results for 80°C stresses of DMP-doped D-1 are shown in Figure 2. The first-order type of behavior which was observed with DMP is illustrated in Figure 3. At all temperatures examined, the amount of total insoluble material formed was directly proportional to the initial concentration of DMP. Furthermore, nitrogen balance calculations are able to account for all of the DMP (after stress) as either unreacted or incorporated into the sediment produced. Nitrogen-specific capillary GC (Hall detector) did not detect any nitrogenous intermediates in the liquid phase.

The sediments produced in all instances have been found to be rich in nitrogen (ca. 12% by weight), and an empirical formula of  $C_6, 3H_6, 7NO_{1.4}$  has been determined (oxygen by direct analysis). The energy of activation for the production of total insolubles was calculated to be 11.7 and 11.6 kcal/mol for fuels D-1 and D-11, respectively. No induction periods were observed.

Filtrate hydroperoxide levels were determined in stressed samples by iodometric titration (ASTM D-1583-60). DMP-doped DFM samples exhibited very low peroxide numbers after stress. The DMP either prevents hydroperoxides from forming, or else reacts with any hydroperoxides which have formed. Results obtained in benzene indicated that formation of hydroperoxides from solvent molecules is not a prerequisite for DMP-promoted sedimentation. Mechanistic studies are continuing. Figure 4 shows the peroxide numbers obtained for D-1 and D-11 fuel blanks (un-doped) after 80°C stress. The antioxidant present in D-11 was seen to protect the fuel out to about 21 days, at which point the peroxide numbers increased sharply. Fuel D-11 contained no detectable hydroperoxide prior to stress.

A survey of other nitrogen compounds as fuel dopants has been undertaken in D-1 fuel. The results of 80°C - 14 day trials (unvented) with 450 ppm N (w/v) of a variety of compound classes are shown in Table I. Alkyl substituted pyrroles were found to be the most active species, with pyridines and quinolines less active. Peroxide numbers were low in the case of most pyrrole trials, and the sediments obtained were rich in nitrogen. Curiously, Knorr's pyrrole (2,4-dimethyl-3,5-dicarbethoxy-) was a most inactive species. Thus, electronic factors may be important for pyrroles.

#### CONCLUSIONS

A common reaction pathway appears to exist for DMP-promoted sedimentation in DFM. Results obtained are consistent with those of other workers (2). A high-precision gravimetric method of fuel storage stability determination has been developed.

#### ACKNOWLEDGMENT

The authors thank Dr. Dennis W. Brinkman of the Bartlesville Energy Technology Center (DOE) for sponsoring this work under DOE contract DE-AI-81BC10525. References to brand names were made for identification only and do not imply endorsement by DOE or NRL.

FIGURE 1  
Time-Temperature Correlation for  
Accelerated Fuel Stability Tests

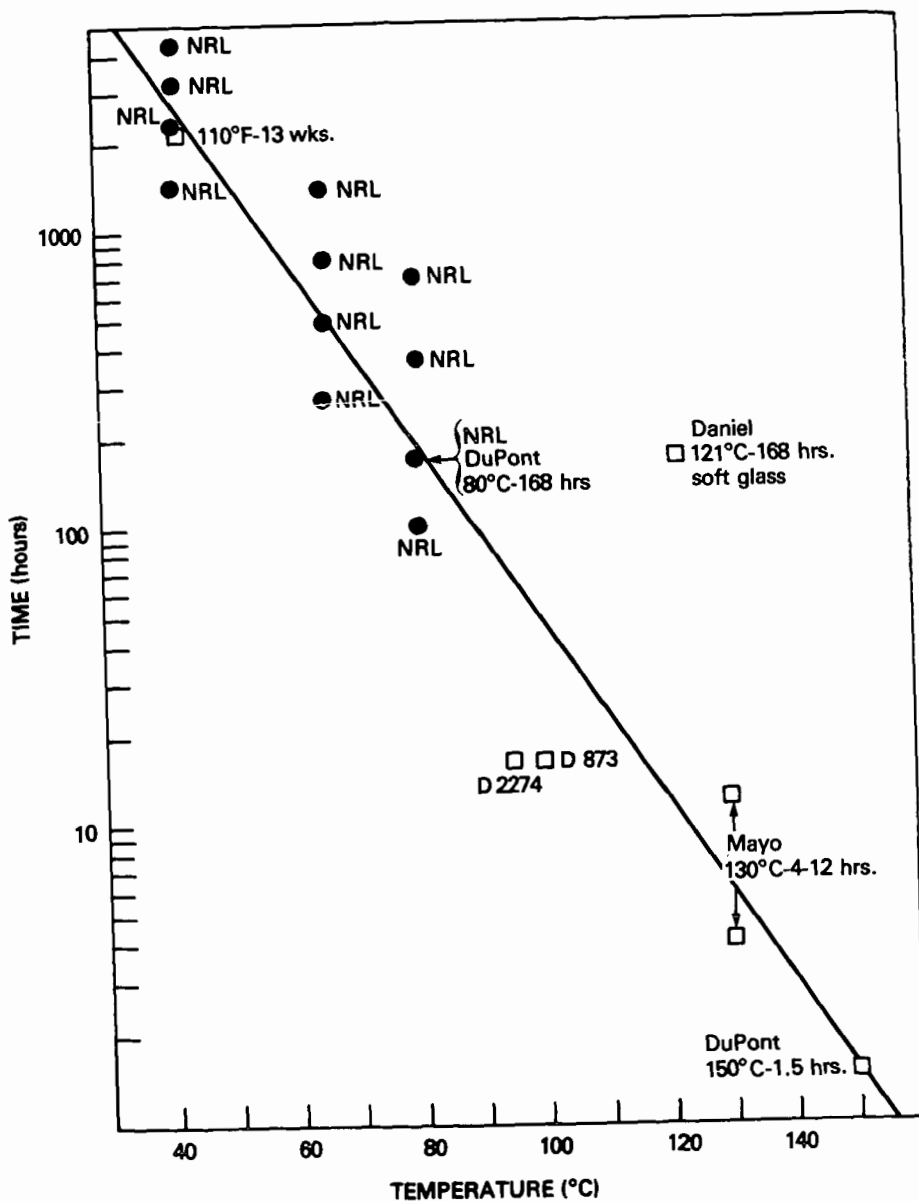


FIGURE 2  
Total Deposits for Shale-II DFM  
(D-1) with DMP Added - 80°C

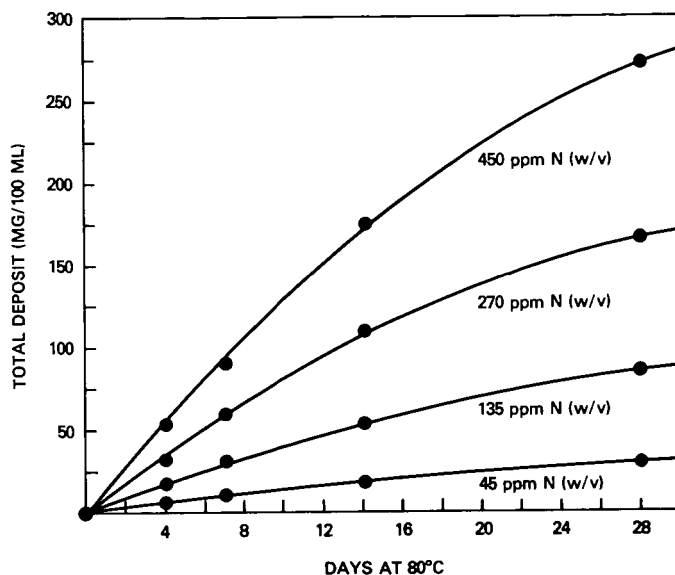


FIGURE 3  
Total Deposit as a Function of Initial DMP  
Concentration Added to DFM (D-11)  
28 Day Stress at 80°C

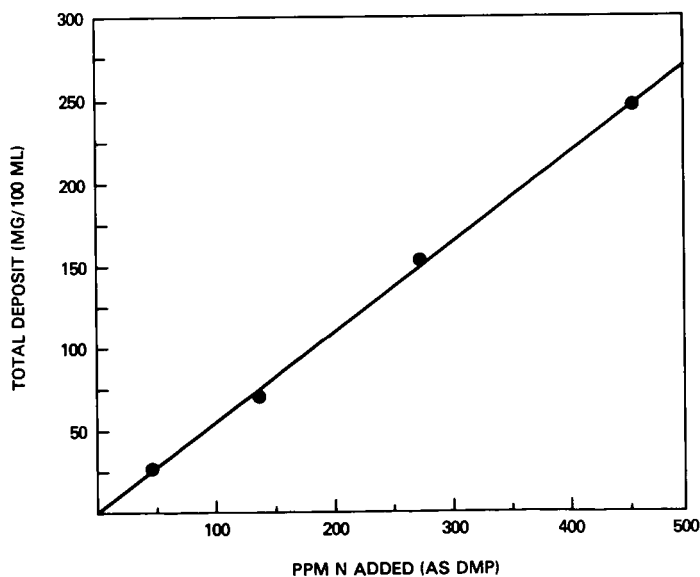


FIGURE 4  
Peroxide Numbers for DFM  
(D-1 and D-11) at 80°C

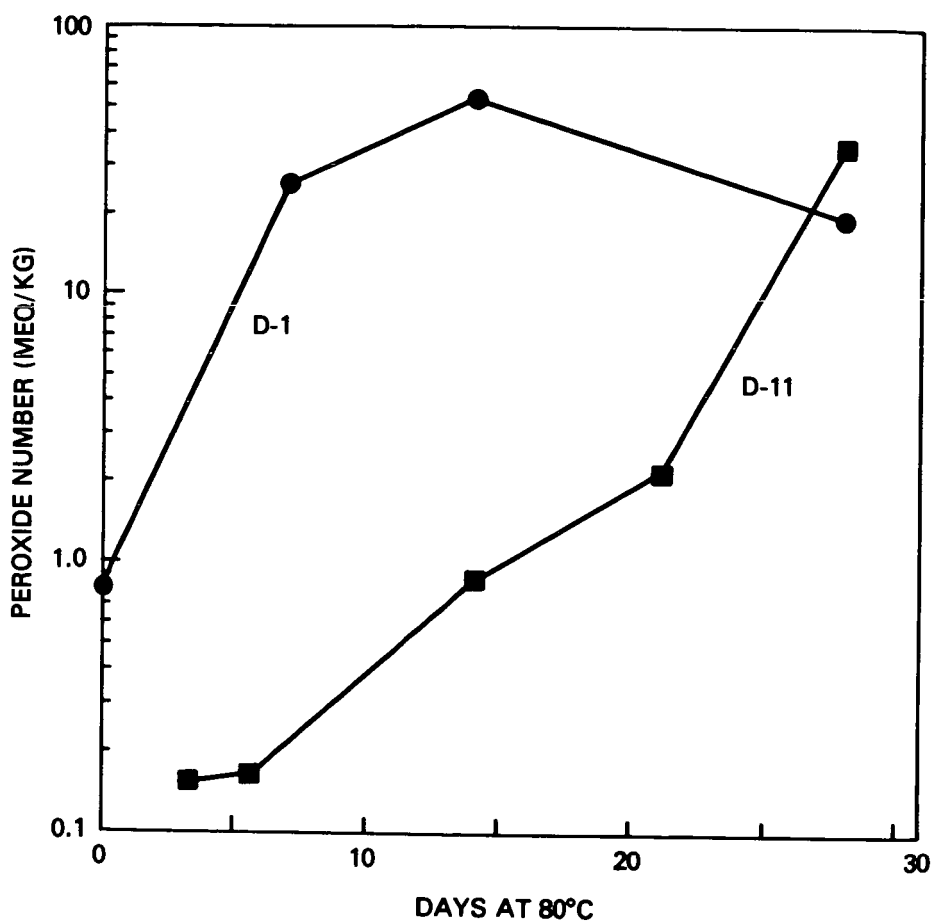


TABLE I  
RELATIONSHIP OF NITROGEN COMPOUND STRUCTURE  
TO SEDIMENTATION IN DFM (D-1)  
(Listed in Approximate Order of Activity)\*

| <u>Group A (&gt;100 mg/100 ml)</u> | <u>Group C (3-10 mg/100 ml)</u> | <u>Group D (&lt;3 mg/100 ml)</u>     |
|------------------------------------|---------------------------------|--------------------------------------|
| 2,3,4,5-Tetramethylpyrrole         | 2,3-Dimethylindoline            | 3,5-Dimethylpyridine                 |
| Dodecahydrocarbazole               | 2,6-Dimethylpyridine            | 3,5-Dimethylpyrazole                 |
| 2,4-Dimethylpyrrole                | 2-Methylpyrrole                 | 4-Methylquinoline                    |
| 2,3-Dimethylpyrrole                | 4-T-Butylpyridine               | 2-Methylquinoline                    |
| 1,2,5-Trimethylpyrrole             | 3-Methylisoquinoline            | 3-Methylpiperidine                   |
|                                    | Pyrrole-2-Carboxaldehyde        | 2-Methylpyrazine                     |
|                                    | 1-Methylpyrrolidine             | 2,5-Dimethylpyrazine                 |
| <u>Group B (10-100 mg/100 ml)</u>  | 2,6-Dimethylquinoline           | Indole-3-Carboxaldehyde              |
| Pentamethylpyrrole                 | 2-Benzylpyridine                | 5,6,7,8-Tetrahydroquinoline          |
| 3-Methylindole                     | 4-Iso-Butylquinoline            | 5-Ethyl-2-Methylpyridine             |
|                                    | 2-Methylpiperidine              | Trans-2,5-Dimethylpiperazine         |
|                                    | Pyrrolidine                     | 2-Methylindole                       |
|                                    | 2-Acetyl-1-Methylpyrrole        | 2-Methylpyridine                     |
|                                    |                                 | 1,2,3,4-Tetrahydroquinoline          |
|                                    |                                 | 2,6-Dimethylpiperidine               |
|                                    |                                 | 2,4-Dimethyl-3,5-Dicarbethoxypyrrole |

#### LITERATURE CITED

- (1) Frankenfeld, J. W., Taylor, W. F., and Brinkman, D. W., "Fundamental Synthetic Fuel Stability Study", EXXON R and E Co., Rpt. No. DOE/BC/10045-12, February 1981 and references therein.
- (2) Frankenfeld, J. W., Taylor, W. F., and Brinkman, D. W., "Fundamental Synthetic Fuel Stability Study", EXXON R and E Co., Rpt. No. DOE/BC/10045-23, March 1982.
- (3) For example: a) Dahlin, K. E., Daniel, S. R., and Worstell, J. H., Fuel, 60, 477 (1981); b) Worstell, J. H., and Daniel, S. R., Fuel, 60, 481 (1981); c) Worstell, J. H., Daniel, S. R., and Frauenhoff, G., Fuel, 60, 485 (1981).
- (4) For more detail: Hazlett, R. N., Cooney, J. V., and Beal, E., "Mechanisms of Syncrude/Synfuel Degradation - First Annual Report: September 15, 1981 - September 30, 1982", Rpt. No. DOE/BC/ (in press), 1983.
- (5) For a thorough review: Stavinoha, L. L., Westbrook, S. R., and Brinkman, D. W., "Accelerated Stability Test Techniques for Middle Distillate Fuels", Southwest Research Institute, Rpt. No. DOE/BC/10043-12, October 1980.

## IGNITION AND COMBUSTION OF COAL PARTICLES

By

C. O. Gomez and F. J. Vastola  
Department of Materials Science and Engineering  
The Pennsylvania State University, University Park, Pennsylvania 16802

### INTRODUCTION

A fundamental understanding of the coal combustion process is important not only in the operation of combustion furnaces but also in the design of equipment for efficient burning, especially now when one of the requirements in the recent emphasis on coal utilization is clean burning. Even when the combustion of coal and char particles has been studied for a long time and extensive literature exists in the subject (1-4), this fundamental understanding has not been established. A clear demonstration is the wide variety of assumptions made in the most recent attempts of modeling the phenomenon (5-10).

The combustion of coal particles is a heterogeneous phenomenon involving a relatively unknown material and occurring in two stages: ignition and burn-out. Ignition depends on a balance between the rates of heat gain and loss to the particle; consequently the particle size, the environmental conditions, and the reactor geometry that defines the fluid dynamics of the system play important roles. The study of this complex phenomenon is difficult, because in addition to its transient character, it involves the simultaneous occurrence of a number of transport processes which apply to a system whose dimensions and characteristics change with time.

Two ignition mechanisms for coal particles are accepted. Their occurrence depends on the relative rates of two phenomena: the heating of the particle surface and the rate of volatile release. When the rate of heating of the particle surface is larger than the rate of volatiles release, the ignition takes place on the particle surface and the mechanism is called heterogeneous. In this case, the particle surface reaches a temperature high enough for reacting and igniting prior to extensive pyrolysis. On the other hand, when the rate of volatile release is larger than the rate of heating of the particle surface, the ignition occurs in the gas phase surrounding the particle and the mechanism is called homogeneous. In this case, the pyrolysis is so rapid that the particle surface is isolated from the external gaseous mixture by a volatile layer. To investigate the conditions which control the mode of ignition we conducted experiments utilizing single particles of coal.

### EXPERIMENTAL

A schematic diagram of the apparatus is in Figure 1. The oxygen-nitrogen mixture is heated in the gas preheater and then sweeps the reaction zone where a single coal particle is introduced by gravity, using a specially designed injector. A light beam at location 1 is used to detect the time of the particles entry into the reaction zone. The gaseous products are rapidly cooled and split to be simultaneously measured by two nondispersive infrared analyzers, one for carbon monoxide and one for carbon dioxide. A photo transistor connected to a light pipe placed within the reaction zone is used to detect combustion generated luminosity. A microcomputer-based data acquisition system records the time of injection, the light generated by the particle's ignition and burnout, as well as the carbon monoxide and carbon dioxide concentration in the product gas stream.

In addition to the time of entry of the coal particle into the reaction zone the time of transit of the product gases from the reaction zone to the detector must be determined. This transit time was measured by injecting a short pulse of carbon dioxide into the reaction zone under the same conditions as used in an ignition run and measuring the time to detector response. To characterize any deformation of the product pulse as it flows from the reaction zone to the detector a similar short pulse of carbon dioxide was directly injected into the detector cell. The shape of the pulse after its travel through the system was compared with that resulting from the injection of the pulse directly into the detector cell. No appreciable difference was detected, indicating that the conditions used are very effective in reducing the deformation of the gas release curves.

A subbituminous coal (PSOC 648), whose characteristics are shown in Table I, was used in this study. Particles from the 850-1000 micron sieve fraction were injected into a reaction furnace swept with air at five temperature levels of 928, 980, 1076, 1118 and 1273°K.



TABLE I  
CHARACTERISTICS OF COAL PSOC 648

|                                |                                  |                  |
|--------------------------------|----------------------------------|------------------|
| Apparent Rank: Subbituminous B | Proximate Analysis (as received) |                  |
|                                | Moisture                         | 22.10%           |
| Reflectance Rank: HVC          | Ash                              | 4.58%            |
|                                | Volatile Matter                  | 33.78%           |
|                                | Fixed Carbon                     | 39.59%           |
| Ultimate Analysis              | <u>As Received</u>               | <u>Dry Basis</u> |
| Moisture                       | 22.10%                           | %                |
| Ash                            | 4.58%                            | 5.88%            |
| C                              | 53.01%                           | 68.05%           |
| H                              | 4.00%                            | 5.13%            |
| S (total)                      | 0.33%                            | 0.42%            |
| N                              | 0.80%                            | 1.03%            |
| O (by difference)              | 15.18%                           | 19.49%           |

## RESULTS AND DISCUSSION

Typical results of the gas evolution during combustion are shown in Figure 2 for selected runs at the different temperatures used in this study. The carbon monoxide and carbon dioxide concentrations are plotted against time with zero time being that time when product gases are first detected. Homogeneous ignition, as evidenced by a peak in the carbon dioxide product curve, is detected at temperatures of 1076°K and higher. The integration of the gas evolution curves will give the total mass of carbon in the original particle, if all the carbon is oxidized to carbon monoxide or carbon dioxide, which means in the case of the combustion of a coal particle, the complete burn-out of the volatiles released in the early stages of the combustion. Experimental results suggest that this was the case, because the most difficult hydrocarbon to be oxidized--methane--detected during the pyrolysis of coal particles, was not found during their combustion.

The occurrence of either of the two mechanisms of ignition previously described can be easily determined from the results of the light intensity measurements presented in Figure 3. When a coal particle ignites homogeneously, the combustion in the gaseous phase of the volatile matter released from the particle produces an initial flash of light, followed by the glowing of the remaining particle as the heterogeneous combustion proceeds. On the other hand, when the ignition mechanism is heterogeneous, the initial flash of light is not observed and only the final glowing is detected.

The ignition mechanisms detected by light intensity and by gas release curves have been summarized in Table II. There is complete agreement between the two techniques, except at the intermediate temperature of 1076°K. This discrepancy however, is consequence of an insufficient amount of volatiles released by the particle for burning with enough intensity to generate a flash of light, when the gas temperature is 1076°K. However, the amount released is enough to be detected before the ignition begins on the surface of the particle. This is a clear advantage of the experimental approach used in this work and shows how both techniques complement each other.

The total combustion time can also be determined from light intensity measurements and from gas evolution curves. A comparison between the results given by the two techniques is presented in Figure 4, where the combustion time measured by carbon dioxide evolution is plotted against the value obtained from light intensity for coal particles. Carbon dioxide was selected over carbon monoxide because of the greater sensitivity of the carbon dioxide detector, which allows the measurement of the combustion time more accurately. The combustion times tend to be larger when they are measured by gas evolution than by light intensity. This tendency is not unexpected because light can be detected only after the particle temperature increases to a point at which it is visible from the background. This high temperature is reached after a period in which gases were already evolving.

An unexpected result is the decrease in the proportion of carbon monoxide in the product gases, as the gas temperature increases. If the measured concentrations of carbon monoxide and carbon dioxide are the results of the chemical reaction on the surface, an increase in the proportion of carbon monoxide is expected as the temperature rises. The opposite trend is a consequence of the gas phase oxidation of carbon monoxide to carbon dioxide, which modifies the relation of the primary products of the reaction. In any case, the occurrence of this gas phase reaction does not affect the results previously discussed, because they are based on the total carbon consumed in the particle, and the gas phase reaction only affects the relative distribution of carbon as carbon monoxide or carbon dioxide, but not the total carbon coming from the particle as the result of the chemical reaction.

TABLE II  
MECHANISMS OF IGNITION DETECTED BY DIFFERENT TECHNIQUES  
IN THE COMBUSTION OF COAL PARTICLES

| Gas<br>Temperature<br>(°K) | Run | Ignition Mechanism Detected by |               |
|----------------------------|-----|--------------------------------|---------------|
|                            |     | Light Intensity                | Gas Evolution |
| 928                        | 150 | Het                            | Het           |
|                            | 151 | Het                            | Het           |
|                            | 152 | Het                            | Het           |
|                            | 153 | Het                            | Het           |
|                            | 154 | Het                            | Het           |
| 980                        | 115 | Hom                            | Hom           |
|                            | 116 | Het                            | Het           |
|                            | 117 | Het                            | Het           |
|                            | 118 | Het                            | Het           |
|                            | 119 | Het                            | Het           |
| 1076                       | 133 | Hom                            | Hom           |
|                            | 134 | Hom                            | Hom           |
|                            | 135 | Het                            | Hom           |
|                            | 136 | Het                            | Hom           |
|                            | 137 | Het                            | Hom           |
| 1118                       | 097 | Hom                            | Hom           |
|                            | 099 | Hom                            | Hom           |
|                            | 100 | Hom                            | Hom           |
|                            | 101 | Hom                            | Hom           |
|                            | 102 | Hom                            | Hom           |
| 1283                       | 081 | Hom                            | Hom           |
|                            | 082 | Hom                            | Hom           |
|                            | 083 | Hom                            | Hom           |
|                            | 084 | Hom                            | Hom           |
|                            | 085 | Hom                            | Hom           |

### CONCLUSIONS

A differential approach has been developed for the study of the combustion process of single coal particles. The experimental technique, based in the simultaneous measure of the carbon monoxide, carbon dioxide, and intensity of the light generated during the combustion, gives quantitative information about the ignition and the subsequent burn-off of the residual particle. The apparatus designed provides the special characteristics required in this study and the transition between the two ignition mechanisms is achieved within the range of operation conditions, for the coal used in this study.

The ignition mechanism is determined not only from measurements of light intensity during the combustion, a technique commonly used in the past, but also from the gas evolution curves which allow the quantification of the whole combustion process. The results show the convenience of using both as complementary techniques in the determination of the ignition mechanism.

### ACKNOWLEDGMENTS

This study was made possible by financial support from the Coal Cooperative Program at The Pennsylvania State University. The authors thank the Penn State Coal Sample Bank and Data Base for supplying the sample and the analysis of the coal used in this study.

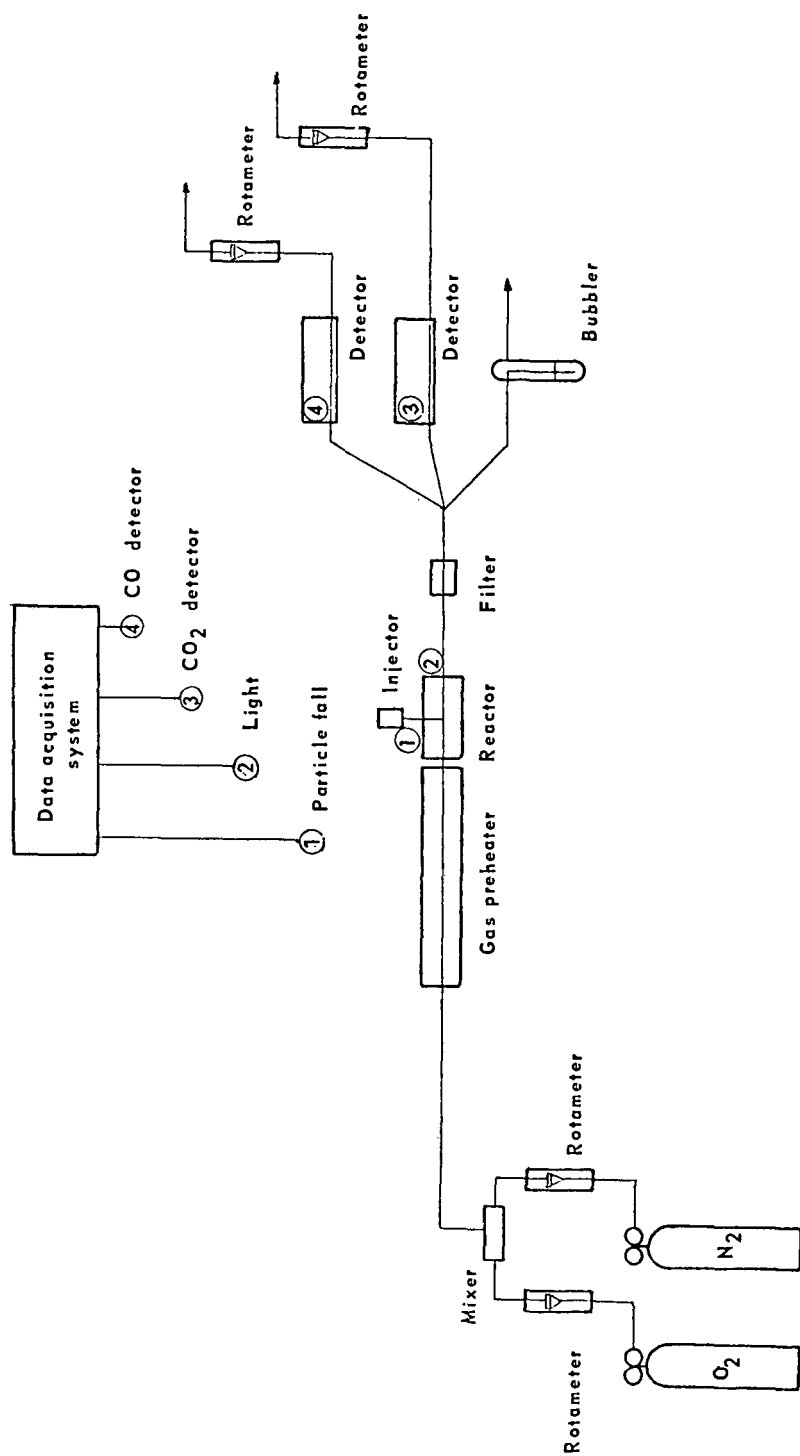


FIGURE 1. SCHEMATIC DIAGRAM OF THE APPARATUS

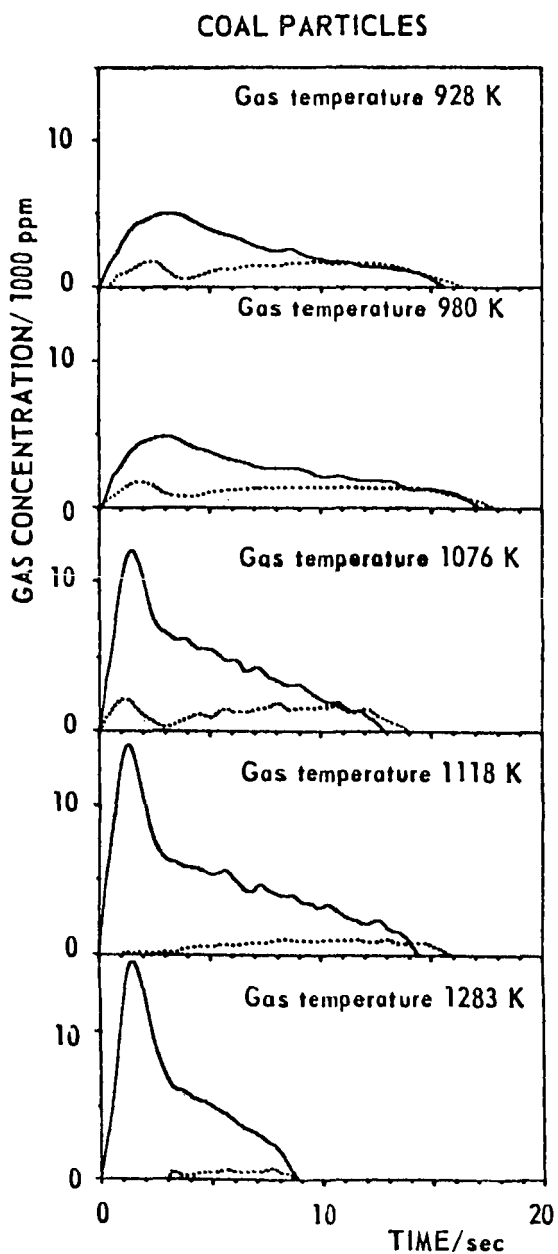


FIGURE 2. TYPICAL GAS EVOLUTION CURVES

( Continuous line  $\text{CO}_2$  – Dotted line  $\text{CO}$  )

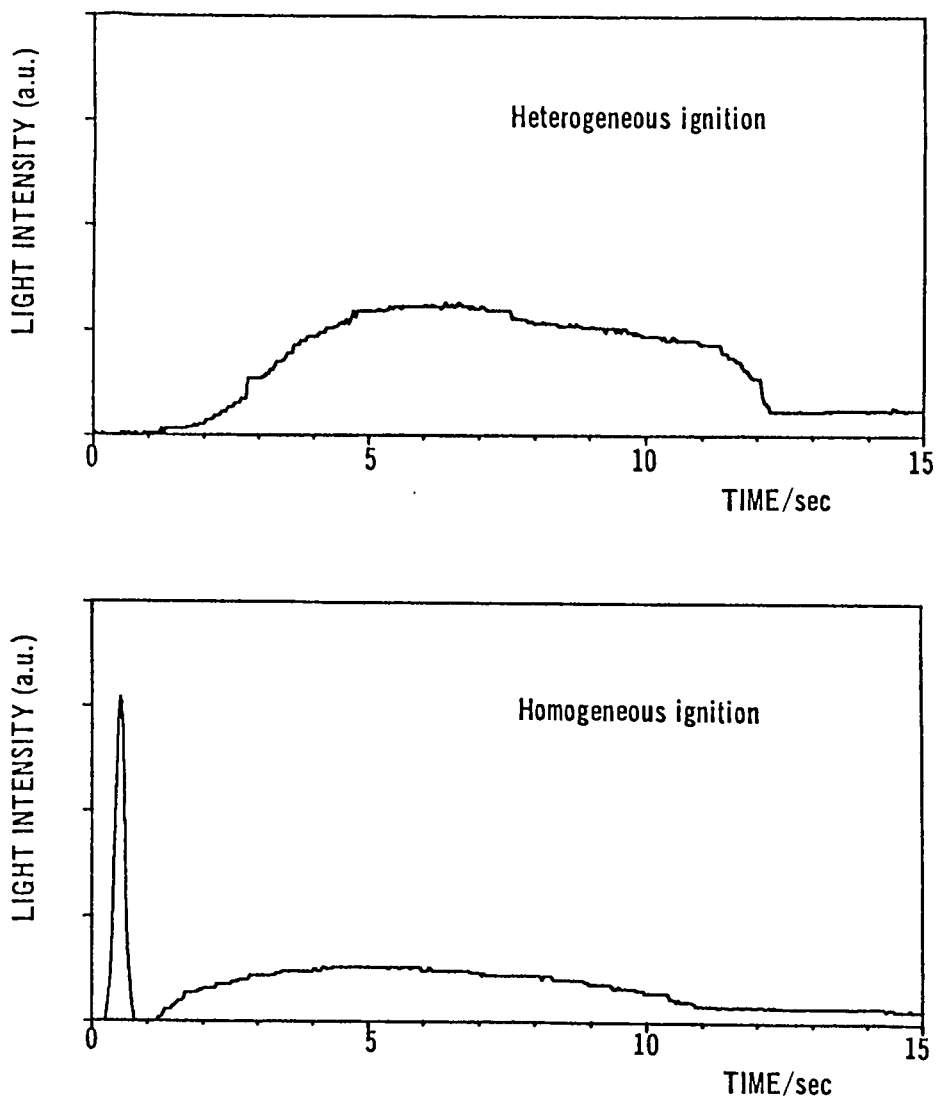


FIGURE 3. TYPICAL RESULTS OF LIGHT EMISSION MEASUREMENTS DURING COMBUSTION OF COAL AND CHAR PARTICLES

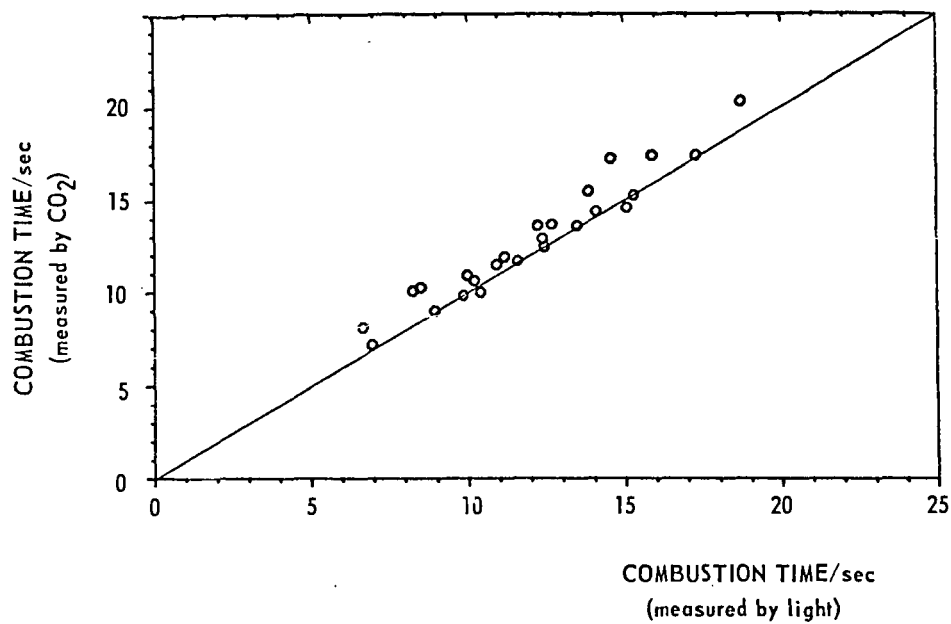


FIGURE 4. COMPARISON BETWEEN THE DIFFERENT TECHNIQUES USED FOR MEASURING COMBUSTION TIMES

#### LITERATURE CITED

- (1) Essenhigh, R. H., J. Inst. Fuel, 34, 239 (1961).
- (2) Essenhigh, R. H., "Chemistry of Coal Utilization, Second Supplementary Volume" (Ed. M. A. Elliot), John Wiley and Sons, 1981, Ch. 19.
- (3) Field, M. A., Gill, D. W., Morgan, B. B., and Hawksley, P. G. W., "Combustion of Pulverized Fuel", British Coal Utilization Research Association, Leatherhead, Surrey, 1967.
- (4) Mulcahy, M. F. R., and Smith, I. W., Rev. Pure and Appl. Chem., 19, 81 (1962).
- (5) Annamalai, K., and Durbetaki, P., Combust. Flame, 29, 193 (1977).
- (6) Bandyopadhyaw, S., and Bhaduri, D., Combust. Flame, 18, 411 (1972).
- (7) Baum, M. M., and Street, P. J., Combust. Sci. Technol., 3, 231 (1971).
- (8) Juniper, D. A., and Wall, T. F., Combust. Flame, 39, 69 (1980).

THE EFFECT OF THE MOLECULAR WEIGHT OF ADDITIVE  
ON THE PROPERTIES OF ANTIMISTING FUELS

By

A. F. Hadermann, J. C. Trippe  
General Technology Applications, Inc., Arlington, Virginia 22209  
and

P. F. Waters  
The American University, Washington, D. C. 20016

INTRODUCTION

Antimisting aircraft fuels, when ignited, do not produce the roaring fireball which often accompanies aircraft crashes (1). This result is attributable to the suppression of the aerosolization of the fuel by added macromolecules which alter the structure of the droplets of fuel emanating from rent fuel tanks after the crash.

The first studies of the antimisting effect of macromolecules on aviation fuel were carried out in Great Britain in 1968 (2). In that early work it was established that there was a qualitative relationship between the suppression of the atomization of the fuel and the molecular weight of the additive above a certain critical concentration; the latter being inverse to the molecular weight of the additive. Subsequent investigations have demonstrated a dependence of the antimisting effectiveness of polyisobutylene in diesel fuel on the viscosity average molecular weight to a power exceeding 2 (3), and in jet-A fuel to the  $2\alpha + 1$  power (4), where  $\alpha$  is the exponent in the Mark-Houwink equation.

In their study Chao et al. were able to demonstrate a strong correlation between the extent of antimisting effectiveness and flammability reduction with the maximum ductless siphon height supported by the solution. They introduced the ductless siphon to the study of antimisting fuels as a measure of the elongational viscosity imparted by the macromolecules to the fuel. The apparatus does not provide a uniform elongational flow field but there is no device, at present, for determining the true elongational viscosity of these solutions and the ductless siphon has the advantage of being easy to assemble and use. The precision of the measurements can be improved by drawing the liquid column in a controlled environment, reading the height optically or with a strain gauge, etc. The principal factor of interest with respect to antimisting fuels, however, is that it has been demonstrated that the ductless siphon is a tool for rapidly screening macromolecules for their effectiveness as antimisting agents.

In this work it is suggested that the ductless siphon might also be used for the rapid estimation of the molecular weight of megadalton macromolecules.

EXPERIMENTAL

Three samples of polyisobutylene (BASF: B-100, B-200, B-200-246) were dissolved in isooctane at room temperature with occasional gentle swirling over several days. The viscosity average molecular weights were determined with an Ostwald viscometer from the Mark-Houwink equation (5):

$$[\eta] = 3.06 \times 10^{-4} \bar{M}_v^{0.65} \quad 1)$$

The values are given in Table I.

The height-at-break of serial dilutions of the stock solutions of the three samples was measured in the apparatus of Figure 1. Six measurements were made on each solution and the measurements were averaged. The averaged heights were plotted against the concentration and the slope of each line,  $h/c$ , was determined by linear regression analysis. The slope values, along with the correlation coefficients,  $r$ , are entered in Table I.

The effect of the molecular weight on the height-at-break property and, by extension, the antimisting effectiveness and the flammability suppression potential of polyisobutylene in isooctane is dramatic.

In a 1975 paper Williams (6) proposed a theory which explains why high molecular weight macromolecules in dilute solution exhibit quite large extensional viscosities relative to lower molecular



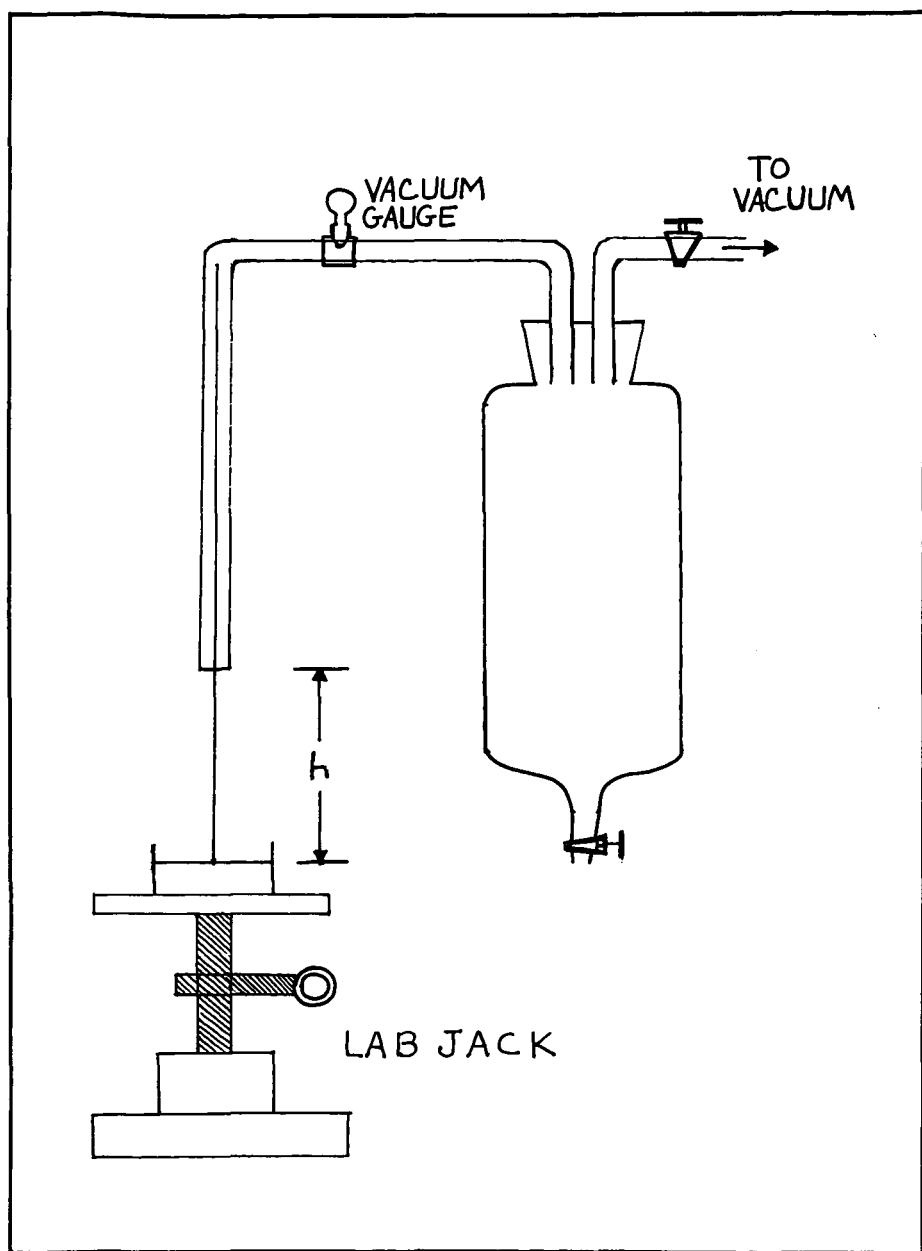


FIG. 1. DUCTLESS SIPHON APPARATUS.

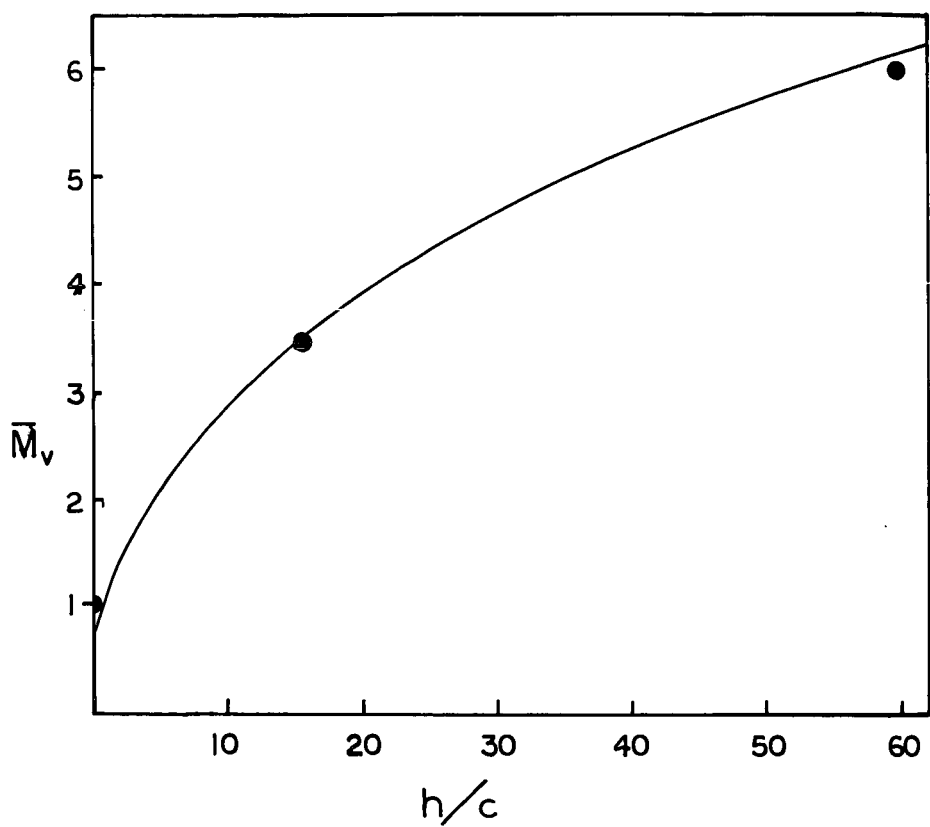


FIG. 2. MOLECULAR WEIGHT VS. SLOPE OF PLOTS OF HEIGHT-AT-BREAK VS. CONCENTRATION OF POLYISOBUTYLENE IN ISO-OCTANE AT 20 °C.

weight species. An extension of the theory applied to the use of the ductless siphon for estimating the extensional viscosity of samples of antimisting fuels was completed last year (7). The working equation is:

$$\frac{\bar{\eta}}{\eta_0} = 3 (1 + \dot{\epsilon} c n_s K^2 M_V (2\alpha + 1) / RT + \dots) \quad 2)$$

where  $\bar{\eta}$  is the extensional viscosity  
 $\eta_0$  is the shear viscosity of the solution  
 $\dot{\epsilon}$  is the elongation rate in pure extensional flow  
 $c$  is the concentration in g/dl  
 $n_s$  is the shear viscosity of the solvent  
 $K$  and  $\alpha$  are the constants of the Mark-Houwink equation.

TABLE I  
 VISCOSITY AVERAGE MOLECULAR WEIGHT AND SLOPES OF  
 HEIGHT-AT-BREAK VS. CONCENTRATION PLOTS FOR  
 SAMPLES OF POLYISOBUTYLENE MEASURED IN  
 ISOCTANE AT 20°C

| Sample    | $M_V \times 10^{-6}$ | $\frac{h}{c}$ | $r$   |
|-----------|----------------------|---------------|-------|
|           | (g/mol)              | (cm/g/dl)     |       |
| B-100     | 1.00                 | 0             | 0.951 |
| B-200     | 3.46                 | 15.7          | 0.999 |
| B-200-246 | 5.96                 | 59.7          | 0.999 |

For a given polymer/solvent, for megadalton samples with the ductless siphon height-at-break measured at the same temperature at which the exponential term in the Mark-Houwink equation is evaluated, we propose the relation:

$$\frac{h}{c} = k \bar{M}_V (2\alpha + 1) \quad 3)$$

where  $k$  is a constant. For the polyisobutylene/isooctane system at 20°C,  $\alpha = 0.65$ . A plot of  $\bar{M}_V$  vs  $h/c$  appears in Figure 2, where the theoretical curve, evaluated from the measured height-at-break values, is given by:

$$\bar{M}_V = 1.05 \times 10^6 \left( \frac{h}{c} \right)^{0.44} \quad 4)$$

Inasmuch as interest in antimisting fuels is growing and ultra high molecular weight macromolecules are markedly superior in their performance in antimisting fuels, this method may be used for rapid estimation of molecular weights when the Mark-Houwink exponential term is known.

#### LITERATURE CITED

- (1) Weatherford, W. D., Jr., and Wright, B. R., AGARD/NATO 45th Meeting, Propulsion and Energetics Panel, London, April, 1975.
- (2) Mossel, J. W., and Waite, F. A., Proc. of the Aircraft Research and Technology for Antimisting Kerosene Conf., Feb. 18-19, 1981, p. 4-1 ff, Report No. FAA-CT-81-181, U.S. Dept. of Trans., June, 1981.
- (3) Investigation of the Application of a Cryogenic Blending Process to Produce Antimisting Diesel Fuels, A. F. Hadermann, P. F. Waters, J. C. Trippe and W. Weitzen, Contract No. DAAK-70-81-C-0134, U.S. Army Mobility Equip. Res. and Dev. Com., Fort Belvoir, Va. Jan. 15, 1982.
- (4) Chao, K. C., Child, C. A., Grens, E. A., and Williams, M. C., Amer. Inst. Chem. Eng. J., in press.
- (5) BASF Tech. Leaflet No. M 2353 E/81538, May, 1978.
- (6) Williams, M. C., Amer. Inst. Chem. Eng. J., 21, 1 (1975).
- (7) Chao, K. K. K., and Williams, M. C., J. Rheology, in press.

## STORAGE STABILITY STUDIES OF U.S. NAVY DIESEL FUEL MARINE

By

L. Jones, D. R. Hardy and R. N. Hazlett  
Naval Research Laboratory, Code 6180, Washington, D.C. 20375

### INTRODUCTION

An increasing trend in recent years is the utilization of heavier crude sources in producing middle distillate fuels. The U.S. Navy's concern about long-term (up to three years) storage stability of its diesel fuel marine (DFM) from such sources is the driving force for this study. The three major objectives of this work are: 1) to improve empirical predictive storage stability tests; 2) to better understand the chemical mechanism involved in middle distillate storage instability; and 3) to examine various commercial and experimental stabilizer additives as possible storage stability improvers suitable to Navy needs.

In this paper we will deal primarily with the first objective and also include some preliminary work and results on the second objective. Some of the problems and severe time restrictions of utilizing empirical predictive storage stability tests will be specifically addressed.

### EXPERIMENTAL

#### Accelerated Storage Stress Test

An empirical gravimetric test which was shown to be very precise for this type of analysis ( $\pm 10\%$  S. E.) of shale-derived diesel fuel marine (DFM) storage stability studies at NRL (1) was adopted for this study. It consists of filtering 300 ml of a fuel through Gelman type A/E glass fiber filters. The filtered fuel is transferred to a clean, dry, borosilicate brown glass 500 ml bottle weighed to the nearest 0.1 mg. The teflon-lined cap is placed on the bottle but not tightened. The bottles are placed in a dark oven held to constant temperatures within  $\pm 0.5^\circ\text{C}$  for a specified number of days ( $\pm 0.1$  days). Temperatures chosen for the accelerated tests were 43, 65, 80 and  $100^\circ\text{C}$ . After removal from the oven the bottles are allowed to cool to ambient temperature and relative humidity in the dark for 24 hours ( $\pm 2$  hours). The fuel is filtered through a Büchner funnel with Gelman type A/E glass fiber filters weighed to the nearest 0.1 mg. The bottles and filter pads are rinsed with  $3 \times 50$  ml of *n*-hexane aliquots to remove fuel and to ensure transfer of all non-adherent material from the bottle. The bottles and filters plus funnels are evacuated in a vacuum oven with a mechanical pump and then heated in vacuo for about 18 hours at  $120^\circ\text{C}$ . The vacuum oven is turned off and allowed to return to room temperature before removing the bottles and filter funnels. The bottles and filter funnels are weighed to the nearest 0.1 mg on a Mettler H315 (1000 g capacity) balance. Adherent gum is the weight difference per bottle corrected for a blank, divided by 300 and reported as mg/100 ml of fuel. Filtrable sediment is the weight difference of the filter pads corrected for a blank, divided by 300 and reported as mg/100 ml of fuel. The sum of these two values is reported as total insolubles in mg/100 ml of fuel. The mean and standard deviation of triplicate runs is generally reported. A blank determination is made for each time and temperature run. The filtrable sediment blank is a funnel and filter pad subjected to the same post stress handling a samples. All sample values reported herein have been corrected for a blank determination.

#### Fuels

In general, fuels used in this work were received in five-gallon metal containers and transferred to five one-gallon epoxy-lined metal containers and stored in a cold room at  $+4^\circ\text{C}$  until used. Most fuels were supplied through the Navy Petroleum Office from refineries and storage depots world-wide. All fuels had conformed to military specifications for Navy DFM at time of receipt by the Navy.

Capillary GC-MS was performed on a Hewlett Packard fused silica 0.3 mm I.D.  $\times$  50 m cross-linked methyl silicone column directly inserted into the electron impact source of a Hewlett Packard 5982A mass spectrometer through a modified solids probe inlet. Flow was adjusted to one ml/min of helium and the injector split ratio was approximately 50:1.

Elemental analyses were performed on a Perkin Elmer Model 240 Elemental Analyzer for carbon, hydrogen, and nitrogen. Oxygen analysis was performed on a Coulometrics Oxygen Analyzer.

## RESULTS AND DISCUSSION

### Stress Tests

Four petroleum derived DFM's covering a wide range of storage stability as defined by ASTM D2774 were selected as the test matrix to determine the statistical variations of the accelerated storage stability test described above. Typical data are reported in Table I (at 80°C for 14 days) with standard errors ranging from 1 to 11% of the mean. Data for a series of triplicate tests run at 80°C for these four fuels at 7-21 days are plotted in Figure 1. All four curves are quadratic least squares best fits. Three fuels exhibit a modest acceleration in sediment formation but 82-10 exhibits a deceleration. The data are further broken down and plotted as total and filtrable sediment for two fuels (81-5 and 82-10) in Figures 2 and 3. The filtered sediment line generally follows the shape of the total sediment curve but Figure 3 shows the exception. This type of behavior underscores the importance of fuel dependence on such measurements.

TABLE I  
WEIGHT OF TOTAL INSOLUBLES IN Mg/100 MI OF FUEL  
STRESSED FOR 14 DAYS AT 80°C

| <u>Fuel</u> | <u>Filtered<br/>Sediment</u> | <u>Adherent<br/>Gum</u> | <u>Total<br/>Insolubles</u> | <u>Mean</u> | <u>S. D.</u> |
|-------------|------------------------------|-------------------------|-----------------------------|-------------|--------------|
| 82-8        | 0.9                          | 2.3                     | 3.2                         | 3.6         | 0.4          |
|             | 0.9                          | 3.0                     | 3.9                         |             |              |
|             | 0.9                          | 2.7                     | 3.6                         |             |              |
| 81-5        | 5.0                          | 1.3                     | 6.3                         | 6.4         | 0.4          |
|             | 4.6                          | 1.6                     | 6.2                         |             |              |
|             | 4.7                          | 2.2                     | 6.9                         |             |              |
| 81-8        | 6.5                          | 2.2                     | 8.7                         | 8.5         | 0.3          |
|             | 6.4                          | 1.8                     | 8.2                         |             |              |
|             | 6.8                          | 1.7                     | 8.5                         |             |              |
| 82-10       | 25.5                         | 3.8                     | 29.3                        | 29.6        | 0.3          |
|             | 25.5                         | 4.3                     | 29.8                        |             |              |
|             | 24.4                         | 5.2                     | 29.6                        |             |              |

Five additional current-use Navy DFM's from petroleum were stress-tested in an effort to 1) broaden the total fuel test matrix and 2) screen for a marginal storage stability type of fuel (one which exhibits relatively high weights of total sediment during short stress tests). Table II gives selected results for four fuels which exhibit different trends in the formation of insolubles as stress temperature and time are increased. These results emphasize the fact that simultaneous, not necessarily related, reactions are proceeding, which form varying amounts of two different types of precipitate in the fuel - adherent and filtrable. The total insolubles formed by any particular fuel increase with increase in stress temperature and stress time. Data from Table II indicate that between 80 and 100°C for the five fuels studied the pseudo-Arrhenius plot of Figure 4 may be discontinuous, i.e., the rate of total sediment formation increases about two to four times faster than expected. This needs to be confirmed by running more fuels and by increasing the number of replicate samples. Figure 4 is plotted for one particular fuel, 81-5, and shows the time required at any particular temperature of stressing to form an equivalent weight of total sediment. The expected straight line relationship is not achieved. This may be indicative that accelerated storage stability tests at temperatures above 80°C may not be predicting correctly either the quantitative or the qualitative aspects of the phenomenon. This is an important consideration in future work in this area involving stabilizer additive studies.

### Chemical Characterization of Sediments

Since the predominant type of sediment formed (adherent or filtrable insoluble) appears to be fuel dependent it will be necessary to carefully characterize each type in order to be able to postulate possible mechanisms of formation. In general the adherent sediment is more soluble than the filtrable sediment. This means that the adherent gum is more amenable to standard gas chromatographic and GC/MS characterization. Adherent gums formed by stressing DFM fuel samples at 100°C for 21 days were analyzed by GC/MS. Chromatograms of the adherent gum are all quite similar to those of the non-stressed fuel. The most striking feature of the chromatograms is the symmetrical appearance of *n*-alkanes ranging from C-9 to C-20 (in the adherent gum) and C-9 to C-24 (in non-stressed fuel). Preliminary work indicates that oxidized hydrocarbons are co-eluting with the higher *n*-alkanes in adherent gum samples.

TABLE II

ALL WEIGHTS ARE GIVEN IN Mg/100 ML OF FUEL. STRESS TEMPERATURES ARE GIVEN IN °C AND STRESS TIMES ARE GIVEN IN DAYS

| <u>Fuel/Temp/Time</u> | <u>Filtered<br/>Sediment</u> | <u>Adherent<br/>Gum</u> | <u>Total<br/>Insolubles</u> | <u>Mean</u> | <u>S.D.</u> |
|-----------------------|------------------------------|-------------------------|-----------------------------|-------------|-------------|
| 82-8/43/52            | 0.0                          | 0.5                     | 0.5                         | 0.4         | 0.4         |
|                       | 0.1                          | 0.6                     | 0.7                         |             |             |
|                       | 0.0                          | 0.0                     | 0.0                         |             |             |
| 82-8/20/21            | 0.8                          | 4.8                     | 5.6                         | 5.1         | 1.1         |
|                       | 0.3                          | 5.5                     | 5.8                         |             |             |
|                       | 0.5                          | 3.3                     | 3.8                         |             |             |
| 81-5/43/52            | 0.2                          | 1.0                     | 1.2                         | 1.4         | 0.4         |
|                       | 0.2                          | 1.7                     | 1.9                         |             |             |
|                       | 0.2                          | 0.9                     | 1.1                         |             |             |
| 81-5/80/21            | 5.7                          | 2.7                     | 8.4                         | 9.0         | 0.6         |
|                       | 6.8                          | 2.7                     | 9.5                         |             |             |
|                       | 6.8                          | 2.2                     | 9.0                         |             |             |
| 82-36/80/21           | 1.3                          | 1.3                     | 2.6                         | 2.6         | 0.2         |
|                       | 1.2                          | 1.3                     | 2.5                         |             |             |
|                       | 1.7                          | 1.1                     | 2.8                         |             |             |
| 82-36/100/6           | 1.1                          | 6.7                     | 7.8                         | 8.0         | 0.3         |
|                       | 1.4                          | 6.8                     | 8.2                         |             |             |
| 82-32/80/21           | 1.5                          | 0.9                     | 2.4                         | 2.3         | 0.1         |
|                       | 1.0                          | 1.2                     | 2.2                         |             |             |
| 82-32/100/6           | 1.0                          | 7.6                     | 8.6                         | 8.4         | 0.3         |
|                       | 1.0                          | 7.2                     | 8.2                         |             |             |
| 82-33/80/21           | 0.5                          | 2.3                     | 2.8                         | 1.3         | 1.3         |
|                       | 0.0                          | 0.3                     | 0.3                         |             |             |
|                       | 0.5                          | 0.2                     | 0.7                         |             |             |
| 82-33/100/6           | 1.3                          | 1.6                     | 2.9                         | 2.9         | 0.0         |
|                       | 1.5                          | 1.4                     | 2.9                         |             |             |
| 82-35/80/21           | 1.1                          | 0.5                     | 1.6                         | 1.3         | 0.5         |
|                       | 0.7                          | 0.8                     | 1.5                         |             |             |
|                       | 0.7                          | 0.0                     | 0.7                         |             |             |
| 82-35/100/6           | 1.0                          | 2.4                     | 3.4                         | 2.3         | 1.6         |
|                       | 0.7                          | 0.5                     | 1.2                         |             |             |

TABLE III

ELEMENTAL ANALYSIS OF FILTRABLE SEDIMENT FROM NRL FUEL 82-10 STRESSED FOR 21 DAYS AT 80°C. ALL VALUES IN WEIGHT PERCENT

| <u>Element</u> | <u>Weight %</u> |
|----------------|-----------------|
| Carbon         | 62              |
| Hydrogen       | 5               |
| Nitrogen       | 3               |
| Oxygen         | 25              |
| Sulfur         | 2               |
| Ash            | 2               |
| Total          | 99              |

The filtrable insoluble sediment is much more difficult to solubilize and is not amenable to standard techniques of MS identification. Preliminary VPO measurements indicate that the filtrable

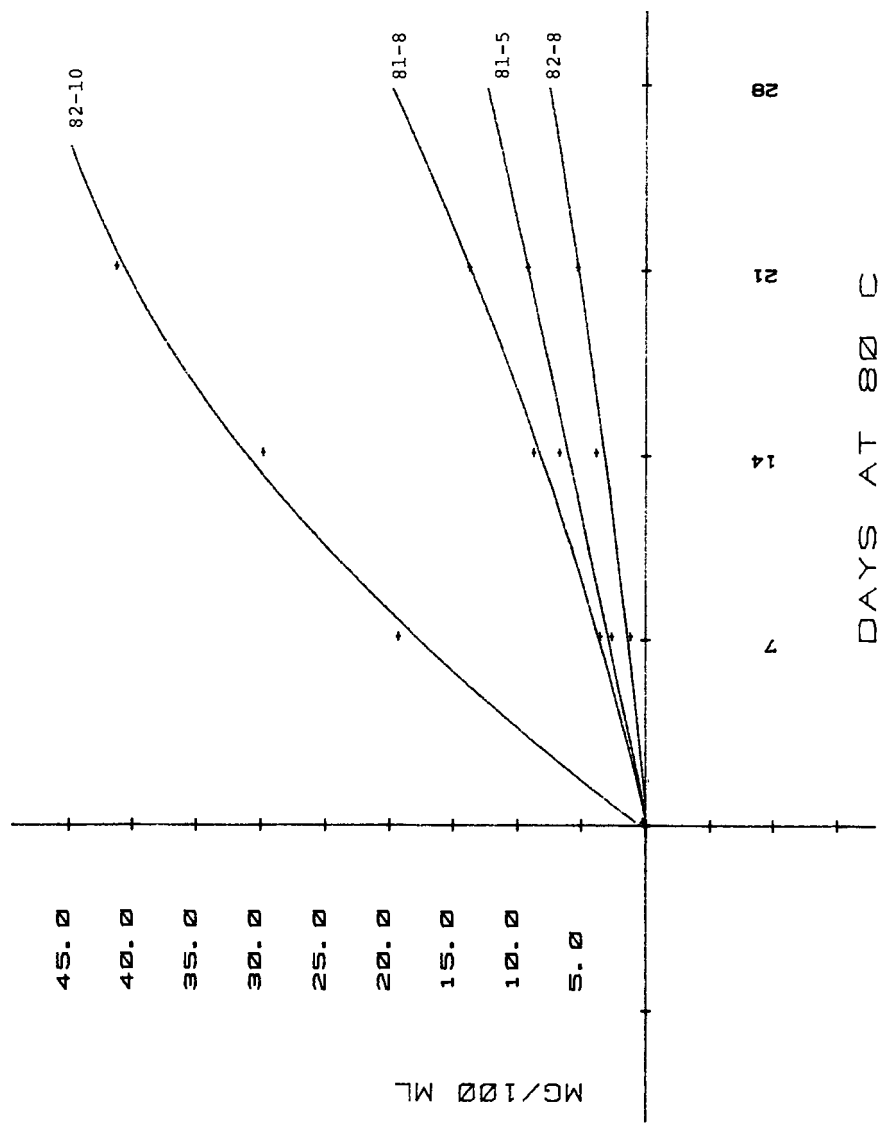


Figure 1. Total insolubles formed for four different DFM fuels stressed at 80°C for 7, 14, and 21 days each. Curves are computer generated quadratic least squares best fits.

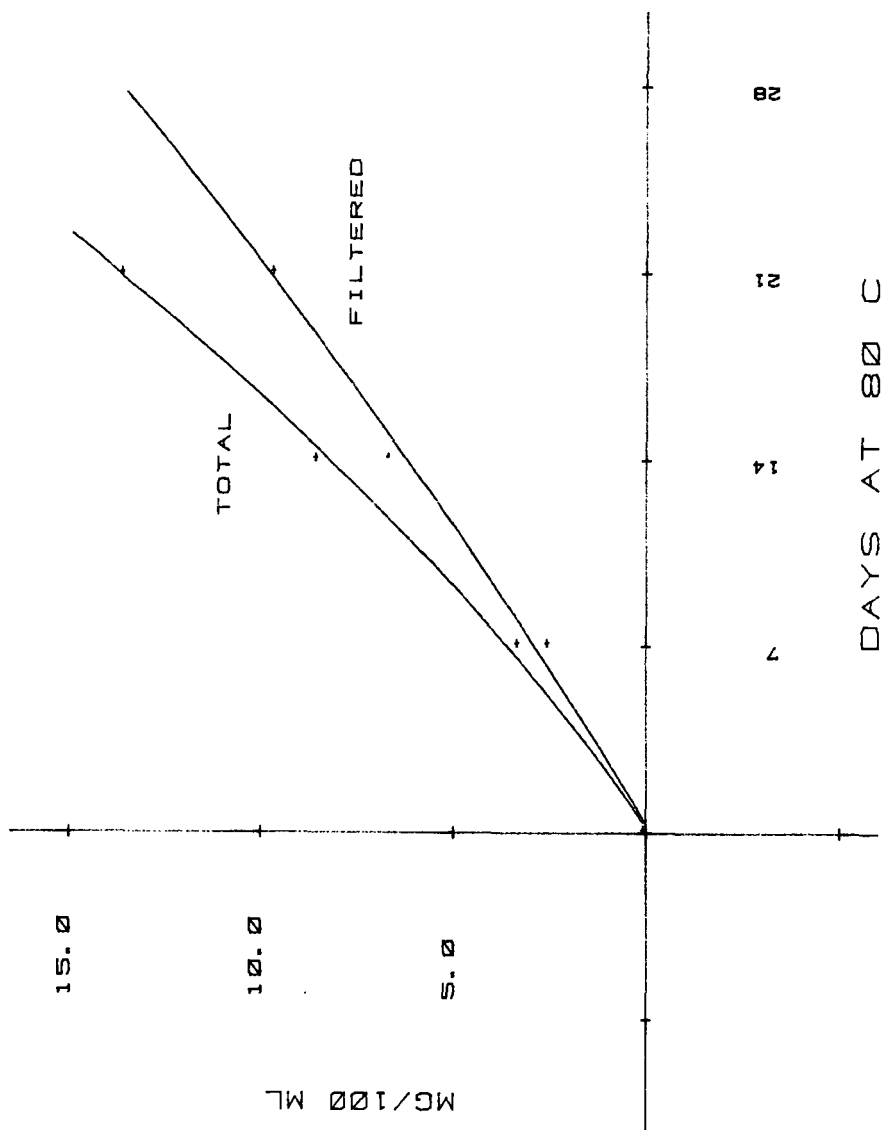


Figure 2. Breakdown of total insolubles into filtered sediment and adherent gum for fuel 81-8 stressed at 80°C for 7, 14 and 21 days. Curves are least squares best fits.



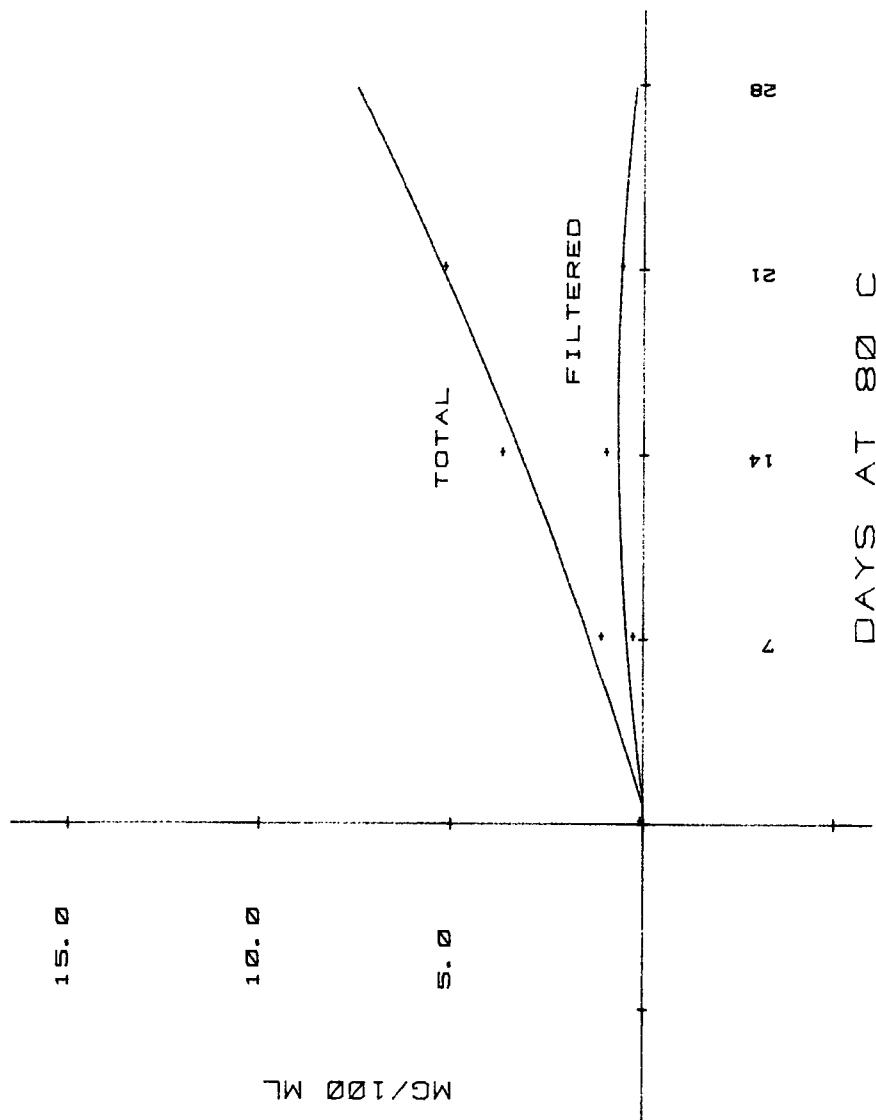


Figure 3. Breakdown of total insolubles into filtered sediment and adherent gum for fuel 82-8 stressed at 80°C for 7, 14, and 21 days. Curves are least squares best fits.

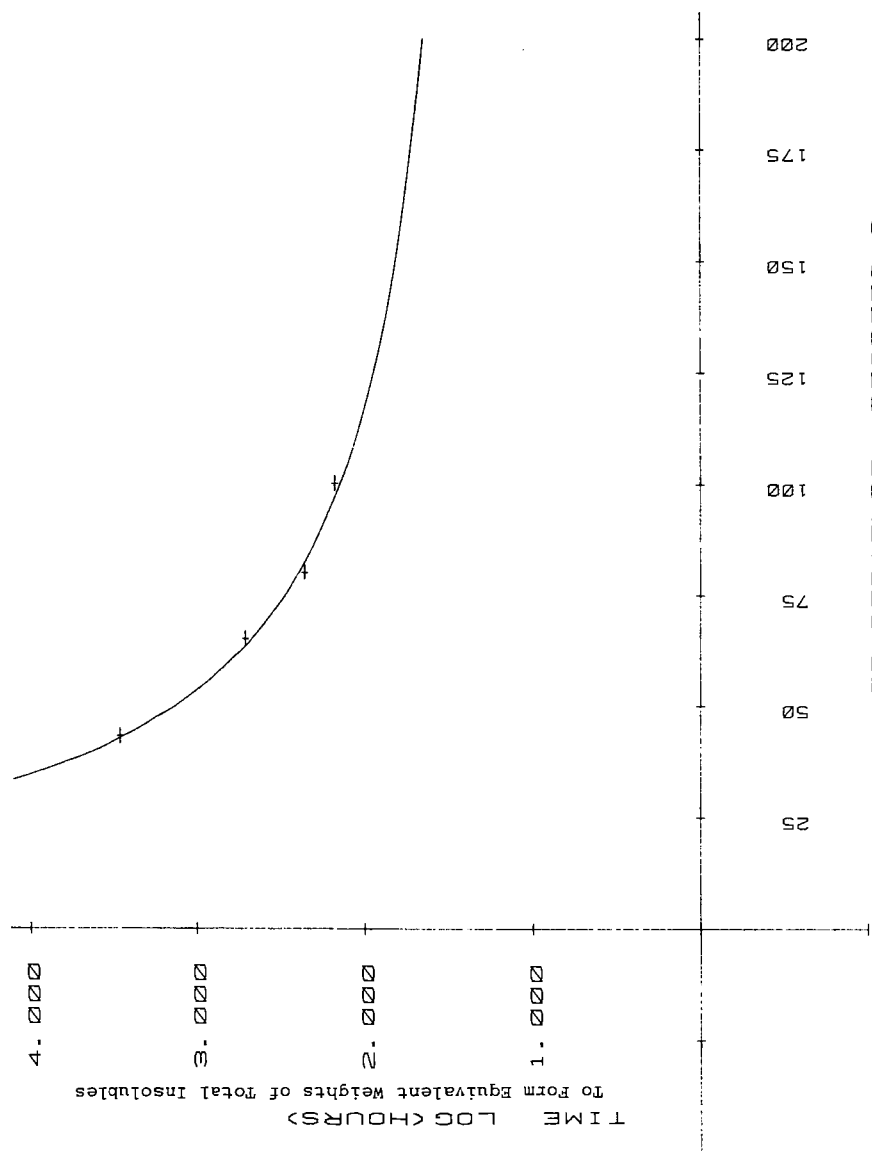


Figure 4. Plot of stress temperature of fuel 81-5 from 43°C to 100°C vs time necessary to form equivalent amount of total insolubles. The curve is a least squares best fit.

insoluble sediment is of higher molecular weight (up to 1500 amu). A typical elemental analysis for filtrable sediment of 82-10 (a particularly unstable DFM) is given in Table III. Oxygen has been directly determined by coulometric measurements. The high heteroatom content is typical for this type of sediment (2). Six major components of a filtered sediment extract in hot THF have been isolated by gas chromatography. Filtered sediments are usually insoluble in most organic solvents. Further analysis of the major fuel degradation components will establish the identity of the reactive species in fuels.

#### LITERATURE CITED

- (1) Hazlett, R. N., Cooney, J. V., and Beal, E. J., First Annual Report, Sept. 15, 1981-Sept. 30, 1982, NRL, Washington, D. C., to be published by USDOE under contract DE-AI-19-81BC10525.
- (2) Nixon, A. C., "Autoxidation and Antioxidants of Petroleum", Chapter 17 in "Autoxidation and Antioxidants", W. O. Lundberg, Ed., John Wiley, New York, 1962.

GENERAL PAPERS - POSTER SESSION  
PRESENTED BEFORE THE DIVISION OF PETROLEUM CHEMISTRY, INC.  
AMERICAN CHEMICAL SOCIETY  
WASHINGTON, D.C. MEETING, AUGUST 28 - SEPTEMBER 2, 1983

RADIOACTIVE ( $^{14}\text{C}$ ) TRACER STUDIES OF METHANOL CONVERSION  
OVER A Ni-ZSM-5 ZEOLITE

By

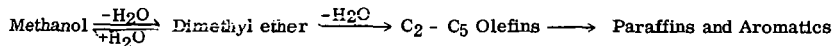
F. S. Hwu\* and J. W. Hightower  
Department of Chemical Engineering, Rice University, Houston, Texas 77251

INTRODUCTION

Within the last few years, researchers at the Mobil Research and Development Corporation (1) have synthesized a novel zeolite catalyst, ZSM-5, which is capable of converting oxygenates, e.g., methanol, into aliphatics and aromatic hydrocarbons in the gasoline boiling range. Since technology exists for making methanol from coal-derived synthesis gas (2), this new process provides an additional source of chemical feedstocks and transportation fuels.

In the conversion of methanol to hydrocarbons over such catalysts, more than 100 different compounds have been identified (3,4). The major hydrocarbon products can be classified into three categories: olefins, paraffins, and aromatics. There is a strong possibility that some of these products, once formed, react further to produce other products. The objective of this research was to investigate this possibility by labeling some of the products and following the transfer of the label to other products.

The reaction is thought to follow the sequence



The interconversion of methanol and dimethyl ether over such catalysts has been confirmed in several studies (5,6). At very low conversion of methanol, dimethyl ether is the major product, and the transformation of methanol into dimethyl ether is 20 to 30 times faster than hydrocarbon formation (6). On the other hand, when dimethyl ether is the starting material, both methanol and hydrocarbons are formed readily (5,6). The intermediate role of dimethyl ether was also confirmed by using a  $^{13}\text{CH}_3\text{-O-}^{13}\text{CH}_3$  tracer technique (6).

The roles played by the lightweight olefins were investigated by Dejaifve et al. (7). They carried out reactions of  $\text{C}_2$ ,  $\text{C}_3$ , and  $\text{C}_4$  olefins over ZSM-5 catalysts and observed similar aromatic product distributions from both methanol and all the olefins. Therefore, they concluded that light olefins were intermediates of methanol conversion to gasoline boiling range products.

This research was aimed at identifying some of the major reactions involved in the overall methanol reaction. A  $^{14}\text{C}$ -labeled tracer technique was developed to explore the roles played by the various species, including olefins, paraffins, and aromatics. The results are described herein.

EXPERIMENTAL

Catalyst

The original ZSM-5 catalyst was prepared at the Exxon Research and Development Laboratories. This material was in the sodium form and was calcined for 2 hours at  $600^\circ\text{C}$ . It was then soaked in a solution of ammonium nitrate (9 wt%) for another 2 hours with constant agitation. After the resulting  $\text{NH}_4\text{-ZSM-5}$  had been washed and filtered, it was impregnated with a solution of 0.0439 g nickel acetate/g of dry zeolite and then heated until dry at  $120^\circ\text{C}$ . This impregnated Ni-ZSM-5 catalyst was subsequently blended with alumina, which served as a binder, in the proportion 0.3 g alumina/g ZSM-5. All catalysts used for these reaction studies were pelletized, crushed, and screened to 30/40 mesh.

Chemicals

Methanol (99.99% purity) was obtained from Fisher Scientific Company. The radioactive compounds, along with their suppliers, are shown in Table I. Both chemical and radiochemical purities of each were checked by the radio-gas chromatograph described later. Since the methanol,

\*Present address: Department of Mechanical Engineering, University of Texas, Arlington, Texas 76019.

propylene, 1-butene, n-hexane, n-heptane, and benzene were satisfactory in both chemical and radiochemical purities, they were used as received. However, radioactive impurities were found in the original ethylene and iso-butane, which necessitated purification with a preparative GLC column (30 ft. long 5/16 in. O. D. Porapak Q at 100-150°C).

#### Reactor System

Figure 1 shows the experimental set-up. Liquid methanol was admitted into a stream of helium carrier gas by a syringe pump. To facilitate rapid vaporization of the liquid reactant, the glass sections immediately before and after the syringe injection port were packed with glass beads and heated by nichrome wire. A 250 ml mixing volume was installed before the reactor to moderate any pulsations in the reactant concentration.

TABLE I  
RADIOACTIVE CHEMICALS

| <u>Compound</u>                 | <u>Specific Activity<br/>(mC/mmole)</u> | <u>Chemical<br/>Purity</u> | <u>Manufacturer*</u> |
|---------------------------------|---|----------------------------|----------------------|
| Methanol                        | 6.7                                     | 98+%                       | PLI                  |
| Ethylene (1,2- <sup>14</sup> C) | 3.5                                     | 98%                        | CBC                  |
| Propylene (1- <sup>14</sup> C)  | 1.0                                     | 98%                        | CBC                  |
| 1-Butene (4- <sup>14</sup> C)   | 5.0                                     | ---                        | ICN                  |
| 1-Butane (2- <sup>14</sup> C)   | 1.02                                    | 98%                        | CBC                  |
| n-Hexane (1- <sup>14</sup> C)   | 1.0                                     | ---                        | ARC                  |
| n-Heptane (1- <sup>14</sup> C)  | 1.0                                     | ---                        | ARC                  |
| Benzene                         | 1.0                                     | ---                        | ARC                  |

\*PLC - Pathfinder Laboratories, Inc.

CBC - California Bionuclear Corp.

ARC - American Radiochemical Corp.

Pulses of radioactive tracers were introduced into the pre-evacuated doser through the standard taper ST1. The pressure in the doser was monitored with a mercury manometer.

The catalyst bed and a bed of vycor chips, located just upstream from and having the same mesh size as the catalyst, were sandwiched in the reactor between two glass wool plugs. The vycor chips served as a preheater and helped develop plug flow in the catalyst bed.

#### Radio-Gas Chromatograph System

A radio-gas chromatograph (RGC) system, shown schematically in Figure 1, was integrated with the reaction system to facilitate periodic sampling and on-line analysis of the products from the reactor. This system consisted of a modified Varian model 3700 gas chromatograph, three different types of detectors (TCD, FID, ICD), a separation column, and a changeable sample loop connected to a 6-port valve V3.

The temperature programmed chromatographic column was a 7-ft. by 1/8-in. O. D. stainless steel tube packed with 15% squalane on 80/100 mesh chromosorb P. Connected to the column exit was a stream splitter which divided the effluent stream into two parts in the approximate ratio 1:10. The smaller stream went to the FID (flame ionization detector) and the larger stream was directed into the ICD (ionization chamber). The argon quench gas was used to sweep the radioactive gases out of the 4.5 ml ionization chamber quickly for improved peak resolution (10).

#### Experimental Procedure

The reaction was carried out in a finite-tracer but continuous-reactant flow manner. This arrangement was used to minimize the consumption of expensive radioactive chemicals and yet to conduct the experiment in the "steady state" so that meaningful kinetic data could be extracted.

With methanol and helium flowing through the reactor, the reaction was brought to the steady state at a fixed set of conditions with the effluent bypassing the sample loop. A very small amount of tracer was introduced into the large pre-evacuated doser (50 ml). The tracer was then diluted with a portion of the reactant stream to make the pressure in the doser the same as that in the reaction system. This made the composition of material in the doser identical to that in the reactant stream except for the small amount of tracer in the doser.

Each radio-tracer experiment was begun by diverting the reactant stream to flow through the doser, and a liquid nitrogen trap collected all the hydrocarbons (except methane) in the product stream. After all the radioactive materials were trapped in the sample loop (usually about 8 minutes),

the sampling valve was returned to its original position, the liquid nitrogen dewar flask was removed, and the products were flashed into the GLC column. The amount of each product was monitored on the FID, and the radioactivity in each peak was measured by the ICD.

The specific activity  $A_i$  in each of the analyzed peaks was calculated by the following equation:

$$A_i = \frac{\frac{\text{(Radioactivity in product i, mC)}}{\text{(Total radioactivity in all hydrocarbon products, mC)}}}{\frac{\text{Moles of product i}}{\text{Total moles of hydrocarbon products}}}$$

## RESULTS

Different types of  $^{14}\text{C}$ -labeled tracers -- olefins (ethylene, propylene, l-butene, paraffins (iso-butane, n-hexane, n-heptane), and aromatics (benzene) -- were used to investigate the roles that these several species play in the overall methanol-to-hydrocarbon reaction.

In all experiments, the reaction was carried out over 100 mg of the Ni-ZSM-5 catalyst at 368°C and 1 atm total pressure. The partial pressure of methanol in the inlet stream was 0.05 atm, and the space time  $\tau$  was 218 mg cat·sec/cm<sup>3</sup>-STP. Other reaction conditions for each experiment are given in Table II.

TABLE II  
REACTION CONDITIONS FOR TRACERS

|   | <u>Ethylene</u> | <u>Propylene</u> | <u>l-Butene</u> | <u>i-Butane</u> | <u>n-Hexane</u> | <u>n-Heptane</u> | <u>Benzene</u> |
|---|-----------------|------------------|-----------------|-----------------|-----------------|------------------|----------------|
| Amount Added (μmole)                                      | 0.51            | 0.76             | 0.76            | 1.14            | 2.53            | 2.53             | 1.03           |
| Radioactivity (μC)  | 1.79            | 0.76             | 0.10            | 1.16            | 0.10            | 0.10             | 0.30           |
| Partial pressure of methanol - 0.05 atm                   |                 |                  |                 |                 |                 |                  |                |
| $\tau$ (Space time) - 218 mg cat·sec/cm <sup>3</sup> -STP |                 |                  |                 |                 |                 |                  |                |
| Reactor temperature - 368°C                               |                 |                  |                 |                 |                 |                  |                |

Table III lists the specific activity  $A_i$  for all the products (or groups of products) when the olefins, ethylene, propylene, and l-butene, were used as tracers. For propylene and l-butene, the radioactivity was almost uniformly spread among all the products, even including the compound initially labeled. However, for ethylene less than 50% of the radioactivity was incorporated into other products with the majority remaining in the ethylene. For this reason, the radioactivity in the ethylene was excluded from the normalization of the radioactivity in each of the products. In other words, the distribution of radioactivity among the various products was based only on the ethylene that reacted, and not on the total radioactive ethylene admitted.

TABLE III  
RADIOACTIVITY DISTRIBUTION AMONG HYDROCARBON PRODUCTS

| <u>Tracer</u>                   | Specific Activity in Products |                      |                      |                      |                                  |                |                |
|---------------------------------|-------------------------------|----------------------|----------------------|----------------------|----------------------------------|----------------|----------------|
|                                 | <u>C<sub>2</sub></u>          | <u>C<sub>3</sub></u> | <u>C<sub>4</sub></u> | <u>C<sub>5</sub></u> | <u>C<sub>6</sub><sup>+</sup></u> | <u>Toluene</u> | <u>Xylenes</u> |
| C <sub>2</sub> H <sub>4</sub>   | ----*                         | 1.29                 | 1.03                 | 1.43                 | 1.00                             | 2.18           | 1.62           |
| C <sub>3</sub> H <sub>6</sub>   | 0.39                          | 1.15                 | 1.00                 | 1.38                 | 0.95                             | 2.27           | 1.81           |
| 1-C <sub>4</sub> H <sub>8</sub> | 0.35                          | 0.91                 | 1.35                 | 1.52                 | 1.18                             | 2.06           | 1.64           |

\*Since more than 50% of the added radioactivity remained in the ethylene, its radioactivity was not included in calculating the specific activity of the other products. Thus, the specific activities given are based only on the ethylene that reacted, not the amount added.

The paraffins were much less reactive than the olefins. For example, in the runs with iso-butane as the tracer, essentially no radioactivity was found in any reaction products other than in the iso-butane. When n-hexane and n-heptane were used as tracers, most (ca. 80%) of the radioactivity

remained in the starting labeled tracer compound. There was a small amount of radioactivity in the C<sub>2</sub> to C<sub>4</sub> aliphatics. Significantly, no radioactivity was detected in the aromatic products.

When labeled benzene was used as a tracer, no radioactivity was found in any of the products except certain aromatics, i.e. there was no measurable radioactivity in the aliphatics. The majority (52%) of the radioactivity remained in the benzene. Considerable radioactivity was in the toluene (26%), followed by (o+m)-xylene (18%), o-xylene (3%), and trimethylbenzene (1%). Since the products contained about 6 times as much (o+p)-xylene as m-xylene, the "specific activity" for these dimethyl aromatics must be the same. Toluene had a higher specific activity (approximately by a factor of 3.4) than the xylenes, while trimethylbenzene had less (about 0.2) relative to the xylenes.

In all cases the conversion of methanol was 100%.

## DISCUSSION

### Olefin Tracers

The observation of radioactivity in all the hydrocarbons from methanol conversion when labeled ethylene, propylene, or 1-butene were used as tracers clearly indicates that these three light olefins play very important roles in the overall methanol-to-hydrocarbon reaction. Especially, the results have verified that even ethylene is involved in the reactions (as postulated by Dejaifve et al. (7) and suspected by Anderson et al. (8)), although ethylene is much less active than are the larger olefins.

In view of the lower reactivity of gaseous ethylene as evidenced by the retention of much more radioactivity in itself than occurred with the labeled propylene and 1-butene, we suggest that the desorption of ethylene is faster than its reactive chemisorption. Moreover, the appearance of radioactive propylene from the initial ethylene tracer supports the claim that the surface reaction of chemisorbed ethylene with methanol is relatively fast. Such a facile reaction of surface ethylene with methanol and/or dimethyl ether, viewed as an autocatalytic step, has been described by Chen and Reagan (9).

The data in Table III show that specific radioactivities of C<sub>2</sub>, C<sub>3</sub>, C<sub>4</sub>, and C<sub>5</sub> aliphatics are of the same order of magnitude. This strongly suggests that the formation of aliphatics proceeds mainly via a C<sub>1</sub> step addition, or more specifically through alkylation with methanol or dimethyl ether.

The detection of much less specific radioactivity in the C<sub>2</sub> aliphatics from the propylene tracer and in the C<sub>2</sub> - C<sub>3</sub> aliphatics when 1-butene was the tracer implies that these small olefins are not cracked substantially but are rather incorporated into higher molecular weight products. These larger hydrocarbons may then be cracked into lower molecular weight compounds.

Similar specific radioactivities were found in both toluene and in the xylenes, regardless of which olefinic tracer was used. This observation illustrates the common role played by these light olefins in the formation of aromatics during methanol conversion of the Ni-ZSM-5 catalyst. Furthermore, since the specific radioactivities in the aromatics are 1.5 to 2.0 times greater than those in the C<sub>3</sub> and C<sub>4</sub> products, it is reasonable to infer that a major pathway of toluene and xylene formation is the reaction between one C<sub>3</sub> and one C<sub>4</sub> or two C<sub>4</sub> species. This conclusion was also drawn by Derouane and co-workers (7).

### Paraffin Tracers

Paraffins are relatively stable final products in the methanol conversion system. The fact that <sup>14</sup>C-tagged iso-butane retains essentially all its radioactivity within itself among the hydrocarbon products shows that neither isomerization of butanes nor alkylation of iso-butane with prevailing olefins is occurring at 368°C.

In methanol conversion over ZSM-5-type zeolites, monomethyl paraffins and olefins predominate over their straight-chain counterparts (5,8). The same was observed with our Ni-ZSM-5 catalyst. In general, this is consistent with thermodynamic equilibrium (the methyl paraffins are more stable than the corresponding straight chain molecules), except for the butanes. At 368°C thermodynamics predicts that n-butane is more stable than iso-butane (57% vs. 43%). Since these two paraffins are not interconverted under reaction conditions, they are probably formed mainly by hydrogen transfer to the respective n-butenes or iso-butene.

### Aromatic Tracers

Benzene is a very thermodynamically stable compound. However, its low concentration among the reaction products causes one to question its function in the overall methanol conversion reactions. The radioactivity distribution among the aromatic products when benzene was used as a tracer reveals that alkylation of benzene to form toluene, the xylenes, and trimethylbenzene is a major route for their formation.

Benzene may be alkylated with methanol or with dimethyl ether to produce toluene, which in turn reacts with more methanol or ether molecules to form first the xylenes and then the trimethylbenzenes. This is consistent with the specific activity ratio following the order toluene > xylenes >

FIGURE 1. REACTION, RADIO-GAS CHROMATOGRAPHIC SYSTEMS

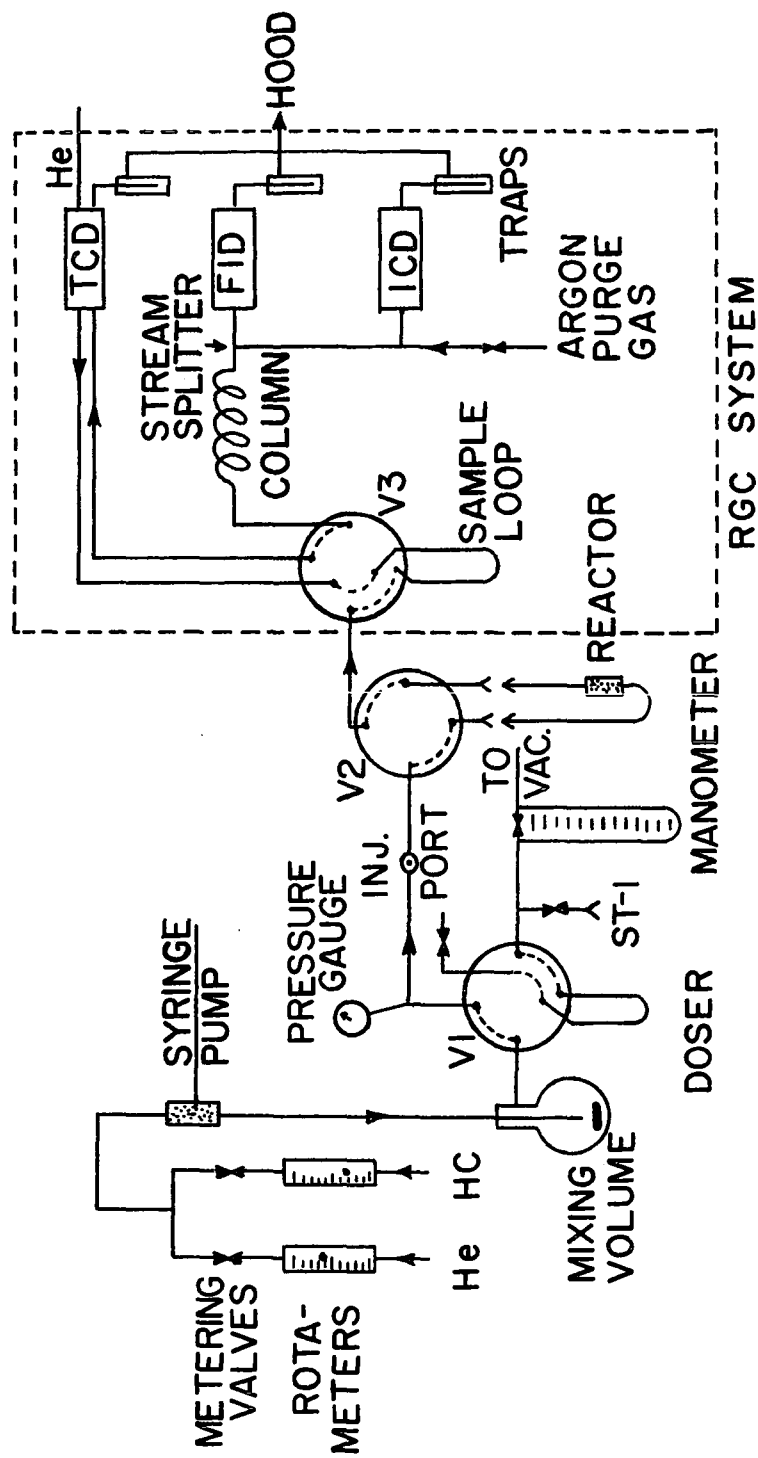
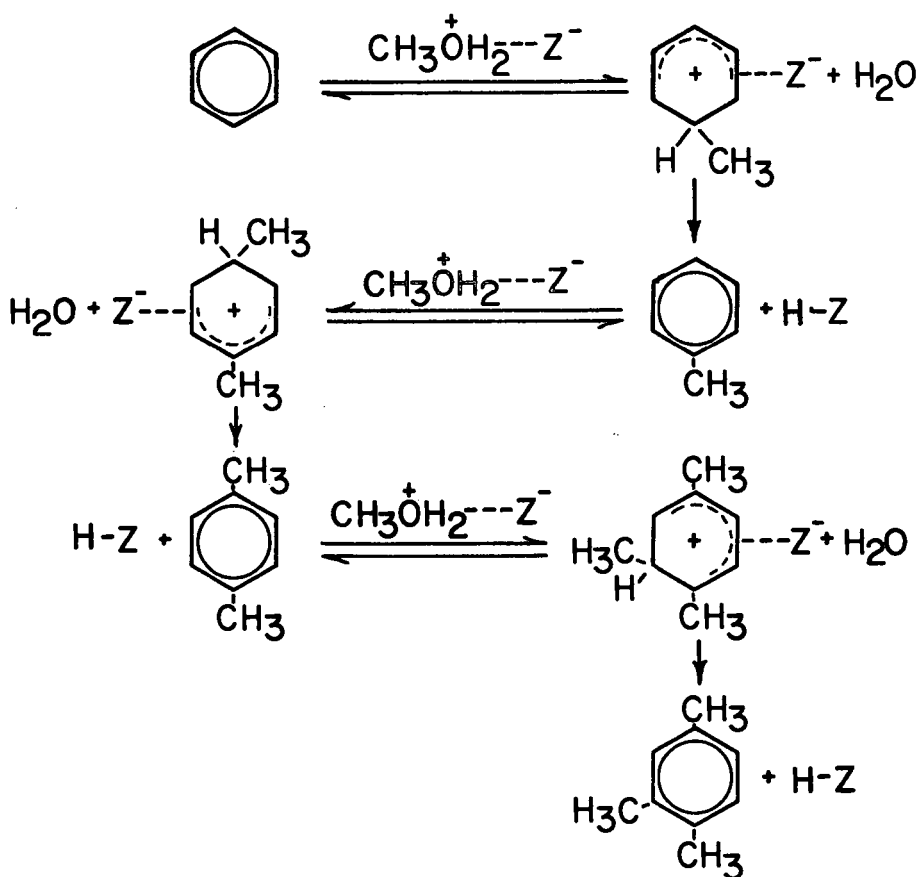




FIGURE 2. ALKYLATION OF AROMATICS



trimethylbenzenes when benzene was used as the tracer.

It is worth noting that the role played by benzene in the formation of alkylated benzenes is quite similar to that of ethylene in the production of higher aliphatics. As observed for the ethylene tracer,  $^{14}\text{C}$ -labeled benzene retains most of its radioactivity intact, again indicating that reactive chemisorption is relatively slow. However, the formation of radioactive toluene suggests that the surface reaction of the chemisorbed benzene with methanol or dimethyl ether occurs readily. These results also seem to point out that the nature of this reaction is autocatalytic, as proposed by Chen and Reagan (9) for ethylene reaction with methanol or dimethyl ether to account for the low concentration of ethylene in the product.

In light of the acidic properties of the ZSM-5 catalyst, a carbenium ion mechanism can be proposed for the formation of alkylated benzenes from benzene as indicated in Figure 2.

### CONCLUSIONS

Through the use of  $^{14}\text{C}$ -labeled tracer compounds, some important secondary reactions have been identified in the overall conversion of methanol to hydrocarbons over a Ni-ZSM-5 catalyst. The major findings are:

1. The alkylation of light olefins with methanol or dimethyl ether is a major pathway for the formation of larger olefins with one more carbon atom.
2. Paraffins are mainly produced by hydrogen transfer reactions to their corresponding olefins, i.e., ones having the same carbon skeleton.
3. Except for minor cracking reactions, paraffins with up to at least 7 C atoms are final stable products; isomerization among paraffin isomers does not take place at 368°C.
4. Light olefins, e.g., ethylene, propylene, and butenes, are reactive intermediates for aromatics formation.
5. Aromatic compounds can also be produced by methanol- or di-methyl ether-alkylation of benzene and subsequent alkylated benzenes.

### ACKNOWLEDGMENTS

The authors are grateful to Dr. H. E. Robson at the Exxon Research and Development Labs for providing a sample of the ZSM-5 zeolite and to the Robert A. Welch Foundation and Haldor Topsøe A/S (Denmark) for financial support.

### LITERATURE CITED

- (1) Meisel, S. L., McCullough, J. P., Lechthaler, C. H., and Weisz, P. B., *Chem. Technol.*, **6**, 86 (1976).
- (2) Danner, C. A., ed, "Methanol Technology and Economics", *Chem. Eng. Progr. Symp. Ser.* No. **98**, 66 (1970).
- (3) Stockinger, J. H., *J. Chromatographic Sci.*, **15**, 198 (1977).
- (4) Bloch, M. G., Callen, R. B., and Stockinger, J. H., *J. Chromatography Sci.*, **15**, 504 (1977).
- (5) Chang, C. D., and Silvestri, A. J., *J. Catal.*, **47**, 249 (1977).
- (6) Perot, G., Cormerais, F., and Guisnet, M., *J. Chem. Res. (S)*, **58** (1982).
- (7) Dejaifve, P., Vedrine, J. C., Bolis, V., and Derouane, E. G., *J. Catal.*, **63**, 331 (1980).
- (8) Anderson, J. R., Foger, K., Mole, T., Rajadhyaksha, R. A., and Sanders, J. V., *J. Catal.*, **58**, 114 (1979).
- (9) Chen, N. Y., and Reagan, W. J., *J. Catal.*, **59**, 123 (1979).
- (10) Hwu, F. S., "Conversion of Methanol and Light Olefins to Gasoline over a Shape Selective Catalyst, ZSM-5", Ph. D. Dissertation, Rice University, 1981.
- (11) Stull, D. R., Westrum, E. F., and Sinke, G. C., "The Chemical Thermodynamics of Organic Compounds", John Wiley and Sons, 1969.

NATURAL GAS BASED TECHNOLOGIES AS REVEALED IN  
POSSIBLE NEW ZEALAND ENERGY PROGRAMS

By

P. Jawetz  
Independent Consultant on Policy, 415 East 64th Street, New York, New York 10021

INTRODUCTION

New Zealand is an exporter of commodities and thus completely dependent on world market conditions. Its large resources of hydro-electricity, forests, natural gas and fish give it the possibility of industrializing. The off-shore debt on March 31, 1982, stood at US \$ 3,263 million or about US \$ 1,052 per head of population - just about as high as the per capita debt of Argentina - a country mentioned when the world banking system started to worry about possible defaults. In the words of Foreign Minister Warren Cooper before the U.N. General Assembly on October 6, 1982 - "As a small trading nation, New Zealand is acutely sensitive to fluctuations in the health of our major trading partners. New Zealand is classed as a developed country, but we share many of the problems of developing countries".

New Zealand has no oil resources and when the country was hit by the Energy Crisis it decided to develop the gas fields at Kapuni and at Maui in the Taranaki province (in the western part of the North Island) in order to collect associated liquid condensates. The gas was first used to fire electrical plants and later readied for reticulation via pipelines in the Northern Island. Eventually, when the condensate became so much more valuable than the gas - despite its quantity being much smaller - it actually led to flaring the gas to waste in order to obtain the condensate. A "take-or-pay" system was negotiated under which the government is contracted to take a given amount of gas per year from the producing partnership. Assuming that future oil prices will rise only a few percent per year in real terms and performing a standard Discount Cash Flow analysis with a 10% discount rate, the conclusion reached was that there was a higher financial value to be obtained from using the condensate - leading to a zero value for the gas and to a financial justification for flaring it. On the other hand, the gas could be used 1) for reticulation, 2) for promoting a CNG industry (compressed natural gas) or 3) for use in petrochemical industries to produce chemicals or further liquid fuels. Following this logic, and attempting to produce the least change in the transportation system, the New Zealand Ministry of Energy went along with a plan to produce synthetic gasoline from what was then seemingly unwanted gas.

The present paper argues that it would be rather to the long range advantage of New Zealand for the Government to stop at the methanol stage and use methanol as a new liquid fuel in addition to CNG motor fuel rather than go all the way to produce the synthetic gasoline from natural gas.

A MISUSED INNOVATION

Mobil Research and Development Corporation laboratories in Paulsboro, New Jersey, developed spongy, shape-selective catalysts to promote a reaction that transforms alcohol into hydrocarbons by excising water molecules. The catalysts are different pore sized aluminum silicates or clays called zeolites (the Greek word for boiling stones - this because the ancient Greeks observed that certain stones when thrown into fire appeared to boil, thus indicating that the interior structure was hollow enough to contain water and that the pore openings were large enough to allow the water to escape). ZSM-5 is a synthetic zeolite whose uniform pore size and shape is such that when treated in a Mobil-developed process will make possible the chemical reactions involved in the elimination of water molecules from the methanol feedstock. (Z stands for Zeolite; S stands for Socony, and M stands for Mobil as "Socony" or Standard Oil Company of New York was an old name for today's Mobil Oil; 5 is a key for the class of the catalyst.)

When producing the hydrocarbons we define as synthetic gasoline, the catalytic process consumes 10-15% of the energy content in the methanol feedstock (1) but what should be remembered as equally important is that half of the volume of the liquid feedstock is lost when the water molecules are eliminated. Then, depending on how the fuels are used, if the energy content as measured in calorimetric units does not express accurately the work yield of the fuel vehicle engine, or if different fuels show different efficiencies when used in the same engine, the fact that we have lost half

the volume may lead to serious differences in work yield. In other words, reducing the liquid fuel volume of the methanol to approximately one half in order to form the twice higher energy-content synthetic gasoline wastes advantages the alcohol has had per energy unit. This is where the most serious inefficiencies of the Mobil MTG (methanol-to-gasoline) process are incurred - more so than in the energy loss of the process itself (2).

The methanol for the Mobil process can be obtained by passing synthetic gas produced from coal over a copper catalyst or starting with natural gas. Mobil Oil has no proprietary technology for the production of methanol and in New Zealand it will be using an I. C. I. process and 40% of the natural gas feedstock energy content will be lost at this stage. The Mobil ZSM-5 catalyst's competing technology is a  $ZnCl_2$  process that was also looked into by the New Zealanders when making their decision (3). To be sure, one does not expect difficulties in upscaling the Mobil MTG process from the four-barrels-a-day pilot unit in Paulsboro, New Jersey to the 13,000-14,000 b.p.d. plant at Motunui, New Zealand, and when completed the plant will most probably deliver as planned but then one could reasonably expect that besides not allowing for a maximum gain to New Zealand from the available natural gas resource, the influx of synthetic gasoline will create an amazing stress on the one and only petroleum refinery in New Zealand that will have to continue to operate on imported crude in order to provide the needed diesel fuel, leading to a future when New Zealand will probably have to import expensive petroleum crude and export cheap gasoline. New Zealand will be left in the process totally dependent on petroleum or "Petroleum-alike" fuels while losing the opportunity it had to move away from petroleum systems by using the natural gas as an entry to a gas and alcohol future to make the two New Zealand islands energy independent indeed. This goal cannot be achieved by providing fuels to existing systems, but rather by adapting its fuel uses to fuels available locally i.e. change its motor vehicle fleets to CNG and methanol cars and opening the future, by establishing now the appropriate end use to biogas, synthetic natural gas from coal, methanol from coal or peat and ethanol from biomass.

New Zealand in answer to its energy needs was destined to experiment with new energy development but it seemingly chose to stay with the old instead of going the way of true innovation. New Zealand, thanks to its geography can go it alone. By not having to worry about cross-border traffic it can isolate itself by going CNG and methanol before the rest of us do so (3).

#### THE PETROLEUM REFINERY

Petroleum refinery design is dictated by the needs of a relatively small number of products, e.g., gasoline, jet fuel, diesel fuel, fuel oil. It is generally recognized that the most important part of any refinery is its gasoline manufacturing facility. As the demand for gasoline increased, more and more of the lighter kerosene components were included in gasoline but the maximum suitable portion depended on the kind of crude oil and rarely exceeded 20%. As such, methods more and more complicated were developed to obtain further products that could be blended into the original gasoline fraction. The customary processing in a refinery is thus no more a fractionation process producing relatively pure hydrocarbons, but rather a very complicated system with flows into a general pool of products - the gasoline produced being a mixture of ingredients with different economic costs. Gasoline blending is thus the combining of components to make up the liquid defined by a given set of properties that enable it to be a fuel in a motor vehicle internal-combustion engine. One of the most important properties that must be satisfied is the required octane value. To produce higher octane ingredients that when blended with the first run low octane product, higher temperatures in cracking processes have to be employed. This more severe and energy intensive process, besides being more costly, as it requires higher energy inputs, also creates less valuable by-products - the upshot being that the economics of production at the refinery change. Furthermore, with the requirement to eliminate the octane boosting tetra-ethyl lead from the gasoline formulation because of environmental reasons some refineries, in most cases the smaller refineries, do not even possess some of the needed equipment for these processes.

Both methanol and ethanol when added at about 3% to low octane gasoline will enhance the gasoline's octane number by one point (that is the average over motor octane and research octane). With 10% of the alcohol the average octane value is improved by about 3 points and with 20% of the alcohol 5 points improvement of the average octane value is achieved. Detailed calculation for savings in petroleum crude, when using alcohol octane boosting additives to gasoline, were presented before the First European Communities Conference on Energy from Biomass (4-6). To recapitulate here - it was found that each Btu of ethanol used this way replaces 3.55 Btu of gasoline or one liter of ethanol replaces at least 2.5 liters of gasoline. Following a similar path one can calculate that when using 5% methanol as an additive to gasoline each Btu of methanol used this way replaces 4 Btu of gasoline or one liter of methanol replaces at least 2 liters of gasoline.

In order to calculate the effective energy balance (in the use as well as in the production of the alcohol) the above values have to be multiplied with the energy balance in the manufacture of the alcohol. For the case of biomass ethanol, using a factor calculated by Professor Melvin Calvin - 1.76 each Btu used as energy input in fertilizers, agricultural machinery or distillation equipment

end up displacing 6.6 Btu of petroleum origin when the ethanol is used as an octane boosting additive to gasoline. When the ethanol is used instead as a fuel in an ethanol driven engine (no gasoline involved) in the effective use of the ethanol the potential gain at the refinery is lost. Also, the Btu content of the engine fuel that in the mixture is decreased only by about 3% will be decreased now by rather 30%, while the octane value of the fuel has been increased in the ethanol-alone case to a value higher than required by an unchanged engine. It is expected thus to decrease from the above calculated advantages for the case of the mixed fuels to net gains of only about 20% above the Btu content of the fuel; each liter of ethanol used replaces now only about 0.8 liters of gasoline and each liter of methanol used replaces only 0.6 liters of gasoline - this leading to higher savings in terms of petroleum resources, but also for economics much more difficult. This alternative becomes a possibility when political decision is taken to avoid dependence on petroleum crude. When mentioning alcohol-gasoline mixtures, despite the favorable results of the Brazilian program and many other programs, i.e., in the U.S., West Germany, South Africa, when a New Zealand journalist visited the Mobil Oil Paulsboro facility he was cautioned against such blends "as liable to cause too many technical and distribution problems". Considering that a second plant in New Zealand was built to produce methanol for export - this in a world market that is already saturated with methanol production capacity - Mobil that is already expected to supply one third of New Zealand's need for gasoline in 1985 suggests to use the additional output of methanol in its Motunui plant (7) thus resulting in a production of synthetic gasoline equal to over 50% of what could reasonably be expected to be the New Zealand need for gasoline by a conventional motor-vehicle fleet. Interestingly Shell and B.P., the other corporate partners of the New Zealand refining corporation, did not agree to participate in the Mobil Oil project.

### POLICY ISSUES

The Marsden Point refinery used, in 1981, 2,300,000 tonnes of crude oil and 440,000 tonnes of gas condensate and produced 1,236,000 tonnes gasoline and 685,000 tonnes of diesel. After the expenditure of over 1 billion for expansion and for building a hydrocracker, the refinery will use 2,884,000 tonnes of crude and 816,000 tonnes of condensate in order to produce 1,050,000 tonnes of gasoline, 430,000 tonnes of aviation fuel, and 1,125,000 tonnes of diesel. This change at the refinery will also double the refinery fuel loss from 165,000 tonnes/year to 330,000 tonnes/year.

On March 31, 1980, New Zealand Motor Vehicle licenses amounted to 1,283,661 passenger cars, 3,134 taxicabs, 3,397 buses and coaches, 176,692 trucks under 2 tonnes, 76,872 trucks over 2 tonnes. When including all other vehicles such as motorcycles, and motor homes, a grand total of 2,157,516 motor vehicles were licensed. New registrations for the year 1981 amounted to a total of 114,842 cars, the majority of which were assembled in New Zealand from parts imported mainly from Japan (73%). Other important countries of origin were the U.K. with 13.6% and Australia with 11.1%. All other countries of origin, including the U.S., amounted to only 2.3% (nevertheless, when analyzing the manufacturing companies it is clear that Ford and General Motors are well represented, mainly through their Australian and U.K. affiliates, amounting to about 30%).

Two of the motor vehicle assembly corporations were responsible for over 21,000 vehicles each while four other corporations were in the 10,000-18,000 range. Thus it is reasonable to assume that a corporation that may not even produce a CNG or methanol car for its own home market may find it advantageous to send such kits to the New Zealand assembly plant. In effect it would just take the cooperation of two such corporations in order to embark on a slow process of changing the motor vehicle fuels system gradually. The funds for such changes could then easily be found from the \$1.5 billion that could be saved by eliminating some changes at the refinery and by eliminating the methanol-to-gasoline stage at the Motunui plant (8).

It is preferable to go to dedicated vehicles - vehicles that were originally built for non-petroleum fuels use - rather than convert vehicles that were originally built to use gasoline fuels. Such conversions, for the CNG case, leave the vehicle with an undesirable seriously decreased trunk space.

### CONCLUSIONS

The Mobil MTG process, to be employed in New Zealand, is being scaled up from the Mobil Oil Paulsboro operation to what could be a commercial size plant. Nevertheless, the economics in the New Zealand case are such that this operation can only prove the technical aspects of the plant but not the economics - the New Zealand economics being figured out on the basis of a practical give-away of the natural gas.

Furthermore, New Zealand being a set of two islands with very little traffic from the outside, could have switched to a transportation system based on CNG and methanol with an intermediary stage that uses the existing Whangarei refinery, without changes, and methanol for an octane enhancer. Such a policy besides having environmental benefits is economically sounder in the long range as 1) it allows for a much larger energy efficiency for the natural gas resource and 2) it prepares

the economy to an eventual switch to other sources of fuel gas and alcohols. New Zealand has large potential for the production of biomass and has as well coal and peat deposits that will eventually form the basis for an industrialization of the South Island. The elimination of the dependence on a petroleum system and the development of an indigenous industry are, reasonably, the real long range interests of New Zealand.

What was said here is in no way an expression of doubt in the technical feasibility of the Mobil MTG process. It is highly possible that for other countries, and in other objective circumstances, this process can be applied in accordance with national interests. Such circumstances could be envisioned for example for the case a country cannot isolate itself when its roads are being used or by cars originating in areas that would not participate in a policy of switching from petroleum fuels.

#### LITERATURE CITED

- (1) "Energy Research Reports", ER Publications Inc., P.O. Box 157, Watertown, MA 02172, U.S.A. (a) December 11, 1978; (b) October 29, 1979.
- (2) Jawetz, P., "Relative Economics of Alcohol Octane Boosting Additives to Gasoline, Alcohol Fueled Cars, and Synthetic Gasoline from Alcohol". Energy from Biomass, Second European Communities Conference, A. Strub, P. Chartier, G. Schlessler, editors, Applied Science Publishers, London, 1983.
- (3) Jawetz, P., "Natural Gas Based Energy Systems - How New Zealand Decided to Act Not In Its Own Best Interest", Monograph No. 83-Pet-28 (1983). The American Society of Mechanical Engineers, 345 E. 47th St., New York, N. Y. 10017.
- (4) Jawetz, P., "The Economics of Improving Octane Values of Gasoline with Alcohol Additives", Palz, W., Chartier, P., and Hall, D.O., editors, "Energy from Biomass", Applied Science Publications, London 1981.
- (5) Jawetz, P., "Alcohol Additives to Gasoline - An Economic Way for Extending Supplies of Fuels and for Increasing Octane Rations", PREPRINTS, Div. of Petrol. Chem., ACS, 24, 798 (1979).
- (6) Jawetz, P., PREPRINTS, Div. of Petrol. Chem., ACS, 25 (1), 99 (1980).
- (7) New Zealand Press Association correspondent, "The Press", Christchurch, March 18, 1983.
- (8) Peace, D. J., Technical Officer for the Auckland Gas Association, in submission for "The Environmental Impact Audit Synthetic Petrol Plant", Volume II, April 20, 1981.

GENERAL PAPERS - POSTER SESSION  
PRESENTED BEFORE THE DIVISION OF PETROLEUM CHEMISTRY, INC.  
AMERICAN CHEMICAL SOCIETY  
WASHINGTON, D. C. MEETING, AUGUST 28 - SEPTEMBER 2, 1983

APPLICATION OF THERMAL ANALYTICAL TECHNIQUES TO  
ENHANCED OIL RECOVERY

By

K. N. Jha  
Research and Development, Saskatchewan Oil and Gas Corporation  
515 Henderson Drive, Regina, Saskatchewan, Canada S4N 5X1

INTRODUCTION

The world, especially in Canada and Venezuela, has extensive resource of oil sands and heavy oils. These resources are characterized by high viscosity, low API gravity, i.e., high density, and large sulfur contents (Table I). Recovery of Lloydminster heavy oils in Canada under primary and secondary processes are less than 9% of initial oil-in-place, whereas that of bitumen from oil sands is nil.

TABLE I  
PROPERTIES OF HEAVY OILS AND OIL SANDS<sup>a-c</sup>

| Source                 | Gravity<br>°API | Viscosity<br>cp(°C)                   | Sulfur<br>Wt% | Asphaltene<br>Wt% | Conradson Carbon<br>Residue Wt% |
|------------------------|-----------------|---------------------------------------|---------------|-------------------|---------------------------------|
| <u>Canada</u>          |                 |                                       |               |                   |                                 |
| Lloydminster           | 10-18           | 2000-20,000 (20)                      | 2.6-3.5       | 8 - 12            | 8 - 12                          |
| S. E. Alberta          | 12-18           | 3000 (T <sub>R</sub> ) <sup>d</sup>   | 3.5           | 12                | 12.2                            |
| Athabasca              | 8-12            | 1-5x10 <sup>6</sup> (T <sub>R</sub> ) | 4.6           | 17                | 13.5                            |
| Cold Lake              | 10-12           | 1 x 10 <sup>5</sup> (T <sub>R</sub> ) | 4.7           | 15                | 12.6                            |
| Peace River            | 8-9             | 1 x 10 <sup>5</sup> (T <sub>R</sub> ) | 5.6           | 20                |                                 |
| Wabasca A              | 8-13            | 8 x 10 <sup>5</sup> (T <sub>R</sub> ) | 5.5           | 19                |                                 |
| <u>Venezuela</u>       |                 |                                       |               |                   |                                 |
| Boscan                 | 10-12           | 26 x 10 <sup>3</sup> (38)             | 5.2           | 9 - 17            | 15.0                            |
| Tia Juana              | 12              | 37 x 10 <sup>2</sup> (38)             | 2.7           | 6                 | 11.2                            |
| Morichal               | 12              | 32 x 10 <sup>2</sup> (38)             | 2.1           | 11                | 14.0                            |
| Jobo                   | 8.4             | 62 x 10 <sup>3</sup> (38)             | 3.7-4.1       | 9                 | 14.1                            |
| <u>U.S.A.</u>          |                 |                                       |               |                   |                                 |
| Asphalt Ridge,<br>Utah | 8-13            | 69 x 10 <sup>6</sup> (25)             | 0.2-0.8       | 12                | 9.1                             |

- a. Work done in our laboratory on Lloydminster, Saskatchewan crudes.
- b. "The Future of Heavy Crude Oils and Tar Sands", Ed. R. F. Meyer and C. T. Steele, McGraw-Hill, Inc., New York (1981), pp. 168, 187, 237.
- c. "The Oil Sands of Canada - Venezuela 1977", Ed. D. A. Redford and A. G. Winestock, CIM Special Volume 17, The Canadian Institute of Mining and Metallurgy, pp. 146, 178, 284.
- d. Reservoir temperature.

For the development and utilization of these resources, enhanced oil recovery (EOR) processes have to be employed (1-3). EOR refers to all techniques used to increase the amount of oil produced after primary recovery. EOR methods encompass pressure maintenance, water-flooding, gas injection, thermal, miscible displacement and chemical processes. The thermal process is most suitable for recovery of heavy oils and oil sand bitumens. In this process oil displacement results from:

- i) viscosity reduction primarily due to heat and secondly due to carbon dioxide dissolution in oil,
- ii) thermal expansion of the oil resulting in increased relative permeability,
- iii) distillation and thermal cracking of oil,
- iv) a solution gas drive from produced gas which facilitates the flow of fluids within the reservoir toward the production wells, and

v) increased pressure gradient imposed by the injected air.

Heat is transferred to the reservoir either by injection of steam/hot water or by *in-situ* combustion. The latter process, of interest to us at present, consists of injecting air/oxygen/water into an oil reservoir to establish a flow path for the movement of fluids, igniting the crude oil and propagating the combustion front by continued air/oxygen injection (Figure 1).

The important factors required to establish the feasibility of initiating an *in-situ* combustion field test are the fuel (coke) content of the oil being burned, the volume of air/oxygen required to sustain combustion and the efficiency of oxygen utilization. These parameters are usually determined by laboratory experiments employing a combustion tube. A sample of the data obtained is presented in Table II. Most of these parameters could be estimated from TGA/DSC data.

TABLE II  
TYPE OF DATA GENERATED FROM COMBUSTION TUBE EXPERIMENTS<sup>a, b</sup>

|   |  |
|---|--|
| Fuel Concentration, Kg/m <sup>3</sup>                     | 16-48  |
| Air-Fuel Ratio, m <sup>3</sup> /Kg                        | 10   |
| Oxygen Utilization, %                                     | 90+  |
| Combustion Front Velocity, m/h <sup>c</sup>               | 0.1  |
| Steam Front Velocity, m/h                                 | 0.1  |
| Vaporization Front Velocity, m/h                          | 0.1  |
| Fuel Required to Sustain<br>Combustion, Kg/m <sup>3</sup> | 20   |
| Maximum Peak Temperature, °C                              | 450-700  |
| Hydrogen to Carbon Ratio of Fuel                          | 0.6-2.0  |
| Oil Recovery, %   | 90   |
| Produced Gas Analysis, Vol. %                             | CO <sub>2</sub> , CO, O <sub>2</sub> , N <sub>2</sub> ,<br>C <sub>1</sub> -C <sub>4</sub> , SO <sub>2</sub> , H <sub>2</sub> |

- a. D. W. Bennion et al., "Proceeding II International Conference on Heavy Crude and Tar Sands", Caracas, February 7-17, 1982.
- b. "The Future of Heavy Crude and Tar Sands", Ed. R. F. Meyer and C. T. Steele, McGraw-Hill, Inc., New York, pp. 413-25, 1981.
- c. Meters per hour.

Although combustion tube experiments generate data useful for the design and operation of the field-pilot, it is imperative that the numerical simulation of the *in-situ* combustion process be carried out in making meaningful predictions of the parameters for planning, construction and optimum operation of field pilots.

Numerical *in-situ* combustion simulation usually requires reservoir description, reservoir fluid properties, thermodynamic, chemical kinetics and well data (4). Experimental data for thermodynamic properties and chemical kinetics required in the area of low temperature oxidation, cracking, combustion and coking reactions are lacking in order to make meaningful predictions of an *in-situ* combustion project (5-7). To this end, we have employed thermal analytical techniques, thermal gravimetric analysis (TGA) and differential scanning calorimeter (DSC) to generate the required data such as energy of activation, pre-exponential factor, rate constant, and heat of reaction for chemical reactions. Thermal techniques can also provide data on minimum ignition temperature of crude oil to sustain combustion, fuel content of the core, fluid-rock interaction, decomposition of the mineral matter present in the core and residue left after heating.

This paper presents TGA and DSC results obtained for two Lloydminster heavy oil core samples under flow of helium, nitrogen and air.

## EXPERIMENTAL

Tests were performed using a DuPont 951 Thermogravimetric Analyzer and a 910 Differential Scanning Calorimeter attached to the 1090 Data Analysis System. A sample size of 25-60 mg and a temperature range of 40° to 900°C for TGA, and 1-3 mg and 40° to 580°C for DSC studies were used. Samples were heated at a rate of 5° or 10°C/min. in air, nitrogen or ultra pure helium flowing at 60 cm<sup>3</sup>/min. for TGA and 20 cm<sup>3</sup>/min. for DSC experiments. Thermograms recorded the percentage weight loss as a function of temperature and its derivative for TGA and heat flow in mW versus temperature for DSC runs. The DSC cell constant was determined to be 1.081 using an indium standard. DSC experiments were performed using hermetic pans.

Samples A and B used for this study had an initial oil saturation of 63 and 85%, a porosity of 29 and 33%, and a permeability of 1.9 and 2.3 Darcies, respectively. Gravity and viscosity of crude oils were 16°API and 236 cp at 38°C for sample A and 11°API and 46,000 cp at 38°C for sample B.



## RESULTS

Thermograms of weight loss versus temperature for Lloydminster core A are shown in Figure 2. The total weight losses were 6.92% in He, 7.57% in N<sub>2</sub>, and 7.79% in air. The higher weight loss under air than under He indicates that the coke produced in the process is oxidized by oxygen, resulting in additional weight loss. The results under N<sub>2</sub> atmosphere imply that N<sub>2</sub> contains oxygen as an impurity.

Figures 3, 4 and 5 show weight loss curves and their derivatives (DTG) against rising temperature for sample A in He, N<sub>2</sub> and air. The derivative curves suggest that there are at least four groups of reactions which can be convoluted in four temperature zones. Kinetics for loss in weight in each temperature zone is described later.

TGA and DTG thermograms are presented in Figures 6 and 7 for core sample B. The total weight loss was 14.8% in He and 15.6% in air in the temperature range 40° to 880°C. The characteristics of the TGA and DTG curves are similar to those obtained for sample A. It should be noted, however, that the oil content of sample B is twice as much as that of A.

For further understanding of reaction kinetics, differential scanning calorimeter experiments were conducted for samples A and B in He and air at a heating rate of 10°C/min. (Figures 8-11). The thermograms produced with He have three peaks, the last one representing the cracking reactions. The large exothermic peak produced under air is attributed to combustion reactions. The peak temperatures for these tests range between 453° and 484°C. Arrhenius and thermal parameters obtained by using the Borchardt and Daniels kinetics data analysis program supplied by DuPont are discussed later (8-10).

## DISCUSSION

Derivatives of TGA thermograms for core samples A and B have demonstrated that there are four temperature regimes for weight loss. The temperature ranges and percentage weight loss for the total material and organic components within each range are listed in Table III. The percentage weight loss in the first region (50°-380°C) was approximately the same under He and air for sample A or B. This weight representing 40 to 55% of the total loss is attributed largely to volatilization and to some extent to low temperature oxidation. The weight loss in the second temperature regime (340°-540°C) was 19% in He and 43% in air for sample A and 27% in He and 54% in air for sample B. This indicates that volatilization and thermolysis of heavy oil present in the core is taking place under He whereas more efficient reactions, such as oxidation and subsequent decomposition and volatilization, are involved in the presence of air. The third regime (450°-630°C) is characterized by cracking, volatilization and combustion reactions whereas the last fraction of the weight loss between 550° and 900°C is assigned to coking, decomposition of mineral matter and oxidation. Oxidation and combustion reactions take place when sample is in contact with oxygen.

Weight loss kinetics for pyrolysis and combustion processes is extremely complex for such systems because of the numerous components present and their simultaneous and competing reactions. Kinetic treatment of the data is described below.

Solid phase thermal decomposition is described by the rate expression (11-12):

$$\frac{d\alpha}{dt} = k(1-\alpha)^n \quad (1)$$

$$\alpha = (\omega_0 - \omega_t) / (\omega_0 - \omega_\infty) \quad (2)$$

$$k = Ae^{-E/RT} \quad (3)$$

where  $k$  is rate constant;  $n$ , order of reaction;  $\omega_0$  initial sample weight;  $\omega_t$  sample weight at time  $t$ ;  $\omega_\infty$  final weight;  $A$ , pre-exponential factor;  $E$ , activation energy;  $R$ , gas constant; and  $T$ , absolute temperature in K. For a linear heating rate,  $\beta$ , °C/min:

$$\beta = dT/dt \quad (4)$$

By combining Equations 1, 3 and 4, rearranging, integrating and taking the natural logarithm and assuming  $n = 1$ , we obtain:

$$\ln \left[ \frac{-\ln(1-\alpha)}{T^2} \right] = \ln \frac{AR}{\beta E} \left[ 1 - \frac{2RT}{E} \right] - \left( \frac{E}{R} \right) \frac{1}{T} \quad (5)$$

A plot of  $-\ln \left[ \frac{-\ln(1-\alpha)}{T^2} \right]$  versus  $1/T$  should result in a straight line of slope  $E/R$ . The value of  $E$  obtained graphically is substituted in Equation 5 to calculate the pre-exponential factor,  $A$ . Typical plots to obtain apparent activation energies are shown in Figures 12-15 for reactions

occurring in the four temperature zones for sample A under He flow.

Equation 3 is used to estimate rate constant at any temperature. Values of E, A, and rate constant at mean temperature for each reaction zone are presented in Table III.

TABLE III  
THERMAL DECOMPOSITION PARAMETERS FOR LLOYDMINSTER  
HEAVY OIL CORES

| Sample<br>(Purge<br>Gas) | Reaction<br>Zone    | Temp.<br>Range, °C | Wt. Loss % |      | E<br>kcal/mol | A<br>s <sup>-1</sup>   | 10 <sup>3</sup> k <sub>mean</sub><br>s <sup>-1</sup> | Fuel<br>(Coke)<br>Kg/m <sup>3</sup> |
|--------------------------|---------------------|--------------------|------------|------|---------------|------------------------|--|-------------------------------------|
| A. (He)                  | 1                   | 50-340             | 3.01       | 2.94 | 4.6           | 1.3 x 10 <sup>-1</sup> | 0.92   | )39.2<br>29.3)                      |
|                          | 2                   | 340-475            | 1.25       | 1.08 | 20.2          | 3.3 x 10 <sup>3</sup>  | 1.1  |                                     |
|                          | 3                   | 475-550            | 0.69       | 0.45 | 49.9          | 2.5 x 10 <sup>11</sup> | 3.3  |                                     |
|                          | 4                   | 550-800            | 1.62       | 1.33 | 18.3          | 1.5 x 10 <sup>1</sup>  | 0.91   |                                     |
|                          | (N <sub>2</sub> ) 1 | 50-360             | 3.09       | 3.01 | 4.9           | 1.3 x 10 <sup>-1</sup> | 0.75   |                                     |
|                          | 2                   | 360-450            | 0.89       | 0.79 | 29.3          | 5.0 x 10 <sup>6</sup>  | 1.8  |                                     |
|                          | 3                   | 450-550            | 1.18       | 0.88 | 36.3          | 3.3 x 10 <sup>7</sup>  | 1.8  |                                     |
|                          | 4                   | 550-900            | 2.32       | 1.98 | 14.8          | 1.8                    | 1.0  |                                     |
|                          | (Air) 1             | 50-340             | 3.17       | 3.10 | 4.9           | 1.2 x 10 <sup>-1</sup> | 0.62   |                                     |
|                          | 2                   | 340-480            | 3.26       | 3.00 | 23.5          | 6.7 x 10 <sup>4</sup>  | 2.0  |                                     |
|                          | 3                   | 480-550            | 0.62       | 0.45 | 45.5          | 1.7 x 10 <sup>10</sup> | 4.1  |                                     |
|                          | 4                   | 550-800            | 0.48       | 0.08 | 14.2          | 2.5                    | 1.3  |                                     |
| B. (He)                  | 1                   | 50-380             | 8.10       | 8.01 | 6.2           | 6.4 x 10 <sup>-1</sup> | 1.1  | )49.1<br>28.8)                      |
|                          | 2                   | 380-500            | 3.90       | 3.66 | 35.3          | 3.8 x 10 <sup>8</sup>  | 5.8  |                                     |
|                          | 3                   | 500-600            | 1.15       | 0.92 | 46.4          | 1.0 x 10 <sup>10</sup> | 4.8  |                                     |
|                          | 4                   | 600-800            | 1.52       | 1.31 | 21.5          | 1.2 x 10 <sup>2</sup>  | 1.8  |                                     |
|                          | (Air) 1             | 50-380             | 6.85       | 6.74 | 6.6           | 8.8 x 10 <sup>-1</sup> | 1.0  |                                     |
|                          | 2,3                 | 380-540            | 8.32       | 7.95 | 39.4          | 1.8 x 10 <sup>9</sup>  | 3.2  |                                     |
|                          | 3,4                 | 540-630            | 0.22       | 0.10 | 29.2          | 2.0 x 10 <sup>5</sup>  | 7.3  |                                     |
|                          |                     |                    |            |      |               |                        |  |                                     |
|                          |                     |                    |            |      |               |                        |  |                                     |
|                          |                     |                    |            |      |               |                        |  |                                     |
|                          |                     |                    |            |      |               |                        |  |                                     |
|                          |                     |                    |            |      |               |                        |  |                                     |

a. Contribution from decomposition of mineral matter was subtracted from % total weight loss to get organic weight loss.

b. Mean temperature.

The apparent activation energy obtained for reaction zone 1, E<sub>1</sub>, varies between 4.6 and 6.6 kcal/mol for samples A and B under He, N<sub>2</sub> and air. E<sub>1</sub> values being very close to the latent heat of vaporization for hydrocarbons confirms our suggestion that weight loss in this reaction zone is mostly due to volatilization (13). E<sub>2</sub> values for sample A range from 20.2 to 29.3 kcal/mol and for sample B 35.3 to 39.4 kcal/mol. These values are similar to those reported for thermolysis and oxidation of hydrocarbons and crude oils (14-16). E<sub>3</sub> values of 49.9 and 46.4 kcal/mol for samples A and B in He are larger than 45.5 and 29.2 kcal/mol for A and B, respectively, in air. Cracking reactions under inert environment are known to have higher E values than under oxidizing atmosphere (5-6). Hayashitani et al. have postulated a series of cracking reactions in helium involving light oil, heavy oil and asphaltene components in the pyrolysis of bitumen extracted from the Athabasca oil sand (17). Activation energies for cracking reactions reported by them range between 57.4 and 65.2 kcal/mol. Bennion et al. have reported that these values of activation energies were divided by 1.37 to be used in numerical simulation in order to obtain reasonable values of temperature and fuel lay-down (5). These activation energies divided by 1.37 produce an average value of 44.1 kcal/mol which agrees with 49.9 and 45.5 kcal/mol obtained by us for reactions in zone 3 under He atmosphere. This indicates that the results obtained from TGA are more meaningful for use in the numerical simulation than those obtained from pyrolysis experiments in a closed system. Activation energies for reactions in zone 4 ranging between 14.2 and 21.5 kcal/mol are typical of reactions involving either coke formation or its oxidation (6).

The fuel (coke) contents of samples A and B have been determined to check if the minimum amount of fuel required to sustain combustion front is available. Calculation of fuel lay-down was based upon percentage organic loss in He in reaction zone 4 because coke is formed in this region. Since the maximum combustion temperature of the fire front listed in Table II ranges between 450° and 700°C, it is expected that for some fireflood tests, weight loss in zone 3 in He will also contribute to fuel lay-down. The fuel content under both scenarios calculated by assuming the density of the sample 2.2 g/cm<sup>3</sup> is included in Table III. Estimated fuel content values under either assumption are greater than the value required (20 kg/m<sup>3</sup>) to sustain combustion.

Activation energies, pre-exponential factors, rate constants at peak temperatures, and heats of reactions obtained from treating DSC data for the last peak using the Borchardt and Daniels kinetics program are listed in Table IV. Order of reaction was assumed to be 1.0. Activation energies for cracking under He of sample A was 55.9 and of sample B was 61.7 kcal/mol and for combustion under air of sample A was 20.5 and of sample B was 28.9 kcal/mol. These values are higher for cracking and lower for combustion reactions than those obtained from kinetic treatment of TGA data in temperature zone 3 (Table III). Although inhomogeneity of core samples is always a problem in generating reproducible data, it is believed that more experimental data is needed before such discrepancy can be resolved. Heats of reaction for tests under air are much larger, 147 for A and 240 cal/g for B, than in He, 38 for A and 91 cal/g for B. It is evident that heat of reaction for sample A is lower than that of B. This is because oxidation reactions are much more exothermic than cracking reactions and oil content of sample A is one-half of B. Table IV includes peak and ignition temperatures derived from DSC thermograms. Ignition temperature is defined here as the temperature to which the product must be heated in the presence of air to sustain combustion. Temperature at the onset point of the combustion peak on DSC thermograms has been assigned to this value. Ignition temperature for sample A is 325°C and for sample B is 345°C.

TABLE IV  
REACTION PARAMETERS FROM DSC EXPERIMENTS<sup>a</sup>

| Sample<br>(Purge<br>Gas) | Peak<br>Temp.<br>°C | Activation<br>Energy<br>kcal/mol | A<br>s <sup>-1</sup> | 10 <sup>3</sup> k <sub>peak</sub><br>s <sup>-1</sup> | Heat of<br>Reaction<br>cal/g | Ignition<br>Temp.<br>°C |
|--------------------------|---------------------|----------------------------------|----------------------|--|------------------------------|-------------------------|
| A. (He)                  | 462                 | 55.9                             | $2.6 \times 10^{14}$ | 5.7  | 38                           |                         |
| (Air)                    | 453                 | 20.5                             | $6.2 \times 10^3$    | 3.9  | 147                          | 325                     |
| B. (He)                  | 484                 | 61.7                             | $4.2 \times 10^{15}$ | 5.2  | 91                           |                         |
| (Air)                    | 480                 | 28.9                             | $9.2 \times 10^5$    | 3.3  | 240                          | 345                     |

- a. Order of reaction was assumed to be 1.0 for estimation of activation energy and pre-exponential factor.

#### SUMMARY

Thermal degradation of Lloydminster heavy oil core samples has been investigated in He, N<sub>2</sub> and air using TGA and DSC techniques. TGA and DTG thermograms demonstrated four distinct types of chemical reactions occurring in four different temperature zones. Reactions in zone 1 are attributed to volatilization and low temperature oxidation; in zone 2 to thermolysis of heavy oil fractions, volatilization and oxidation; in zone 3 to cracking and combustion; and in zone 4 to coking, decomposition of mineral matter and oxidation of the coke produced. Oxidation reactions take place when the sample is in contact with air. Fuel (coke) contents of sample A ranged between 29.3 and 39.2 Kg/m<sup>3</sup> and that of B, 28.8 and 49.1 Kg/m<sup>3</sup>. Arrhenius and thermal parameters obtained for reactions in TGA/DSC studies are listed in Tables III and IV.

Data generated from TGA/DSC experiments are essential for running numerical simulation of the in-situ combustion process and verifying their match to the laboratory results. In addition, TGA/DSC data can be manipulated to yield air-fuel ratio, oxygen utilization, combustion front velocity, produced gas composition and hydrogen-to-carbon ratio of the fuel. It is evident that thermal analytical techniques have the potential to produce data which can be used for planning, design and construction of the field in-situ combustion tests and for numerical simulation to predict process variables and economics.

#### ACKNOWLEDGMENTS

I wish to thank G. Perron for technical assistance and A. Leu for calculation of some of the data. Partial financial support from Saskatchewan Energy and Mines is acknowledged for this work.

Figure 1. Schematic diagram of in-situ combustion process.

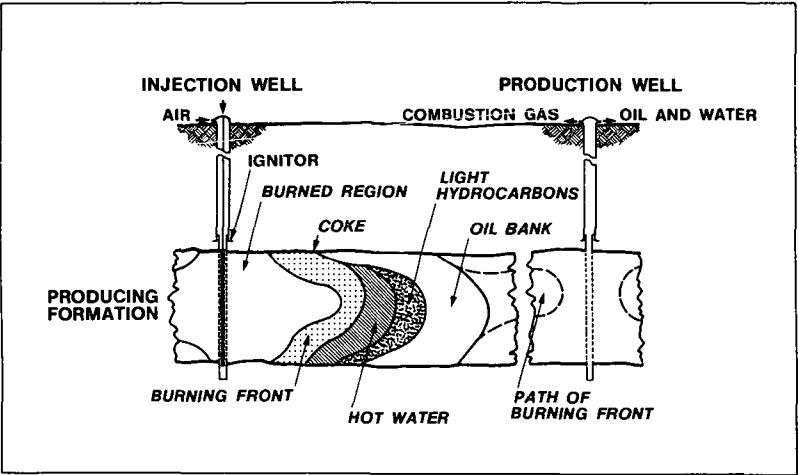


Figure 2. TGA thermograms of core sample A under the flow of He, N<sub>2</sub> and air.

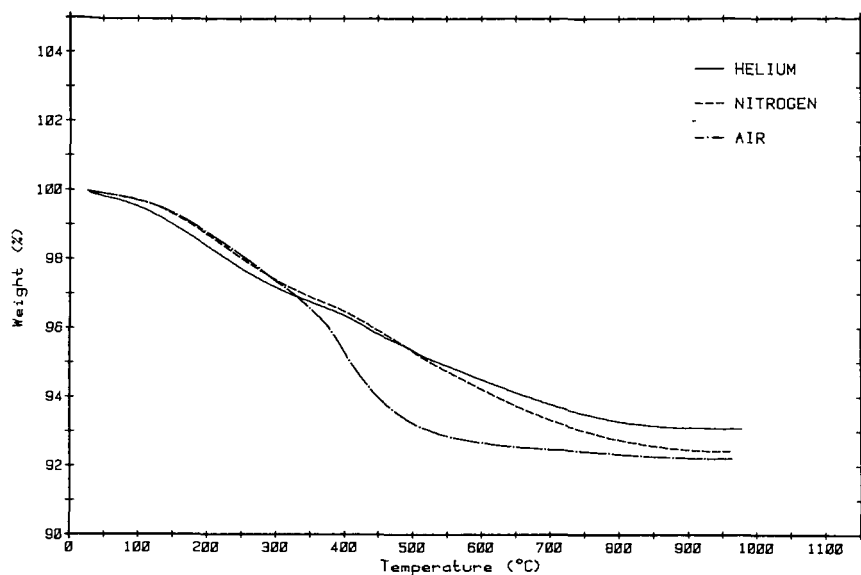


Figure 3. TGA and DTG thermograms of core sample A under He.

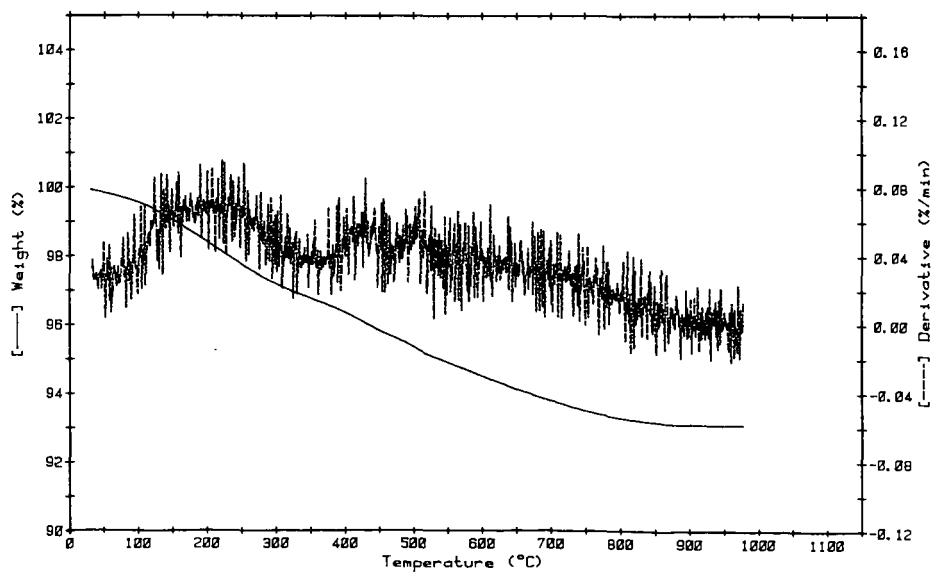


Figure 4. TGA and DTG thermograms of core sample A under N<sub>2</sub>.

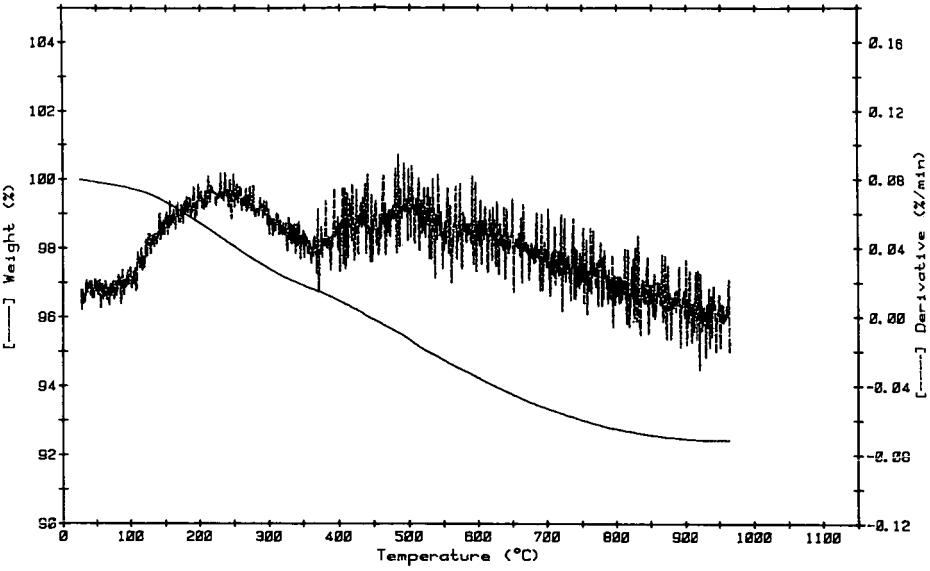


Figure 5. TGA and DTG thermograms of core sample A under air.

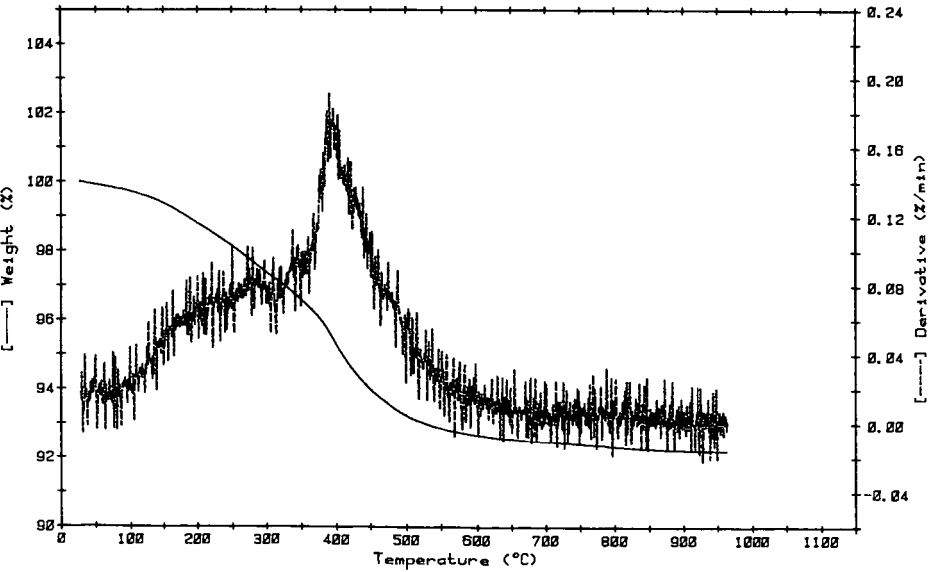


Figure 6. TGA and DTG thermograms of core sample B under He.

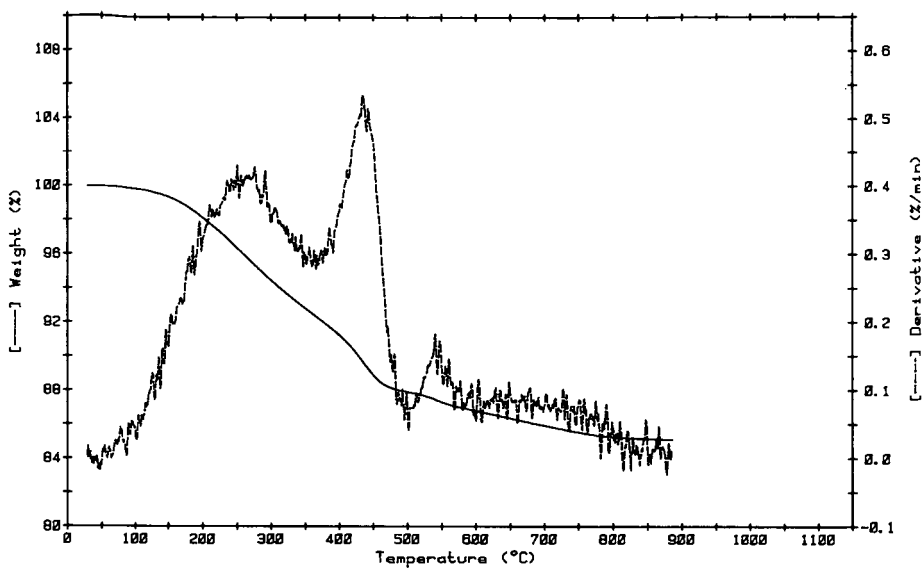


Figure 7. TGA and DTG thermograms of core sample B under air.

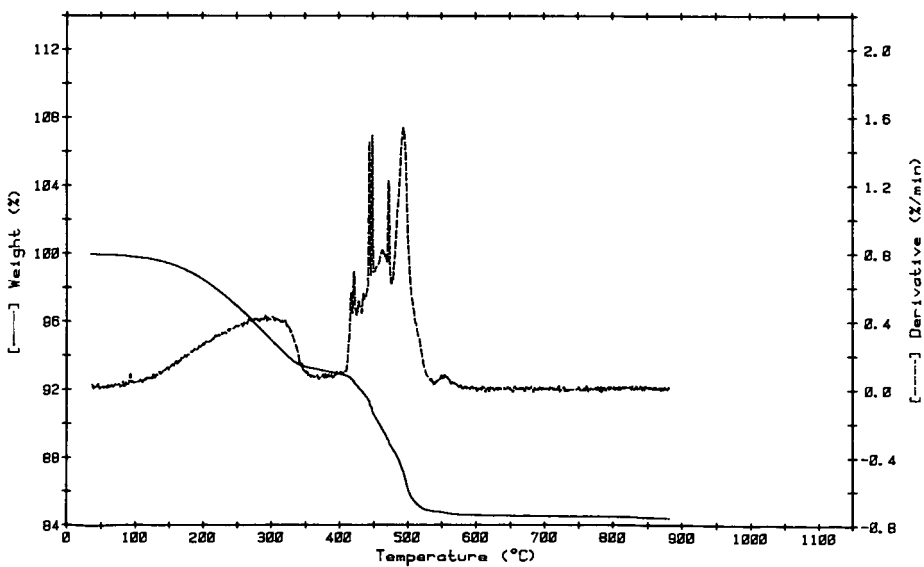


Figure 8. DSC thermograms of sample A under He.

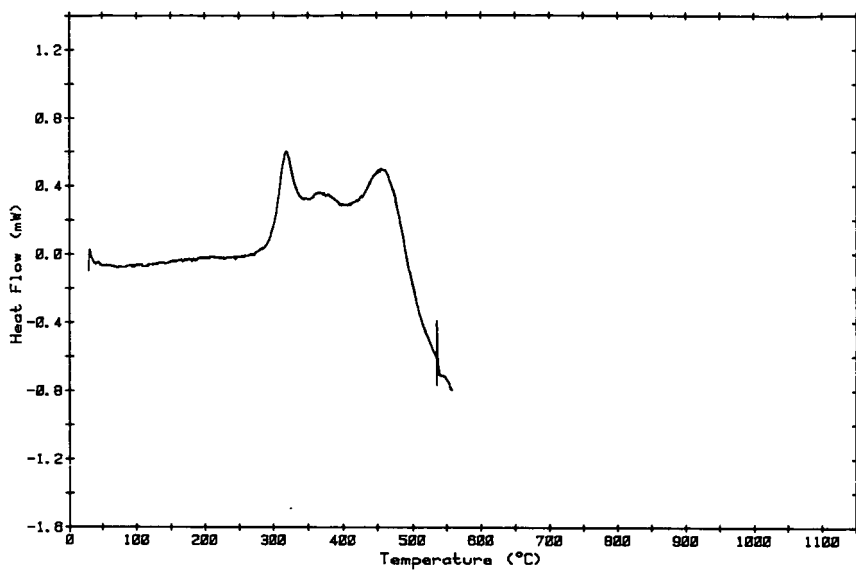


Figure 9. DSC thermograms of sample A under air.

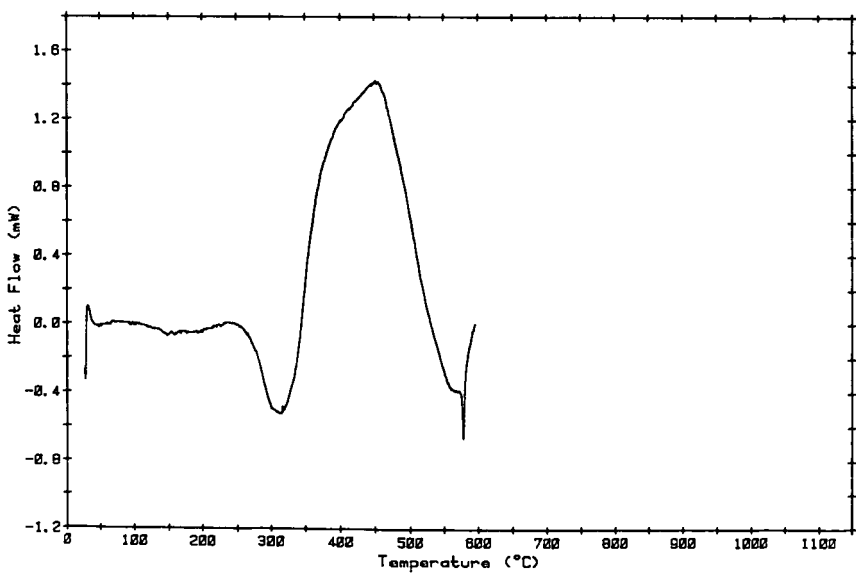




Figure 10. DSC thermograms of sample B under He.

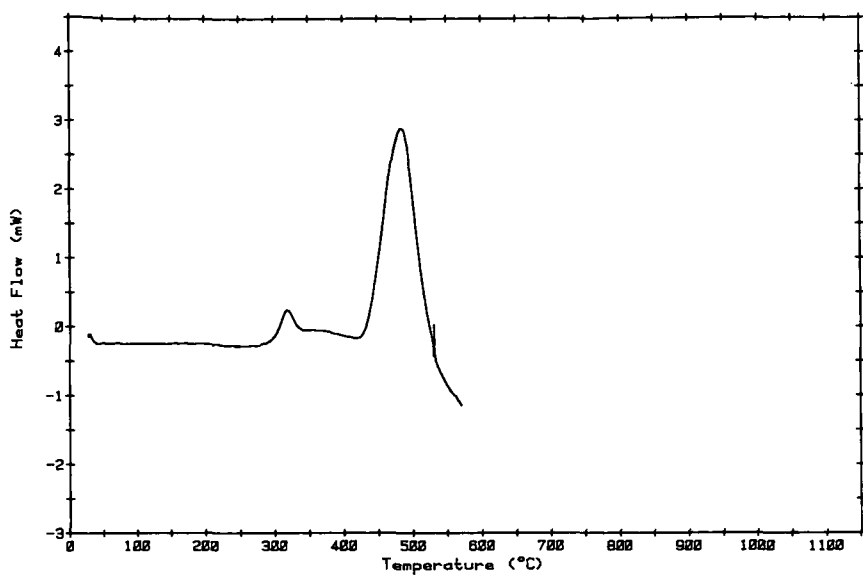


Figure 11. DSC thermograms of sample B under air.

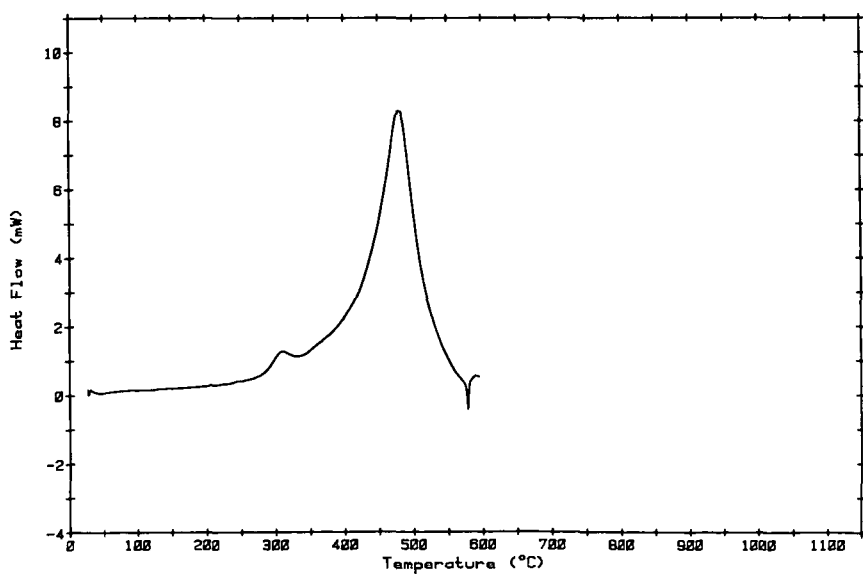


Figure 12. Arrhenius plot for sample A under helium between 50° and 340°C.

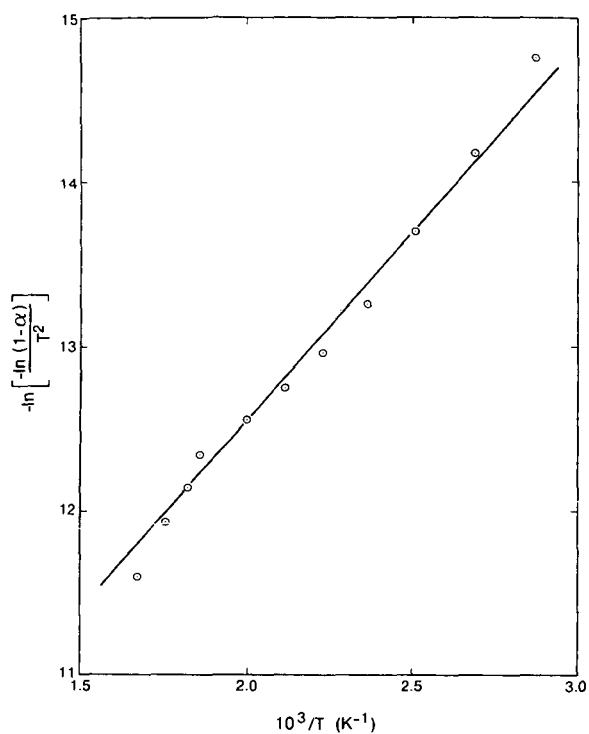


Figure 13. Arrhenius plot for sample A under helium between 340° and 475°C.

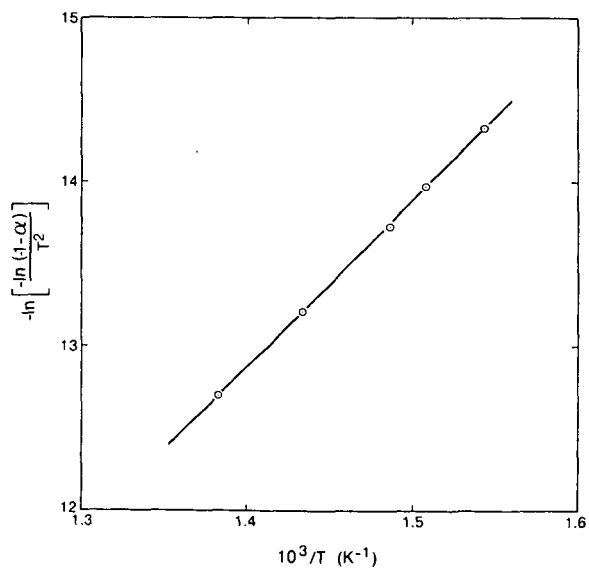


Figure 14. Arrhenius plot for sample A under helium between 475° and 550°C.

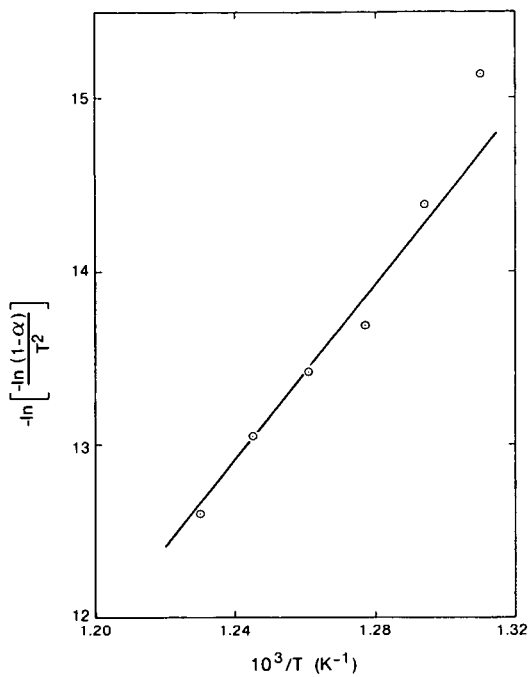
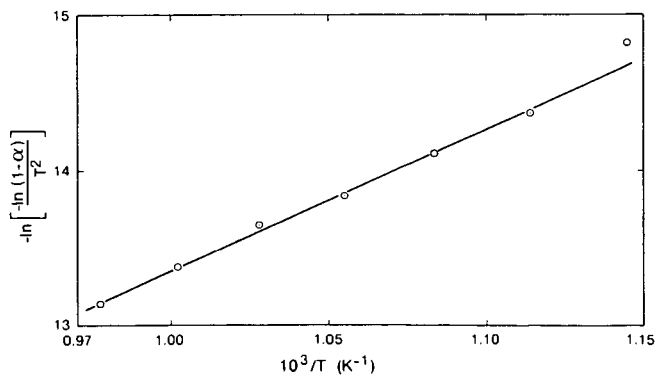


Figure 15. Arrhenius plot for sample A under helium between 550° and 800°C.



# LITERATURE CITED

- (1) Jha, K. N., Chemistry in Canada, pp. 19-26, September 1982.
- (2) Jha, K. N., and Verma, A., Proc. II International Conf. on Heavy Crudes and Tar Sands in Caracas, Venezuela, Vol. IV, Feb. 7-17, 1982.
- (3) "Fundamentals of Enhanced Oil Recovery", K. H. van Poolen and Assoc. Inc., PennWell Books, Tulsa, Oklahoma, U.S.A., 1980.
- (4) "Fully Implicit In Situ Combustion and Steam Model", ISCOM User Manual, Version 2.2, April, 1981, Computer Modelling Group, Calgary, Alberta, Canada.
- (5) Bennion, D. W., Moore, R. G., Donnelly, J. K., and Erian, A., Proc. II International Conf. on Heavy Crudes and Tar Sands in Caracas, Venezuela, Vol. II, February 7-17, 1982.
- (6) Lin, C. Y., Chen, W. H., Lee, S. T., and Culham, W. E., 57th Ann. Fall Tech. Conf., Soc. Pet. Engg. SPE 11074, New Orleans, U.S.A. September 26-29, 1982.
- (7) Vossoughi, S., Barlett, G. W., and Willhite, G. P., 57th Ann. Fall Tech. Conf., Soc. Pet. Engg. SPE 11073, New Orleans, U.S.A., September 26-29, 1982.
- (8) Borchardt, H. J., and Daniels, F., J. Am. Chem. Soc., 79, 41-46 (1957).
- (9) Grentzer, T. H., Holsworth, R. M., and Provder, T., National ACS, 3/81, ORPL.
- (10) "Borchardt and Daniels Kinetics Data Analysis Program", PN994377-912, DuPont, Wilmington, Delaware, U.S.A., August 1982.
- (11) Coats, A. W., and Refdern, J. P., Nature, 201, 68-69 (1964).
- (12) Thakur, D. S., Nuttall, H. E., and Cha, C. Y., Preprint, Div. Fuel Chem., 27 (2), 131 (1982).
- (13) Yaws, C. L., "Physical Properties", Chem. Engg., McGraw-Hill Co., New York, p. 205 (1977).
- (14) Baldwin, R. R., Bennett, J. P., and Walker, R. W., 16th International Symp. on Combustion, MIT, Cambridge, Mass., U.S.A., August 15-20, 1976.
- (15) Jha, K. N., Rao, P. M., and Stausz, O. P., Preprint, Div. Fuel Chem., 23 (4), 91 (1978).
- (16) Campbell, J. H., Koskinas, G. H., and Stout, N. D., Fuel, 57, 372 (1978).
- (17) Hayashitani, M., Bennion, D. W., Donnelly, J. K., and Moore, R. G., "The Oil Sands of Canada-Venezuela 1977", Ed. Redford, D. A., and Winestock, A. G., Can. Ins. Mining and Met., pp. 233-247 (1977).

GENERAL PAPERS - POSTER SESSION  
PRESENTED BEFORE THE DIVISION OF PETROLEUM CHEMISTRY, INC.  
AMERICAN CHEMICAL SOCIETY  
WASHINGTON, D. C. MEETING, AUGUST 28-SEPTEMBER 2, 1983

DEVELOPMENT OF AN ALTERNATIVE S.A.R.A. METHOD FOR THE  
CHARACTERIZATION OF COAL-DERIVED LIQUIDS

By

F. M. Lancas, H. S. Karam and H. M. McNair  
Department of Chemistry, Virginia Polytechnic Institute and State University  
Blacksburg, Virginia 24061

INTRODUCTION

Coal-derived liquids have been studied extensively, because of their potential applications in many fields such as fuel and feedstocks generation (1). One of the most popular methods by which to characterize fossil fuels is by fractionation of the sample into saturates, aromatics, resins and asphaltenes (S.A.R.A.). Two different approaches are widely used for this purpose: solvent extraction and liquid chromatography. Although much work has been done using these two approaches, characterization of fossil fuels is still unsatisfactory and exhaustive research is still required. Solvent extraction methods currently used, though simple and inexpensive, present problems with reproducibility, time consumption, solvent evaporation, co-extraction and loss of volatiles (2, 3). In most of the liquid chromatographic methods used, the fossil fuel extract is first treated with a non-polar hydrocarbon (such as n-pentane) to precipitate the asphaltenes and the remaining solution is applied to an Attapulgis clay column to separate resins from oils. Finally, the oils are fractionated to saturates and aromatics on alumina and/or silica columns (4). All these steps, in addition to being unnecessary and inconvenient, do not provide the actual group-type distribution in the extract since part of the resins could be co-precipitated with asphaltenes (5). With these problems in mind, we have developed and applied an alternative S.A.R.A. method for the characterization of Brazilian coal-derived liquids.

RESULTS AND DISCUSSION

Fractionation by Solvent Extraction

Coal was finely ground, sieved through a 60 mesh (U. S. Standard) sieve, extracted with different solvents for 30 minutes using a magnetic stirrer (100 ml of solvent to 10 g of coal). Results showed that stirring time is not critical. After one hour of stirring with hexane, the unextracted coal was 96.6% of the original sample, while after 12 hours it was 95.6%. Following extraction, the solvent was evaporated and the extract redissolved in 2 ml of solvent. Asphaltenes were precipitated by adding 80 ml of n-pentane to the concentrated extract solution (volume ratio of 40 to 1). In all experiments solvents were evaporated by a combination of rotary evaporation for sample concentration and controlled heating under nitrogen flow until dryness of the extract. Figure 1 shows the results of a study comparing the relative amounts of asphaltenes and maltenes present in the "Mina do Leao" (high-ash Brazilian coal). The relative amounts extracted by the different solvents are displayed in Figure 2. Although pyridine is the best solvent examined, we decided to use tetrahydrofuran (THF) since it has a similar performance and it is less toxic and less polar.

In a different set of experiments, the fractionation of the THF coal extract into asphaltols, asphaltenes and oils was carried out utilizing the schematic shown in Figure 3. The results of this study appear in Table I.

Fractionation by Column Chromatography

A 50 cm (L) x 11 mm (I.D.) glass column fitted with a teflon stopcock was dry or slurry packed for comparison purposes. Dry packing was done by constantly tapping the column while adding 2 g of the packing material in small portions. A plug of glass wool and a layer of white sand (ca. 0.5 cm) on the top were used to support the solid adsorbent and to prevent it from washing through the stopcock. Slurry packing was performed by first adding the solid adsorbent a little at a time to hexane in a beaker, swirling the beaker and pouring the slurry into a draining column (previously filled about 1/3 full with the first eluent, hexane). The results of a comparative study using different packing techniques and materials are displayed in Table II. A set of five identical columns was employed, to determine the reproducibility of each system as applied to a hexane coal extract. For this study, the hexane soluble materials were filtered following extraction into a 100 ml

volumetric flask. 10 ml of this stock solution was loaded into the chromatographic column. The eluents used to generate the fractions were hexane (50 ml), toluene (75 ml) and methanol (50 ml) for saturates, aromatics and resins, respectively, following precipitation of asphaltenes, in accordance with the Phillips method (6). The results show that slurry packing with silica is the most reproducible system investigated. (It is well-established in the literature that asphaltols are highly adsorbed on alumina, while fewer substances are adsorbed on silica gel because of its mildly acidic properties (7, 8).)

TABLE I  
SOLUBILITY CHARACTERISTICS OF HIGH-ASH BRAZILIAN COAL THF EXTRACT

| Sample | Wt % Asphaltols | Wt % Asphaltenes | Wt % Oils |
|--------|-----------------|------------------|-----------|
| 1      | 38.5            | 35.2             | 26.3      |
| 2      | 38.5            | 32.4             | 29.1      |
| 3      | 37.8            | 36.9             | 25.4      |
| 4      | 36.4            | 37.6             | 26.0      |
| 5      | 42.1            | 34.8             | 23.1      |
|        | $\bar{x}$       | 38.7             | 35.4      |
|        | $\sigma$        | 2.1              | 2.0       |
|        | R. S. D.        | 5.4              | 5.7       |
|        |                 |                  | 8.3       |

TABLE II  
COMPARISON OF DIFFERENT PACKING SYSTEMS AS APPLIED TO HEXANE COAL EXTRACT

| Group Type | Column Type <sup>a</sup> : | 1    | 2    | 3    |
|------------|----------------------------|------|------|------|
| Saturates  | Wt %                       | 40.4 | 35.3 | 24.3 |
|            | $\sigma$                   | 8.8  | 3.4  | 2.3  |
|            | R. S. D.                   | 22   | 9.8  | 9.5  |
| Aromatics  | Wt %                       | 30.1 | 22.4 | 30.1 |
|            | $\sigma$                   | 5.9  | 3.1  | 2.2  |
|            | R. S. D.                   | 20   | 14   | 7.1  |
| Resins     | Wt %                       | 29.4 | 42.3 | 45.6 |
|            | $\sigma$                   | 10   | 2.5  | 1.8  |
|            | R. S. D.                   | 35   | 5.8  | 4.0  |

a. 1=dry-packed alumina; 2=slurry-packed alumina;  
3=slurry-packed silica.

Since the best performance was shown with THF as extracting agent and silica gel as an adsorbent for slurry packing technique, we have applied the whole coal extract (a maximum of 200 mg) to the column to avoid problems associated with the asphaltenes precipitating in non-polar solvents. The characteristics of the chromatographic elution utilizing this new system as well as the relative group type distribution of the THF coal extract appear in Table III.

TABLE III  
CHROMATOGRAPHIC ELUTION CHARACTERISTICS AND RELATIVE GROUP TYPE DISTRIBUTION OF THF COAL EXTRACT

| Eluent   | Volume of Eluent | Color of Eluent | Identity    | Wt % |
|----------|------------------|-----------------|-------------|------|
| Hexane   | 50 ml            | Colorless       | Saturates   | 3.3  |
| Toluene  | 75 ml            | Orange          | Aromatics   | 20.2 |
| Methanol | 50 ml            | Red-Wine        | Resins      | 51.8 |
| THF      | 50 ml            | Dark Brown      | Asphaltenes | 24.7 |

100.0

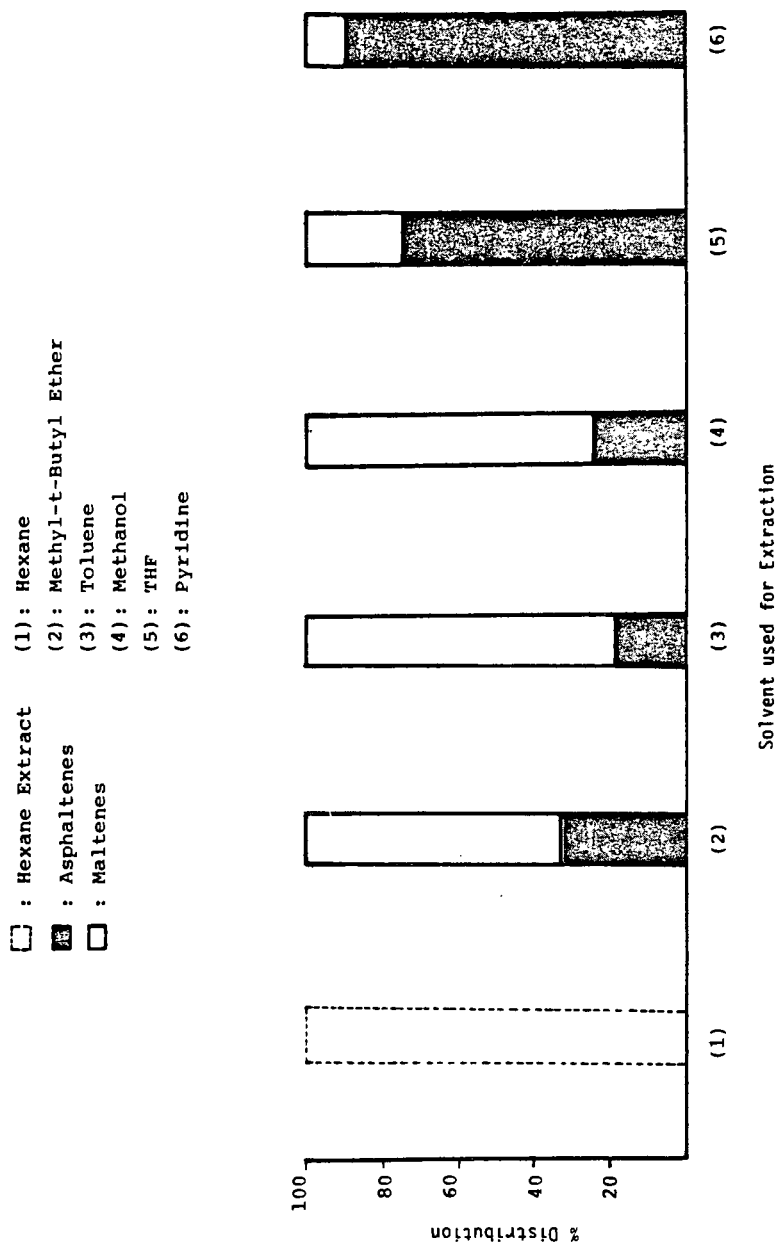


Figure 1. Relative amounts of asphaltenes and maltenes in the high-ash Brazilian coal.

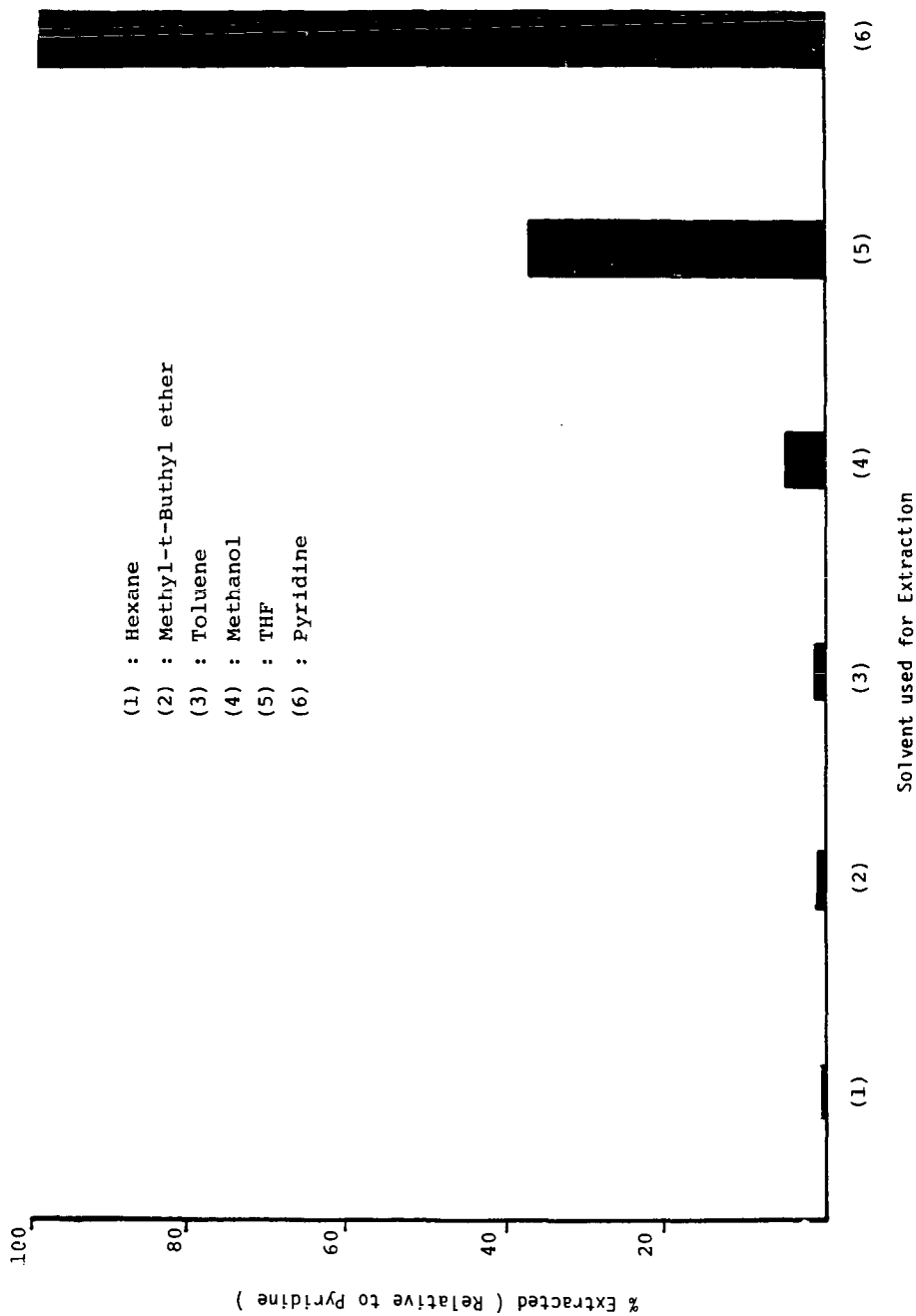
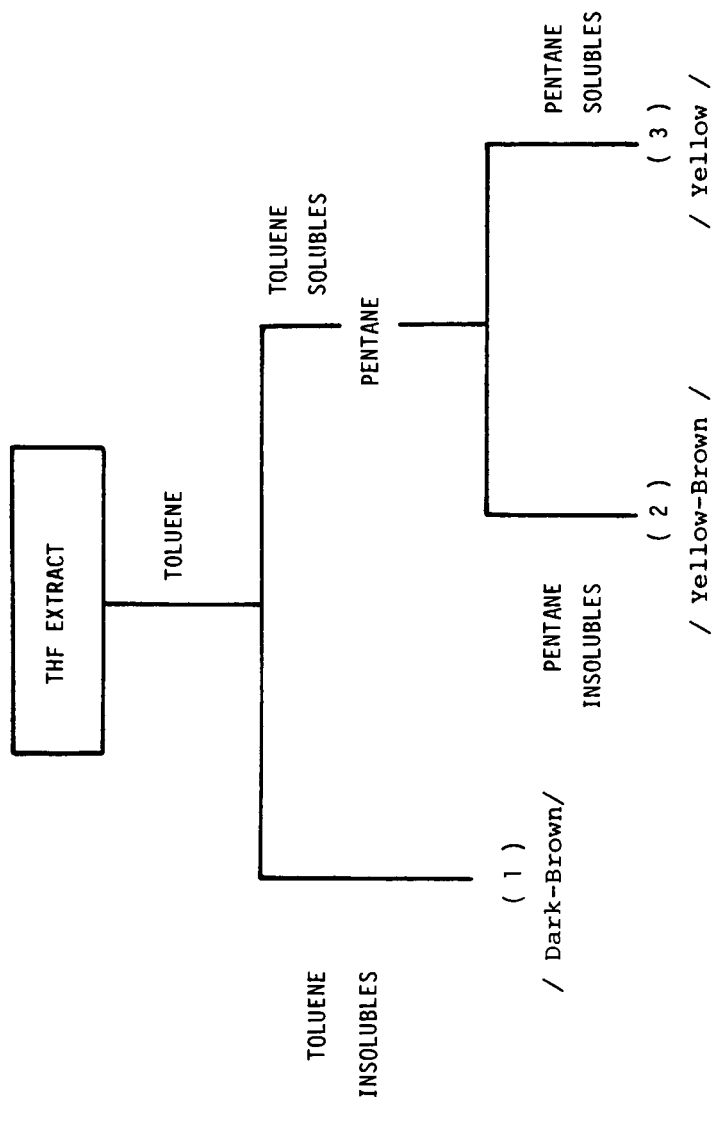


Figure 2. Percentage extracted (relative to Pyridine) using different solvents.





- (1): Asphaltols  
 (2): Asphaltenes  
 (3): Oils

Figure 3. Fractionation schematic of the THF extract

## CONCLUSION

Compared with methods of characterization of coal extract described in the literature, the method we have developed has the following advantages:

1. Extraction Step: Using THF instead of hexane, pyridine, toluene, etc., gives more reproducible results and avoids extracting very polar compounds and loss of volatiles during the evaporation step. Magnetic stirring instead of manual stirring or Soxhlet extraction is an easier, faster and more reproducible extraction procedure.

2. Column Chromatography: Slurry packing with silica permits a better stationary bed and, at the same time, avoids irreversible adsorption. By fractionating the whole THF coal extract, one avoids the precipitation of asphaltenes prior to column chromatography. In addition, fractionating the whole extract permits collection of the four S.A.R.A. (saturates, aromatics, resins and asphaltenes) fractions for further characterization.

## ACKNOWLEDGMENTS

F. M. Lancas would like to thank Fundacao de Amparo a Pesquisa do Estado de Sao Paulo (FAPESP) for the fellowship (Processo 16-Quimica 81/0557-2) and Universidade de Sao Paulo for the free absence.

## LITERATURE CITED

- (1) Whitehurst, D. D., Mitchell, T. O. and Farcasiu, M., "Coal Liquefaction. The Chemistry and Technology of Thermal Processes", Academic Press, NY (1980).
- (2) Boduszynski, M. M., Hurtubise, R. J. and Silver, H., Anal. Chem., 54, 372 (1982).
- (3) Bockrath, B., Schroeder, K. T. and Steffgen, F. W., Anal. Chem., 51, 1168.
- (4) Galya, L. G. and Suatoni, J. C., J. of Liquid Chromatogr., 3, 229 (1980).
- (5) Bunger, J. W. and Li, N. C., eds., "Chemistry of Asphaltenes", Advances in Chem. Series, No. 195, AMS (1981).
- (6) Phillips Petroleum Company, Research and Development, Method 8045-AS (1980).
- (7) Whitehurst, D. D., Farcasiu, M. and Mitchell, O., "The Nature and Origin of Asphaltenes in Processed Coals", EPRI Annual Report (1976).
- (8) Given, P. H., Cronauer, D. C., Spakman, K., Lovell, H. L., Davis, A. and Biswas, B., Fuel, 54, 34 (1975); 54, 40 (1975).

A CORRELATIVE INVESTIGATION OF THE EFFECTS OF OXIDATION ON THE MINERALS,  
MACERALS AND TECHNOLOGICAL PROPERTIES OF COAL

By

M. C. Lin, F. E. Huggins, G. P. Huffman and D. E. Lowenhaupt  
U. S. Steel Corporation, Research Laboratory, 125 Jamison Lane  
Monroeville, Pennsylvania 15146

INTRODUCTION

The oxidation of coal by natural weathering processes is well known to degrade those properties important for cokemaking (1, 2). Conversely, the loss of fluidity and enhancement of char reactivity resulting from low-temperature coal oxidation are desirable properties for coal gasification (3). Thus, better understanding of the oxidation mechanisms of coal components and of the effect of such oxidation on technological processes is highly desirable.

<sup>57</sup>Fe Mossbauer spectroscopy and diffuse reflectance infrared Fourier transform (DRIFT) spectroscopy were used to investigate the oxidation of minerals and macerals, respectively, and measurements of the Gieseler plasticity were made as representative of an important technological property, coal fluidity, that is affected by oxidation. The relative sensitivity of these techniques to coal oxidation were compared by correlating measurements made on a variety of bituminous coals.

SAMPLES AND EXPERIMENTAL TECHNIQUES

The naturally oxidized coal discussed in this paper is a low-volatile bituminous coal obtained from a strip mine on the Pocahontas No. 4 seam in West Virginia. Samples were collected from an outcrop (most oxidized) and the mine highwall (least oxidized), and at an intermediate location to obtain an oxidation profile across the strip pit.

Two high-volatile bituminous coals (Pittsburgh and Harlan seams) were used in long-term, room-temperature oxidation treatments. The -60 mesh coals were put into several 100-ml beakers and stored separately in dry, ambient and humid air atmospheres at room temperature in the laboratory for 950 days. The dry environment was simulated by placing the coals in a desiccator containing Drierite, whereas the humid environment was simulated by placing the coal in a similar desiccator vessel, but with water present. The ambient samples were stored in beakers open to the laboratory atmosphere.

Channel samples of two additional bituminous coals, one collected from the Pittsburgh seam in Pennsylvania and the other from the Pocahontas No. 3 seam in West Virginia, were used in two simulated weathering treatments. In one treatment, -40 mesh coal was placed in a gas-tight oven at 50°C. The moisture level of the air in the oven was maintained at approximately 65% RH ( $6.9 \pm 0.2\%$  H<sub>2</sub>O). In the other treatment, stockpiled samples of -1/8-inch coal were exposed to the atmosphere in 20-pound aliquots in plywood boxes.

The iron-bearing minerals in the various coals were investigated by <sup>57</sup>Fe Mossbauer spectroscopy. Details of sample preparation and data reduction procedures can be found in previous papers (4, 5, 6). The diffuse reflectance infrared Fourier transform (DRIFT) spectra were measured on a Nicolet 7000 series FTIR spectrometer with data reduction capability. Samples for FTIR were either -60 mesh or -200 mesh coals without KBr dilution. Typical measurement times were 285 seconds and the resolution of the spectra was typically  $4\text{ cm}^{-1}$ .

Standard ASTM methods were used for Gieseler plastometer measurements. The extent of coal oxidation was also monitored by an alkali extraction test (7).

RESULTS AND DISCUSSION

Gieseler Plastometer Measurements

Results of Gieseler plastometer measurements on the strip-mined coal samples are summarized in Table I. The thermal plasticity of the coal samples decreases markedly as a result of oxidation. The softening temperature increases and solidification temperature decreases by approximately 30°C, narrowing the plastic range from 90°C to 30°C. The maximum rate of rotation,

which corresponds to the maximum fluidity of coal samples, decreased by several orders of magnitude to the level of essentially no fluidity at all for the outcrop coal.

TABLE I

RESULTS OF LIGHT TRANSMISSION VALUES AND GIESELER PLASTOMETER MEASUREMENTS  
FOR POCAHONTAS NO. 4 SEAM

| Coal     | Percent<br>Transmission | Max.<br>ddpm | Soft<br>Temp. | °C                     |                 |                  |
|----------|-------------------------|--------------|---------------|------------------------|-----------------|------------------|
|          |                         |              |               | Max.<br>Fluid<br>Temp. | Solid.<br>Temp. | Plastic<br>Range |
| Highwall | 97                      | 3.5          | 401           | 461                    | 491             | 90               |
| Middle   | 58                      | 2.3          | 412           | 457                    | 481             | 71               |
| Outcrop  | 28                      | 0.2          | 413           | 448                    | 463             | 30               |

The results of the alkali extraction test, also summarized in Table I, correlate fairly well with results of Gieseler plastometer measurements. This test is used in the metallurgical coal industry to detect coal oxidation prior to the coking operation. Usually, a coal with a light transmission value less than 80% is regarded as too oxidized for metallurgical usage (7). It is noted that the badly oxidized coal taken from the outcrop of the pit has a transmission value of only 30%, while the least oxidized highwall coal has a value of 97%.

Similar plasticity behavior as a result of oxidation was also found for the Pittsburgh and Harlan seam coals stored in dry, ambient and wet atmospheres for over 950 days at room temperature, as summarized in Table II. These results indicate that the extent of oxidation depends greatly on the humidity of the coal environment, with high humidity accelerating coal oxidation.

TABLE II

GIESELER PLASTOMETER RESULTS OF COALS "WEATHERED"  
FOR 950 DAYS AT ROOM TEMPERATURE

| Sample                  | Max.<br>ddpm | Soft<br>Temp. | Max.<br>Fluid<br>Temp. | Solid.<br>Temp. | Plastic<br>Range |
|-------------------------|--------------|---------------|------------------------|-----------------|------------------|
| Pittsburgh<br>(dry)     | 22400.0      | 347           | 410                    | 464             | 117              |
| Pittsburgh<br>(ambient) | 1600.0       | 365           | 422                    | 467             | 102              |
| Pittsburgh<br>(wet)     | 580.0        | 366           | 420                    | 459             | 93               |
| Harlan<br>(dry)         | 18.0         | 365           | 410                    | 440             | 75               |
| Harlan<br>(ambient)     | 9.0          | 387           | 432                    | 459             | 72               |
| Harlan<br>(wet)         | 5.0          | 391           | 427                    | 454             | 63               |

An extremely rapid decrease of Gieseler plasticity due to oxidation is shown in Figure 1, where the maximum fluidity is plotted versus time of oxidation treatment for coals treated at 65% RH and 50°C. Accompanying this rapid reduction of fluidity, there is also a significant decrease of the plastic range. The -1/8-inch stockpiled samples of the same coals show similar but less rapid changes.

57

Fe Mossbauer Spectroscopy

The distribution of iron among minerals obtained by low-temperature Mossbauer spectroscopy is summarized in Table III for the strip-mined Pocahontas No. 4 samples. The data indicate that the pyrite has been completely converted to iron oxyhydroxide in both the middle and outcrop coals. Additionally, with increasing oxidation, a decrease in the percentage of iron contained in clay minerals and an increase in the percentage of iron present as an unidentified ferric phase ( $\text{Fe}^{3+}$ ) are observed. This  $\text{Fe}^{3+}$  phase is most probably either a ferric sulfate or  $\text{Fe}^{3+}$  in clays.

TABLE III

MOSSBAUER DATA ON DISTRIBUTION OF IRON AMONG MINERALS FOR  
POCAHONTAS NO. 4 COAL SAMPLES

| Sample   | Percentage of the Total Sample Iron Contained in: |          |        |          |                      |                  |
|----------|---|----------|--------|----------|----------------------|------------------|
|          | Clay  | Siderite | Pyrite | Jarosite | Iron<br>Oxyhydroxide | Fe <sup>+3</sup> |
| Highwall | 76  | 13       | 6      | 1        | -                    | 4                |
| Middle   | 64  | 14       | -      | 1        | 10                   | 12               |
| Outcrop  | 51  | 11       | -      | -        | 21                   | 17               |

Results of Mossbauer spectroscopy investigations on the room-temperature oxidation of Pittsburgh and Harlan coals are summarized in Tables IV and V. The data indicate that in Harlan coal, the clay and siderite are apparently little affected by oxidation, whereas the pyrite is extensively oxidized and transformed to jarosite, iron oxyhydroxide and a ferric iron phase. For the Pittsburgh coal, the pyrite was transformed to ferrous sulfate initially and then to ferric sulfates and iron oxyhydroxide. As discussed elsewhere (8), this and other differences in mineral oxidation reflect the significantly different sulfur content and mineralogies of the two coals.

TABLE IV

MOSSBAUER DATA ON THE DISTRIBUTION OF IRON AMONG MINERALS FOR  
PITTSBURGH COAL SAMPLES

| Sample  | Phases                        | % Fe <sup>a</sup> |
|---------|-------------------------------|-------------------|
| Fresh   | Pyrite                        | 100               |
| Dry     | Pyrite                        | 96                |
|         | Szomolnokite                  | 4                 |
| Ambient | Pyrite                        | 76                |
|         | Szomolnokite                  | 20                |
|         | Rozenite                      | 4                 |
| Wet     | Pyrite                        | 26                |
|         | $\alpha$ -FeOOH               | 23                |
|         | Jarosite                      | 4                 |
|         | Fe <sup>3+</sup>              | 25                |
|         | Unidentified Fe <sup>+2</sup> | 22                |

a. Percentage of the total iron in the sample contained in the indicated phase.

The low-temperature Mossbauer spectra of Pittsburgh coal, treated in the experimental oven (50°C, 65% RH) and coal stockpiled out of doors, are shown in Figure 2. For both Pittsburgh and Pocahontas No. 3 coals treated in the oven, the iron sulfate, szomolnokite, was detected after 40 and 124 days of treatment, respectively. As the oxidation proceeds, the iron sulfate content continues to increase at the expense of pyrite. However, for the coals stockpiled out of doors, iron oxyhydroxide is the oxidation product of pyrite and no iron sulfate has yet been detected. This indicates that different oxidation processes or different rate-determining steps are involved in the oxidation of pyrite in the two environments.

Diffuse Reflectance Infrared Fourier Transform (DRIFT) Spectroscopy

The infrared spectra of the strip-mined coal samples are shown in Figure 3. The most obvious trend with increasing oxidation is increases in intensity of various carbonyl bands between 1600 cm<sup>-1</sup> and 1800 cm<sup>-1</sup>. These increases in intensity were also accompanied by an increase in intensity of the region between 1100 cm<sup>-1</sup> and 1300 cm<sup>-1</sup>, which is associated with the C-O stretching vibration and O-H bending modes of phenols, ethers and esters (9, 10). Similar increases in intensity can also be found in the absorption bands of hydroxyl groups ranging from 3200 cm<sup>-1</sup> to

3600  $\text{cm}^{-1}$ . However, the intensity of absorption bands at 2860, 2920 and 2950  $\text{cm}^{-1}$ , which correspond to the aliphatic C-H stretching modes, show systematic decreases from the least oxidized to the most oxidized coal samples. Similar decreases in intensity also occur for the aromatic C-H stretching mode at 3040  $\text{cm}^{-1}$ , and the absorption bands between 700 and 900  $\text{cm}^{-1}$ , which correspond to the aromatic C-H out-of-plane bending modes.

TABLE V

MOSSBAUER DATA ON THE DISTRIBUTION OF IRON AMONG MINERALS FOR HARLAN COAL SAMPLES

| Sample  | Phases            | % Fe <sup>a</sup> |
|---------|-------------------|-------------------|
| Fresh   | Pyrite            | 53                |
|         | Clays             | 43                |
|         | Siderite          | 4                 |
| Dry     | Pyrite            | 46                |
|         | Clays             | 43                |
|         | Siderite          | 5                 |
|         | Jarosite          | 6                 |
| Ambient | Pyrite            | 42                |
|         | Clays             | 43                |
|         | Siderite          | 6                 |
|         | Jarosite          | 9                 |
| Wet     | Pyrite            | 12                |
|         | Clays             | 42                |
|         | Siderite          | 6                 |
|         | Jarosite          | 20                |
|         | Iron Oxyhydroxide | 7                 |
|         | Fe <sup>+3</sup>  | 13                |

a. Percentage of the total iron in the sample contained in the indicated phase.

For the laboratory-oxidized Pittsburgh and Harlan coal samples, the carbonyl and carboxylic-acid absorption bands between 1600  $\text{cm}^{-1}$  and 1800  $\text{cm}^{-1}$ , which are found in naturally oxidized coals from strip-mines and are closely associated with effects of coal oxidation, were not detected. This suggests that the oxidation of these coal samples is still at a relatively early stage, although both Mossbauer spectroscopy and Gieseler plastometer measurements clearly show changes due to oxidation. This observation is further supported by the DRIFT results obtained after severely oxidizing the dry and wet Pittsburgh coal samples in air at 110°C for seven days. Figure 4 shows that, in addition to the 1650  $\text{cm}^{-1}$  and 1735  $\text{cm}^{-1}$  bands observed before, carbonyl and carboxyl bands near 1585, 1680, 1690, 1710 and 1765  $\text{cm}^{-1}$  also appear after this rather severe oxidation treatment.

DRIFT spectra were also obtained from all oven-oxidized and stockpiled coal samples. No significant difference between the treated and fresh coals was found. This indicates that DRIFT spectroscopy is not sufficiently sensitive to detect the early stages of oxidation that cause the large decreases observed in plasticity.

## CONCLUSIONS

Mossbauer spectroscopy shows that pyrite in coal is readily altered by low-temperature coal oxidation. The oxidation of pyrite in coals subjected to simulated weathering treatments at constant temperature and humidity in the laboratory gives rise to a variety of iron sulfates. This is in contrast to coal samples stockpiled out-of-doors and strip-mined coals, in which the principal pyrite oxidation product is iron oxyhydroxide.

A reduction in intensity of aliphatic and aromatic bands with increasing oxidation of a strip-mined coal is detected in DRIFT spectra. These changes accompany the enhancement in intensity of certain carbonyl and carboxyl bands. However, these carbonyl bands are not detected in spectra of laboratory oxidized coals until oxidation is quite extensive.

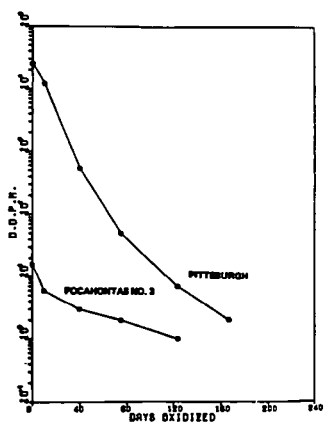


Fig. 1 Variations of maximum fluidity as measured by Gieseler plastometer with days of oxidation at 50°C, 65% RH.

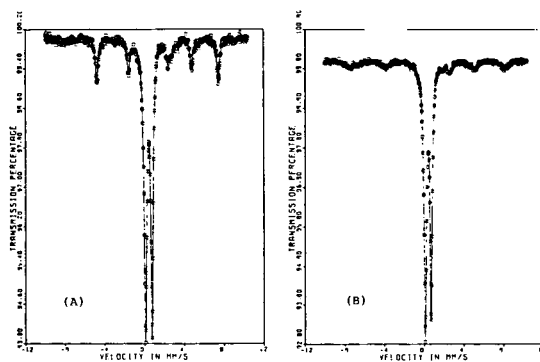


Fig. 2 Low-temperature Mossbauer spectra of Pittsburgh coals: (A) treated in 50°C, 65% RH for 167 days; (C) stockpiled out of doors for 139 days.

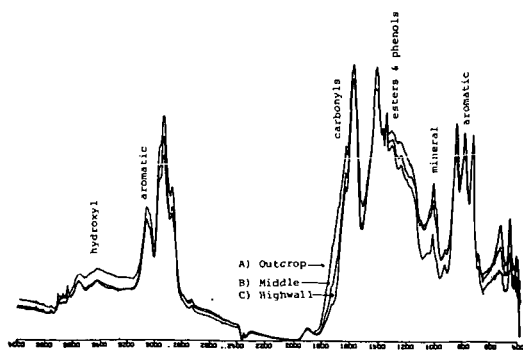


Fig. 3 FTIR spectra of Pocahontas No. 4 seam coals: (A) outcrop, (B) middle, (C) highwall.

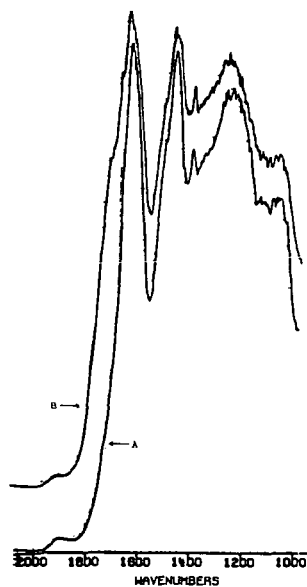


Fig. 4 FTIR spectra of (A) Pittsburgh coals oxidized for over 30 months in wet air atmosphere at room temperature; (B) wet Pittsburgh coal oxidized in air at 110°C for seven days.



The plastic properties of coal, as determined by Gieseler plastometer measurements, are extremely sensitive to oxidation. The maximum fluidity shows a very rapid reduction with oxidation. There is also a significant narrowing of the plastic range. Of the three techniques, the Gieseler plasticity measurement is the most sensitive and DRIFT spectroscopy the least sensitive to the initial stages of coal oxidation. This order of sensitivity is inverse to their applicability to coals as the Gieseler measurements are restricted to coking bituminous coals and Mossbauer techniques are best applied to high pyrite coals, whereas DRIFT spectroscopy can be applied to all coals with little or no modification.

The extreme sensitivity of the thermoplastic behavior of coal to initial oxidation as determined by the Gieseler measurements is in contrast to the insensitivity of DRIFT spectroscopy and the relative minor oxidation of pyrite detected by Mossbauer spectroscopy, both of which are bulk-oriented techniques. The explanation must be attributed to the fact that the first stages of coal oxidation are surface controlled, as are most oxidation processes. Even though plasticity is determined by a macroscopic measurement, it is dependent upon the fusing together of separate coal particles. Consequently, it is likely to be highly sensitive to very thin surface layers on the coal particles. Further investigations involving the characterization of oxidized coal surfaces are currently underway.

#### LITERATURE CITED

- (1) Gray, R. J., Rhoades, A. H. and King, D. L., Trans. AIME, Soc. Min. Engineers, 260, 334 (1976).
- (2) Crelling, J. C., Schrader, R. H. and Benedict, L. G., Fuel, 58, 542 (1979).
- (3) Mahajan, O. P., Komatsu, M. and Walker, P. L., Jr., Fuel, 59, 3 (1980).
- (4) Huffman, G. P. and Huggins, F. E., Fuel, 57, 592 (1978).
- (5) Huggins, F. E. and Huffman, G. P., Analytical Methods for Coal and Coal Products, Clarence Karr, Jr., ed., Academic, New York, Vol. 3, Chapter 50 (1979).
- (6) Huggins, F. E., Huffman, G. P. and Lee, R. J., Coal and Coal Products: Analytical Characterization Techniques, E. L. Fuller, Jr., ed., ACS Symp. Series No. 205, p. 239 (1982).
- (7) Lowenhaupt, D. E. and Gray, F. J., Internatl. Journal of Coal Geology, 1, 63 (1980).
- (8) Huggins, F. E., Huffman, G. P. and Lin, M. C., to be published in Internatl. Journal of Coal Geology (1983).
- (9) Painter, P. C., Snyder, R. W., Starsinic, M., Coleman, M. M., Keuhn, D. W. and Davis, A. H., Applied Spectroscopy, 35, 475 (1981).
- (10) Painter, P. C., Snyder, R. W., Pearson, D. E. and Kwong, J., Fuel, 59, 282 (1980).

GENERAL PAPERS - POSTER SESSION  
PRESENTED BEFORE THE DIVISION OF PETROLEUM CHEMISTRY, INC.  
AMERICAN CHEMICAL SOCIETY  
WASHINGTON, D. C. MEETING, AUGUST 28-SEPTEMBER 2, 1983

EFFECT OF FRACTURE MODES ON SHAPE AND SIZE OF COAL PARTICLES  
AND SEPARATION OF PHASES\*

By

J. M. Lytle and L. R. Bunnell  
Battelle, Pacific Northwest Laboratory, Richland, Washington 99352  
and  
K. A. Prisbrey  
University of Idaho, Moscow, Idaho 83843

INTRODUCTION

Studies of coal grinding are becoming one of the most important and interesting areas of coal research. Consequently, the Department of Energy sponsored "Study Group on Research Planning for Coal Utilization and Synthetic Fuel Production" emphasized size-dependent phenomena during coal grinding as one of the seven most important areas of research needed for development of an advanced coal and synfuels industry (1, 2). Nearly every use of coal involves grinding to some extent and modern processes are requiring finer and finer coal powders. Knowledge of the properties of these coal powders is essential in developing these processes. For example, knowledge of shapes and sizes of particles is important in defining the viscosity and transport behavior of coal-liquid slurries for combustion or pipeline transport. Knowledge of separation of phases is important in developing beneficiation processes to remove impurities.

The study reported in this paper used microscopy, shape, size and sulfur analyses to show the influence of fracture modes and mechanisms on shape and size of coal particles and separation of phases. The preferential lines of fracture during coal grinding were identified microstructurally and related to the size and shape of particles produced and the separation of mineral and organic phases. For example, weaker phases that were lean in organic sulfur were observed to concentrate into finer particle size ranges and stronger phases that were rich in organic sulfur concentrated into coarser particle size ranges.

EXPERIMENTAL

Two coals of widely differing rank were selected for this study: a lignite from the Fort Union Bed near Savage, Montana and a medium volatile bituminous (MVB) from the Beckley seam near Duo, West Virginia. These two coals (PSOC-837 and PSOC-985) were obtained from the Pennsylvania State University's coal sample bank.

Prior to ball milling, the coals were preground in nitrogen to minus 20 mesh (U. S. standard screen, 840  $\mu$ m opening size) in a wheel-type pulverizer. The coal (350 g) was transferred in the N<sub>2</sub> atmosphere to a 1.8 L steel ball mill, which was then evacuated and backfilled with helium. During rotation of the mill, coal powders were withdrawn in a long, cylindrical scoop inserted along the axis of rotation through a hole plumbed with a rotary union and ball valves to maintain the atmosphere.

RESULTS AND DISCUSSION

During coal grinding, particle microstructure affected the fracture modes which in turn affected shape and size of particles and separation of phases. Optical micrographs of polished particle cross-sections (Figure 1) illustrate the tendency for separation of organic phases in the early stages of grinding. With both lignite and MVB, fracture tended to proceed preferentially along organic-to-organic interfaces, as shown by the separate and microstructurally more uniform particles already present after the pregrind step and the incomplete but progressing fractures along interfaces in the particles, indicated by arrows.

Fracture also tended to preferentially proceed along mineral-to-organic interfaces and

\* The Pacific Northwest Laboratory is operated by Battelle Memorial Institute for the Department of Energy. The research was sponsored by the Basic Energy Science, Division of Material Science, under Contract DE-AC06-76RLO 1830.

cracks and pores. This tendency is illustrated by the scanning electron micrographs of particle cross sections shown in Figure 2. In the lignite particles, cracks and pores--highlighted in the photographs by electron microscope edge effects--were apparent in the pregrind particles but were depleted after 7 h of grinding. In the MVB particles, mineral inclusions were separated from the organic phases during grinding as shown by the presence of separate mineral particles after 7 h.

Distinct organic phases that were separated during the pregrind step tended to grind at their own individual rates during subsequent grinding (3). The particles that were microstructurally more heterogeneous and contained more cracks and pores were rapidly ground according to the larger set of particle size-dependent rate constants shown in Table I. The stronger particles were ground more slowly according to the set of smaller rate constants.

TABLE I

Breakage rate constants,  $S_i^a$ , ( $10^{-3} \text{ min}^{-1}$ ) for lignite grinding where the weaker particles were rate controlling for the first 30 min of grinding. After weaker particles were reduced to fines, the stronger particles controlled the grinding rate.

| Particles | Particle size, $\mu\text{m}$ |     |     |      |      |      |      |       |       |
|-----------|------------------------------|-----|-----|------|------|------|------|-------|-------|
|           | 210                          | 149 | 105 | 74   | 53   | 83   | 30   | 20    | 15    |
| Weaker    | 10.1                         | 8.2 | 5.6 | 4.0  | 2.8  | 2.0  | 1.6  | 1.0   | 0.77  |
| Stronger  | 4.2                          | 2.5 | 1.4 | 0.79 | 0.46 | 0.26 | 0.18 | 0.090 | 0.046 |

$$a. \text{ rate} = \frac{dm_i}{dt} = -S_i^a m_i + \sum_{j=1}^{i-1} S_j^b b_{ij} m_j$$

$m_i$  = mass fraction of size  $i$

$S_i^a$  = breakage rate constant for size  $i$

$b_{ij}$  = primary breakage fragment distribution

During lignite grinding, the stronger particles contained more organic sulfur than the weaker particles, as can be seen from the particle-by-particle compositional analysis done previously (4). The weaker, more porous, particles averaged 0.26% organic sulfur whereas the stronger, less porous, particles averaged 0.46% (4). During grinding, the sulfur content of a given particle size range steadily increased as the weaker particles passed through that size range and the stronger particles lingered (see Table II). Thus, during grinding, sulfur-rich and sulfur-lean particle size ranges developed, depending on the grinding time.

TABLE II

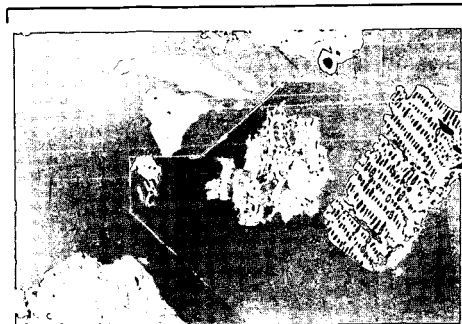
Average organic sulfur content (percent) of lignite particles as determined by particle-by-particle analysis of particle cross sections using X-ray fluorescence in a scanning electron microscope.

| Particle Size, $\mu\text{m}$ | Grinding Time, Minutes |      |      |
|------------------------------|------------------------|------|------|
|                              | 15                     | 60   | 420  |
| 20 - 30                      | 0.37                   | 0.38 | 0.45 |
| 5 - 10                       | 0.11                   | 0.19 | 0.23 |

The microstructure of coal is a major factor in the sizes and shapes of particles produced during grinding. One of the best examples of the effect of microstructure on shape is the needle-like and plate-shaped particles produced from the fracture of the weaker particles during the initial stages of grinding (Figure 3). As seen in Figure 3, in the 10 to 15  $\mu\text{m}$  particle size range, many needle-like or plate-shaped particles were present after 15 min of grinding, but these particles were no longer present in this size range after 60 and 420 min. The microstructure of the stronger particles did not lead to needle-like or plate-shaped particles but instead blocky and rounded particles were produced throughout grinding. The stronger particles of the 20 to 30  $\mu\text{m}$  size range did, however, become increasingly spherical during grinding, as shown by an increasing shape factor (4 x cross sectional area/perimeter squared) which would be one if the projected shape was a circle.

LIGNITE

MEDIUM VOLATILE BITUMINOUS



100  $\mu\text{m}$  


FIGURE 1. OPTICAL MICROGRAPHS OF POLISHED, PREGRIND PARTICLE CROSS SECTIONS SHOWING SEPARATION OF ORGANIC PHASES DURING THE EARLY STAGES OF GRINDING. ARROWS INDICATE FRACTURE PROGRESSING ALONG INTERFACES.

LIGNITE

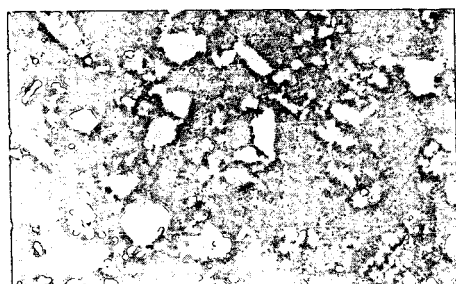
MEDIUM VOLATILE BITUMINOUS




PREGRIND

100  $\mu\text{m}$  

100  $\mu\text{m}$  



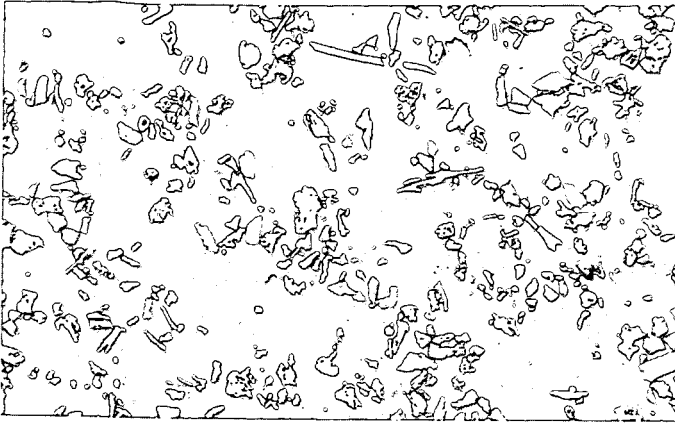
AFTER 7 hrs  
GRINDING

100  $\mu\text{m}$  

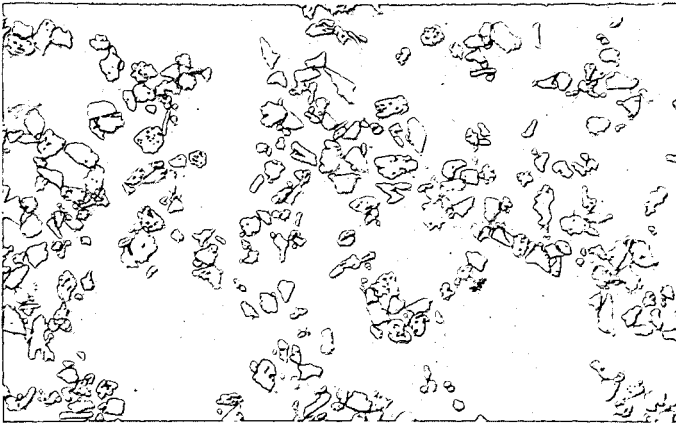
100  $\mu\text{m}$  

FIGURE 2. SCANNING ELECTRON MICROGRAPHS OF PARTICLE CROSS SECTIONS SHOWING THE DEPLETION OF PORES AND CRACKS AND THE SEPARATION OF MINERAL INCLUSIONS.

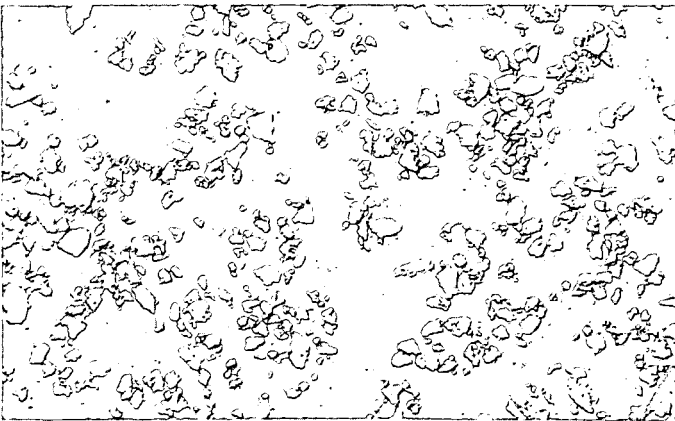
GRINDING TIME



15 min



60 min



420 min

FIGURE 3. OPTICAL MICROGRAPHS OF 10 TO 15  $\mu\text{m}$  LIGNITE PARTICLES AFTER VARIOUS GRINDING TIMES.

The shape factor was 0.47, 0.47 and 0.62 after 15, 60 and 420 min of grinding, respectively.

## CONCLUSIONS

During coal grinding, the modes and mechanisms of fracture change with time and particle size. Fracture tends to proceed preferentially first along organic-to-organic interfaces, then along mineral-to-organic interfaces and cracks and pores: first, through the largest cracks and pores, then through gradually smaller cracks and pores as encountered by the stress field. Thus, particles with limited porosity and mineral inclusions are the stronger particles that tend to grind at lower rates.

Modeling studies indicate that two sets of comminution rate constants are required to model the grinding of lignite because weaker components control the rates initially and stronger components control the rates later in grinding.

These modes and mechanisms of fracture cause changes in the shape and size of particles and the separation of phases. The shapes and sizes of particles are first changed by fracture through organic-to-organic interfaces, then by the microstructure of the weaker phases and finally by the microstructure of the stronger phases. During lignite grinding, the weaker phases produce needle-like or plate-shaped particles that are changed to more blocky and rounded shaped particles as particle size is decreased. The stronger phases produce blocky and rounded shaped particles that become more rounded with longer grinding times.

In both coals the organic phases are separated initially by the tendency for fracturing preferentially through organic-to-organic interfaces. Then the stronger phases are ground more slowly than the weaker phases. The stronger phases of lignite have greater organic sulfur content than the weaker phases. Thus, there is a stage in grinding where low-sulfur particles are concentrated in the fines and high-sulfur particles are concentrated in the larger size ranges.

Mineral phases are separated from the organic phases during grinding. The extent of separation depends on the size distribution of the mineral phases and the extent of grinding.

The size and shape of particles and the separation of phases are important factors in modern coal processes. For example, in producing and using coal-liquid slurries important factors include coal-to-liquid ratio, rheological properties of slurry, particle size distribution and mineral content. The results of this study impact all of those factors. The shapes of particles can have a marked effect on slurry viscosity as well as the packing density of slurries, thus, it may be advantageous to grind a coal more extensively in some cases to produce more rounded particles. The potential for removal of mineral impurities increases with grinding time. However, the potential for removal of organic sulfur may be greater at an intermediate stage of grinding. Thus, detailed knowledge of the coal grinding process can greatly increase the potential for more efficient and environmentally safe ways of using coal.

## LITERATURE CITED

- (1) Robinson, A. L., "Can Physicists Clean Up Coal's Act?", *Science*, 213, 1484 (1981).
- (2) Study Group on Research Planning for Coal Utilization and Synthetic Fuel Production, B. R. Cooper, Chairman, *Rev. Mod. Phys.* 53 (4, Part 2) (1981).
- (3) Lytle, J. M., Daniel, J. L. and Prissbrey, K. A., "The Effect of Microstructure on the Size and Shape of Coal Particles During Comminution", submitted to *Fuel* (1983).
- (4) Lytle, J. M., Daniel, J. L. and Tingey, G. L., "Concentration of Sulfur and Mineral-Rich Components in Particle Classes During Coal Comminution", submitted to *Fuel* (1982).

GENERAL PAPERS - POSTER SESSION  
PRESENTED BEFORE THE DIVISION OF PETROLEUM CHEMISTRY, INC.  
AMERICAN CHEMICAL SOCIETY  
WASHINGTON, D.C. MEETING, AUGUST 28 - SEPTEMBER 2, 1983

RAPID DISSOLUTION OF COAL FOR ANALYSIS FOR  
SULFUR, IRON, AND OTHER ELEMENTS

By

R. Markuszewski, B. C. Wheeler, and R. S. Johnson  
Iowa State Mining and Mineral Resources Research Institute  
Iowa State University, Ames, Iowa 50011

and

C. C. Hach  
Hach Chemical Company, P.O. Box 389, Loveland, Colorado 80537

ABSTRACT

Most dissolution methods necessary for the determination of major, minor, and trace constituents in coal are tedious and require unusual procedures. A rapid dissolution method is based on heating 250 mg coal with 10 ml of a 4:3:3 mixture of  $\text{HNO}_3$ ,  $\text{HClO}_4$  (72%), and  $\text{H}_3\text{PO}_4$  (85%). In numerous analyses of 8 subbituminous and bituminous coals using a simple digestion apparatus, the entire sample was dissolved in 20-45 min., leaving silica in a pure form suitable for determination by filtration, ignition, and weighing as  $\text{SiO}_2$ . In the clear filtrate, total sulfur was determined by a turbidimetric measurement of  $\text{BaSO}_4$ . For the 8 coals, containing 0.41-4.20% S, the results agreed well with those obtained by using a combustion method followed by automatic iodometric titration of the  $\text{SO}_2$ . In other aliquots of the same filtrate, total iron was determined spectrophotometrically using FerroZine. For an iron range of 0.113-1.762%, the standard deviations were 0.001-0.050. The clear digest can be also used to determine other elements by spectrophotometric, atomic absorption, or other procedures.

GENERAL PAPERS - POSTER SESSION  
PRESENTED BEFORE THE DIVISION OF PETROLEUM CHEMISTRY, INC.  
AMERICAN CHEMICAL SOCIETY  
WASHINGTON, D. C. MEETING, AUGUST 28-SEPTEMBER 2, 1983

GUM AND DEPOSIT FORMATION FROM JET TURBINE AND DIESEL FUELS

By

F. R. Mayo and B. Y. Lan  
SRI International, Menlo Park, California 94025

INTRODUCTION

The objective of this work is to determine the chemistry of deposit formation in hot parts of jet turbine and diesel engines and, thus, to predict and prevent deposit formation.

Previous work in the field has been extensive (1, 2), but a real understanding of deposit formation has been elusive. Work at SRI started on the basis that deposit formation from fuels must take place stepwise and is associated with autoxidation and the hydroperoxide produced (3). More recent work (4) showed that in the absence of dissolved oxygen, higher temperatures are required for deposit formation. Our recent report (5) indicated that gum and deposit formation proceed mainly through oxidation products of the parent hydrocarbon, coupling of these products to dimeric, trimeric and higher condensation products (partly or wholly by radicals from hydroperoxides) and precipitation of insoluble products. We know of no information on how these first precipitates are converted to the ultimate, very insoluble, carbonaceous materials that cause engine problems.

The present paper describes measurements of rates of oxidation and soluble gum formation in both pure hydrocarbons and mixed hydrocarbon fuels. Some patterns appear that can be largely explained on the basis of what is known about co-oxidations of hydrocarbon mixtures.

EXPERIMENTAL PROCEDURES

All of our hydrocarbons and fuels were distilled at about 10 torr before use. This step eliminated the highest boiling 2-5% of the fuels, but was essential to eliminate whatever gum had accumulated before the fuel was distilled. The fuels were then stored under nitrogen at -8°C until used. Some of the purchased "pure" hydrocarbons exhibited marked induction periods on oxidation, but in all such cases, chromatography through acidic alumina resulted in faster oxidations at fairly steady rates.

All of our oxidations were carried out in an oil bath at 130°C, with shaking under air. At intervals, 70- $\mu$ L samples of gas were withdrawn and analyzed for oxygen/nitrogen ratio by gas chromatography on a 6' x 1/8" O.D. stainless steel column packed with 13X molecular sieve and attached to a thermal conductivity detector. Soluble gum was determined by evaporating a weighed 5-mL sample of fuel in a gentle stream of nitrogen at 160°C (without spattering). The residue (~0.1 mL) was then transferred with 1-2 mL of acetone to a tared aluminum dish weighing about 50 mg. This sample was then brought to constant weight (3-10 h) in a gentle stream of nitrogen in a furnace at 200°C. Weighings were made on a Perkin Elmer AD-22 electromicrobalance. This method gave results reproducible within 20% at low levels of gum, usually within 5% at higher levels.

Fuels A and C are very stable and very unstable jet turbine fuels supplied by NASA-Lewis Research Center. Fuels 1, 10, 13, 14 and 15 are diesel fuels supplied by the U. S. Army Fuels and Lubricants Research Laboratory.

RESULTS

Table I summarizes our work on pure hydrocarbons and several fuels; it shows that gum formation is closely associated with oxidation. Indene and N-methylpyrrole (NMP) are listed separately at the bottom of the table because they are special cases. The other materials are listed in the first column of figures according to decreasing rates of oxygen absorption under air at 130°C. There is a clear distinction between the pure compounds, which oxidize faster and the fuels, which oxidize slower. The second column of figures lists the same materials in order of decreasing rate of gum formation, which is nearly the same as the order for oxidation. The figures in the last column are the quotients of the rates for the indicated fuels in the previous columns. This column shows that the pure, fastest oxidizing compounds usually require the most oxygen to produce a milligram of gum, or that the fuels at the bottom of this column produce the most gum for the oxygen absorbed. The quotient is constant with time for Fuel A; similar information is lacking for other fuels.



TABLE I

|                     | umole O <sub>2</sub><br>g fuel/hr | Mg gum<br>100 g fuel/hr |      | 100 umole O <sub>2</sub><br>mg gum |     |
|---------------------|-----------------------------------|-------------------------|------|------------------------------------|-----|
| 1-Phenylhexane      | 27.5                              | EtN                     | 6.4  | 1-PH                               | 40  |
| Phenylcyclohexane   | 27.2                              | PCH                     | 5.7  | DOD                                | 15  |
| n-Dodecane          | 24.0                              | C                       | 5.1  | BCH                                | 4.8 |
| Bicyclohexyl        | 18.5                              | BCH                     | 3.9  | PCH                                | 4.7 |
| 2-Ethyl-naphthalene | 4.7                               | DOD                     | 1.6  |                                    |     |
|                     |                                   | 1-PH                    | .71  | 14                                 | 1.3 |
| Fuel C              | 3.8                               |                         |      | A                                  | .80 |
| Fuel 14             | .78                               | 14                      | .58  | C                                  | .75 |
| Fuel 13             | .20                               | 13                      | .48  | EtN                                | .73 |
| Fuel 15             | .17                               | 15                      | .28  | 10                                 | .65 |
| Fuel 10             | .09                               | 1                       | .19  | 15                                 | .59 |
| Fuel 1              | .06                               | 10                      | .14  | 13                                 | .42 |
| Fuel A              | .05                               | A                       | .05  | 1                                  | .34 |
| N-Methylpyrrole     | 97                                | IND                     | 1282 | NMP                                | .14 |
| Indene              | 91                                | NMP                     | 684  | IND                                | .07 |

Table I shows that the rate of gum formation increases with the rate of oxygen absorption. Although the unstable Fuel C oxidizes and produces gum 80-100 times as fast as stable Fuel A, the oxygen required to make a milligram of gum is the same for the two fuels.

The special cases of indene and NMP are now considered. The other compounds and fuels in Table I apparently give mostly hydroperoxides as primary oxidation products. Other products are peroxide decomposition products and small yields of condensation products (gum). However, indene (6) and probably NMP copolymerize with oxygen to give alternating polyperoxides that are nonvolatile until they decompose thermally. The rates of oxygen absorption and gum formation are very high and more gum is left after decomposition of the polyperoxide and, therefore, less oxygen is required to produce this gum than for any other pure compound or fuel in Table I.

Study of the data in Table I gives rise to the question: Why do all the fuels oxidize slower than all the pure compounds, even though the fuels contain mostly compounds like the models? How does Fuel A differ from Fuel C? What are the important minor components in the fuels?

The classic work of Russell (7) on the co-oxidation of cumene and tetralin and the expansions by Mayo and coworkers (8) and Sajus (9) provide examples of rates of oxidation of hydrocarbon mixtures. Figure 1 is a plot of Russell's data on the rate of oxidation of cumene-tetralin mixtures at 90°C at a constant rate of chain initiation. Although tetralin alone oxidizes faster than cumene alone under these conditions, 4% of tetralin significantly retards the rate of oxidation of cumene. The high reactivity of pure tetralin with tetralylperoxy radicals can offset the high reactivity of tetralylperoxy radicals with each other (chain termination), but in dilute tetralin, which reacts with peroxy radicals much faster than cumene, the effect of fast chain termination predominates. Figure 1 shows that increasing proportions of tetralin may either decrease (at <4% tetralin) or increase (at >4% tetralin) the rate of oxidation of a mixture that is mostly cumene.

Figure 2 shows how these principles apply in mixtures of indene (which oxidizes much faster) and dodecane. At the lowest concentrations of indene, rates of oxidation are lower than for either pure hydrocarbon, at least until the indene is depleted, but with 1 M indene in dodecane, the rate of oxidation is faster than for dodecane alone and approaches the rate for indene in an inert solvent. NMP has a similar effect. The curves in Figure 3 show that the oxidation of Fuel A is so slow that it is not clear whether the initial oxidation is retarded by a little NMP. But the rate of oxidation increases as more NMP is added. These results are qualitatively satisfying, but they cannot be treated quantitatively. The Russell treatment (6) requires a constant rate of chain initiation, which is uncontrolled in our experiments. Our results do not suggest any catalytic effects of impurities or additives; as far as we can tell, these accelerators and retarders are consumed when they produce effects.

Several of our distilled fuels have been passed through acidic alumina to remove minor polar components, which have sometimes been returned to chromatographed fuel to reconstitute the original fuel. Figure 4 shows triplicate experiments with Fuel 10. The chromatographed fuel oxidizes faster initially than the distilled fuel (the usual situation) and the reconstituted fuel behaves

like the distilled fuel. Figure 4 shows the reproducibility of both the oxygen absorption and gum measurements (numbers at final points on curves). There is a close parallel in Figure 4 between the oxygen absorbed and the gum found.

The data in Tables II and III provide a comparison of Fuel A with Fuel C. By H/C ratio, Fuel C contains more aromatic material than Fuel A. Both fuels were examined by field ionization mass spectroscopy by Dr. S. E. Buttrill, Jr. and Mr. G. A. St. John, with the results shown in Table III. The instrument used could not distinguish between paraffins and alkyl naphthalenes, but to be consistent with the differences in H/C ratios in Table II, Fuel C must be higher in alkyl naphthalenes.

TABLE II  
ANALYSES OF FUELS

|                  | %C   | %H   | %N    | %S    | %<br>(diff.) | H/C  |
|------------------|------|------|-------|-------|--------------|------|
| Fuel A           | 86.4 | 13.3 | <0.02 | <0.02 | <0.36        | 1.83 |
| Gum from A + NMP | 68.0 | 5.9  | 6.2   | 19.9  | O + S        | 1.03 |
| NMP, calc        | 74.3 | 7.1  | 17.3  | 0     | 0            | 1.40 |
| Fuel C           | 87.6 | 11.9 | <0.02 | 0.03  | <0.19        | 1.63 |

TABLE III  
CLASSES OF HYDROCARBONS BY MOLE % IN FUELS A AND C

| Hydrocarbon<br>Class → | Alkanes<br>+C <sub>10</sub> H <sub>7</sub> R | Ring or C=C |      |     | PhR  | Indanes,<br>Tetralins | $\bar{M}_n$ |
|------------------------|--|-------------|------|-----|------|-----------------------|-------------|
|                        |  | 1           | 2    | 3   |      |                       |             |
| Fuel A                 | 20.0   | 16.9        | 15.7 | 5.0 | 28.3 | 14.1                  | 151         |
| Fuel C                 | 45.4   | 10.3        | 6.9  | 2.9 | 19.3 | 15.2                  | 159         |

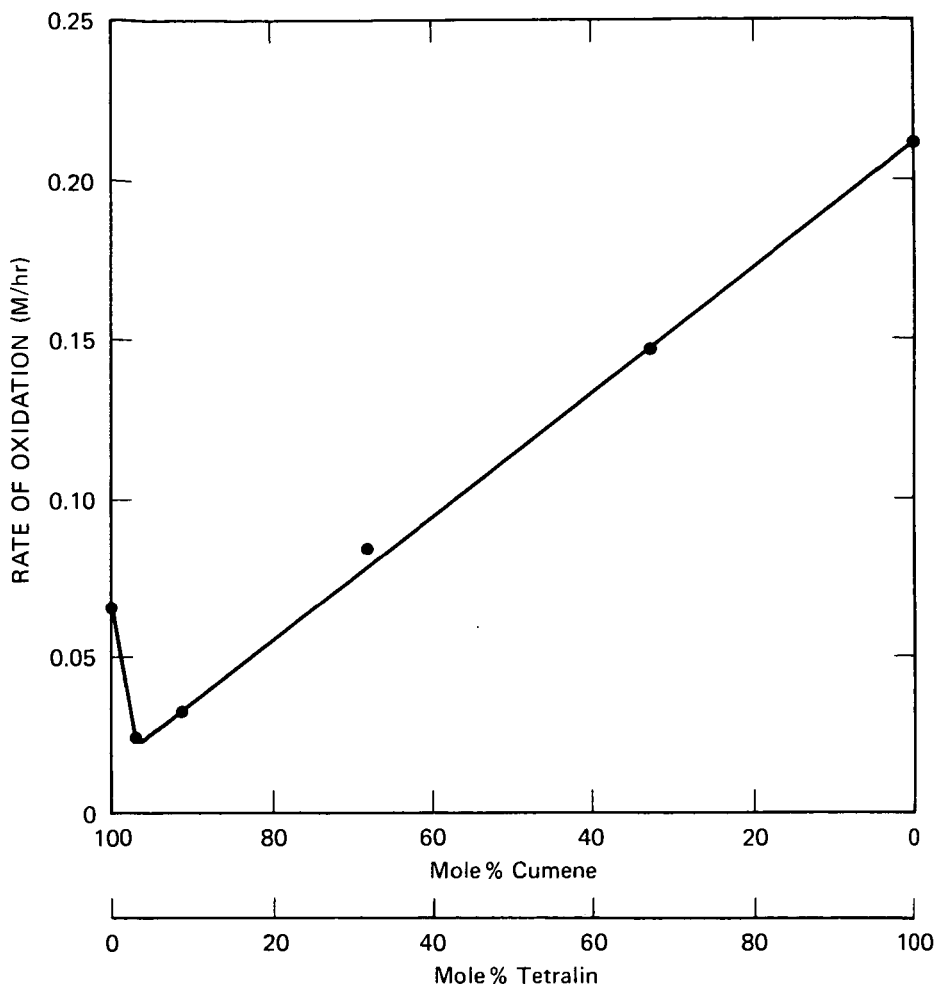
Table IV lists analyses of polar concentrates from three fuels. The polar concentrates contain more oxygen, nitrogen and sulfur than Fuels A and C and two of them are especially high in oxygen, suggesting that the fuels had undergone some oxidation before they reached us. The polar components of Fuels 10 and 13 were also analyzed by gas chromatography/mass spectroscopy. The Fuel 10 residues were rich in fluorene and phenanthracene/anthracene and their alkyl derivatives. Fuel 13 contained a wider range of products, in which carbazole and alkylcarbazoles were identified.

TABLE IV  
ANALYSES OF POLAR CONCENTRATES

|         | %C   | %H  | %N   | %S   | %<br>(diff.) | H/C  |
|---------|------|-----|------|------|--------------|------|
| Fuel C  | 74.9 | 6.0 | 0.20 | 18.9 | O + S        | 0.98 |
| Fuel 10 | 85.8 | 8.5 | 0.94 | 1.87 | 2.85         | 1.18 |
| Fuel 13 | 80.0 | 9.1 | 1.14 | 0.85 | 9.0          | 1.35 |

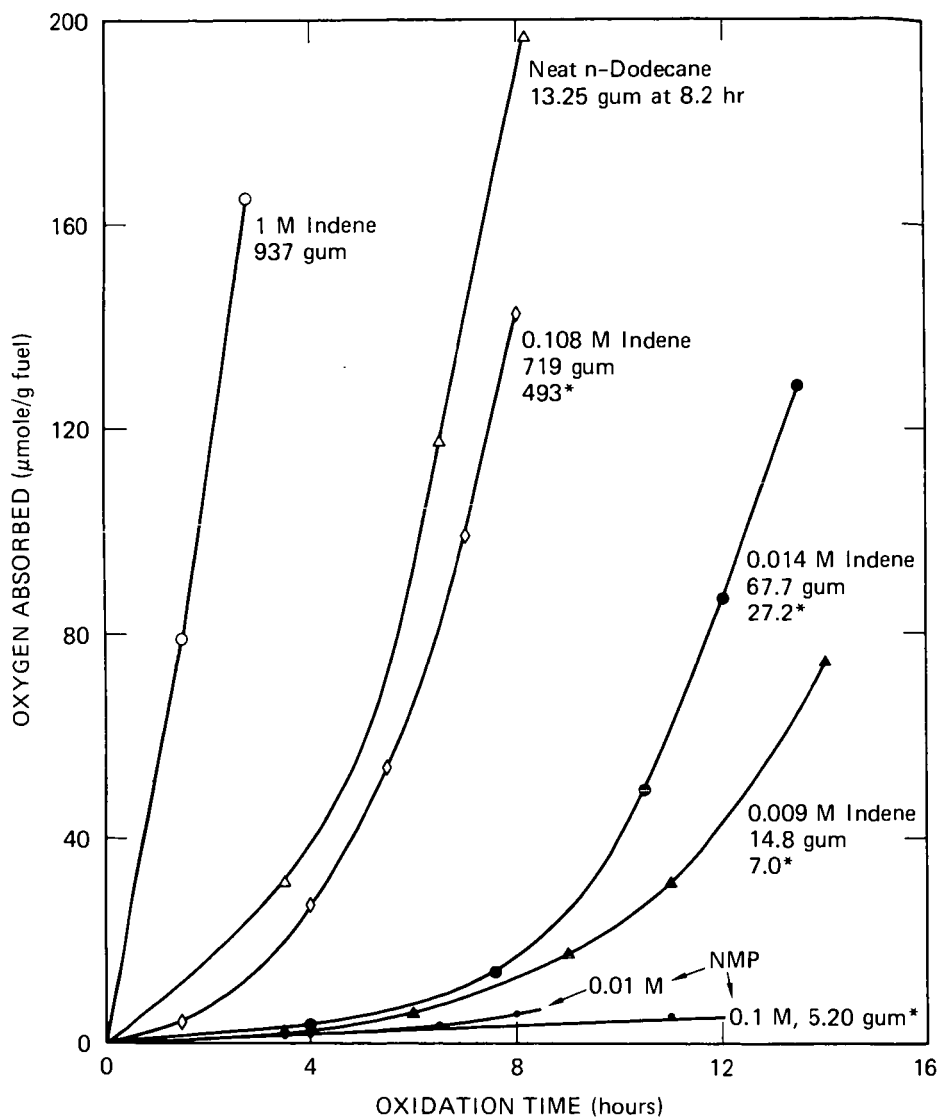
#### CONCLUSIONS

Our present working hypothesis is that deposits on hot engine parts come mostly from soluble gum formed on storage but maybe partly during heating of the fuel in the engine. The compounds that copolymerize with oxygen to give polyperoxides require the least oxygen to give a milligram of gum, but among other pure hydrocarbons and fuels, the rates of gum formation and oxygen absorption decrease together. It appears that the coupling of fuels and their primary oxidation products to form products of higher molecular weight, soluble gum and deposits is a small part of the chain termination reaction in which some of the free radicals that are involved in oxidation couple (terminate) instead of propagating. The faster the oxidation, the more coupling occurs. The dependence of rate of oxidation on rate constants for initiation, propagation and termination is expressed by the well known equation,



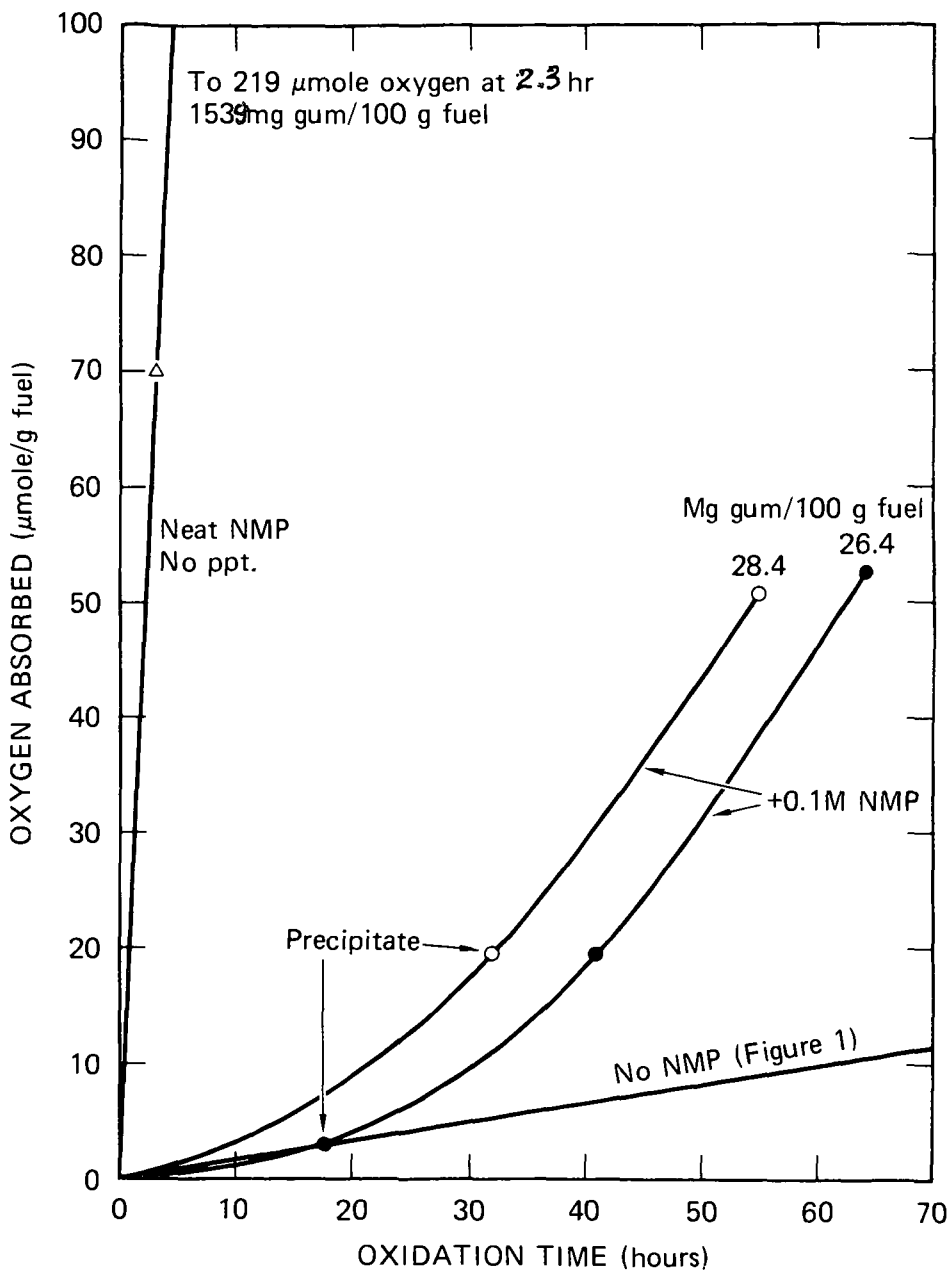
JA-2115-18

FIGURE 1 COOXIDATION OF CUMENE AND TETRALIN WITH 0.02 M  $t\text{-BuO}_2\text{Bz}$  AT  $90^\circ\text{C}$   
Data of G. A. Russell (ref. 6)



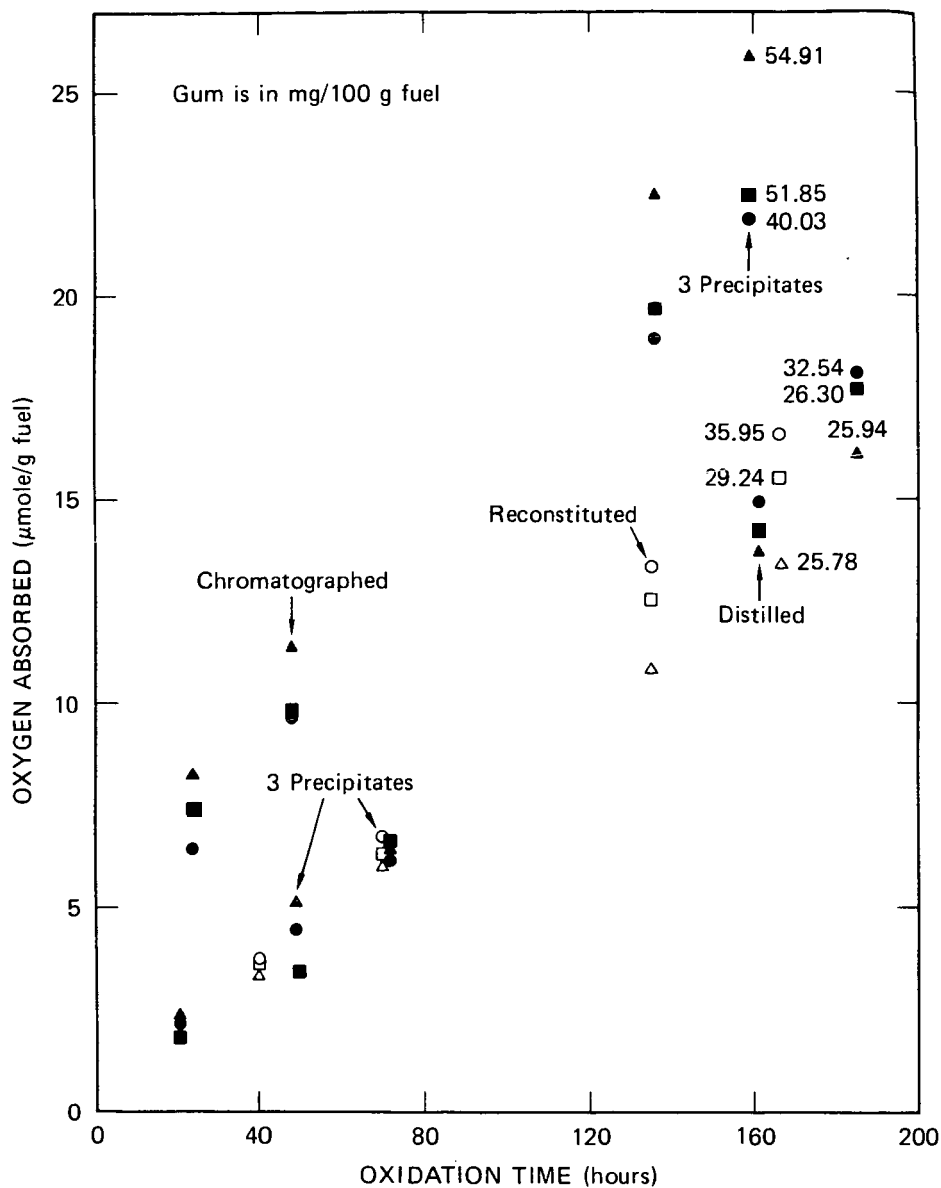
JA-2115-16A

FIGURE 2 OXIDATIONS OF n-DODECANE WITH INDENE AND NMP AT 130°C  
Gum is in mg/100 g fuel, determined at 100°C except when marked \* for 200°C.



JA-2115-22

FIGURE 3 OXIDATION OF FUEL A AND NMP AT 130°C



JA-1924-16

FIGURE 4 OXIDATION OF FUEL 10 IN AIR AT 130°C

$$R_O = (k_i/k_t)^{1/2} k_p [RH]$$

For fuels that contain mostly paraffins, naphthenes and alkylbenzenes, the  $k_p$ s should be quite similar. We think that  $k_t$  is the most susceptible of the three constants to the effect of other fuel components, which may explain why nearly all the fuels oxidize and produce gum slower than the pure hydrocarbons. Although  $k_i$  can be affected moderately by minor components, any effect on increasing the rate of peroxide decomposition will be offset by a decrease in the steady state concentration of peroxides. It is known that polynuclear aromatic hydrocarbons and their alkyl derivatives are very reactive toward peroxy radicals and that their chain termination constants in oxidation vary over a wide range (10).

Although a non-radical condensation mechanism has not been excluded and although details of a radical condensation mechanism are lacking, it appears to us now that the most fruitful approach to understanding and reducing gum and deposit formation in fuels is through the effects of condensed aromatic and heterocyclic compounds on the rates of oxidation of fuels.

Other factors that appear to be critical in gum and deposit formation are the effects of oxygen concentration and metals and the mechanism by which soluble gum evolves into insoluble deposits. Our conclusions based on oxidation at 130°C should eventually be confirmed by tests at storage temperatures, although the relative stabilities of fuels appear not to change much between 40 and 150°C (11).

#### ACKNOWLEDGMENT

This research was supported by the U. S. Army Research Office and NASA-Lewis Research Center.

#### LITERATURE CITED

- (1) Nixon, A. C., Chapter 17 in *Autoxidation and Antioxidants*, W. O. Lundberg, ed., Wiley Interscience, NY (1962).
- (2) CRC Literature Survey on the Thermal Oxidation Stability of Jet Fuel, Report No. 509 of Coordinating Research Council, Inc., Atlanta (1979).
- (3) Mayo, F. R., Richardson, H. and Mayorga, G. D., PREPRINTS, Div. of Petrol. Chem., ACS, 20 (1), 33 (1975).
- (4) (2), pg. 71.
- (5) Mayo, F. R., Buttrill, S. E., Jr., Lan, B., St. John, G. A. and Dulin, D., Preprints, Div. of Fuel Chem., 27 (2), 76 (1982).
- (6) Russell, G. A., J. Amer. Chem. Soc., 78, 1035, 1041 (1956).
- (7) Ibid., 77, 4583 (1955).
- (8) Mayo, F. R., Syz, M. G., Mill, T. and Castleman, J. K., Adv. Chem. Series, 75, 38 (1968).
- (9) Sajus, L., Adv. Chem. Series, 75, 59 (1968).
- (10) Huntington, J. G., Mayo, F. R. and Kirschen, N. A., Fuel, 58, 31 (1979).
- (11) Stavinocha, L. L., Westbrook, S. R. and Brinkman, D. W., DOE/BC/10043-12 (1980).

GENERAL PAPERS - POSTER SESSION  
PRESENTED BEFORE THE DIVISION OF PETROLEUM CHEMISTRY, INC.  
AMERICAN CHEMICAL SOCIETY  
WASHINGTON, D.C. MEETING, AUGUST 28 - SEPTEMBER 2, 1983

FT-IR MEASUREMENTS OF ALIPHATIC AND AROMATIC  
C-H GROUPS IN COAL

By

B. Riesser, M. Starsinic, A. Davis, and P. C. Painter  
College of Earth and Mineral Sciences  
The Pennsylvania State University, University Park, Pennsylvania 16802

ABSTRACT

The experimental difficulties involved in the study of coal structure are both notorious and well-documented. Nevertheless, recent improvements in spectroscopic instrumentation have allowed the determination of what are thought to be reasonably accurate parameters describing an average coal structure. For example, Fourier transform infrared spectroscopy (FT-IR) has been applied to the determination of aromatic and aliphatic hydrogen. Unlike measurements of aromaticity by NMR, however, infrared methods rely on calibrating the intensities of specific bands to the concentration of the appropriate functional groups, using model compounds or other procedures. We have recently found that the values obtained depend heavily on the choice of bands and the methodology employed. In addition, the calibration coefficients vary considerably with rank. We will discuss the various approaches we have employed and the errors involved in each. Our results indicate that the best that can be achieved is the definition of a band of values of aromatic and aliphatic hydrogen.



## SULFUR COMPONENTS ANALYSIS IN HYDROCARBON MATRIX BY GAS CHROMATOGRAPHY

By

O. Puzic

Esso Chemical Canada, P. O. Box 3004, Sarnia, Ontario, Canada N7T 7M5

### INTRODUCTION

Determination of low concentrations of sulfur-containing gases has received considerable attention in recent years (1-6). The need is particularly acute in the petroleum industry, since the trace amounts of sulfur compounds cause corrosion and poison catalysts. Because of their reactivity and labile nature, as well as diversity of stream composition, determination of sulfur components in hydrocarbon matrix is a complex and intricate task. This paper presents a method for GC analysis of trace levels (0-200 ppm) of sulfur compounds in gaseous hydrocarbon streams.

### EXPERIMENTAL

#### Chromatography

Varian Model 3700 Gas Chromatograph equipped with a Dual Flame Photometric and a Flame Ionization Detector (FPD and FID, respectively) and Vista 401 Dual Channel Data System was employed. Material used for sample transfer lines, 1 cc gas sample loop and the column was high grade, acetone-washed nickel. The gas sample was introduced onto the column via a six port teflon Valco valve. Two certified standard gas blends, compressed in an aluminum gas cylinder from Scott Specialty Gases, were used as calibration gases. Standard 1 contained: hydrogen sulfide, methyl mercaptan, ethyl mercaptan, dimethyl sulfide and dimethyl disulfide in nitrogen matrix. Standard 2 contained: dimethyl sulfide, methyl ethyl sulfide, diethyl sulfide and diethyl disulfide in nitrogen matrix. The concentration of each component was certified within  $\pm 2\%$ . Ultra high purity He was used for the carrier gas and high purity hydrogen and air for the flame gases in the two detectors. The optimal flow rates for the flame photometric detector fuel gases were found to be:  $H_2$ , 142 ml/min; air #1, 80 ml/min; air #2, 170 ml/min. In the first flame, decomposition of the sample takes place. Combustion products from sulfur-containing compounds will produce optical emission in the second flame from the  $S_2$  radicals formed. The Varian flame photometric detector employs a filter with maximum optical transmission at 365 nm for sulfur detection. For the flame ionization detector, the fuel gas flow rates were:  $H_2$ , 30 ml/min; and air, 300 ml/min. The carrier gas flow rate was 26 ml/min.

The type of column packing material used for trace sulfur analysis depends on the stream composition and the hydrocarbon concentration. For most applications, a complete separation of various sulfur species as well as resolution between hydrocarbons and sulfur compounds such as  $H_2S$ ,  $C_1$  and  $C_2$  mercaptans, sulfides and disulfides was achieved using a 6' x 1/8" acetone-washed nickel column packed with oxo-propionitrile/Porasil C - Durapak 80-100 mesh. However, when analyzing  $H_2S$  in propylene rich streams (propylene concentration greater than 10%), there is no longer a baseline separation between  $H_2S$  and propylene with this column. A phenomenon referred to as "quenching effect" takes place in the detector, whereby the decrease in sulfur response is apparently due to inactivation of the excited  $S_2$  species by its combination or collision with a hydrocarbon and its degradation products (5, 7). Silicone, QF-1 (5%) on Porapak QS column packing material will provide the necessary separation in the  $H_2S$  region when high propylene concentration is expected (6).

An effluent splitter (ratio 50:50) is placed on the outlet of the column to send identical gas streams to the FPD and the FID, thereby allowing detection of components on both detectors simultaneously. The temperature programming profile suitable for most applications was: initial temperature, 70°C; final temperature, 100°C; hold, 45 min.; rate 10°C/min. Retention times for various sulfur compounds obtained using the chromatographic conditions described above are presented in Table I.

#### Calibration and Analysis

For quantitative analysis of sulfur species, an external standard method was used for calibration. After the sample loop had been purged with the calibration gas for several minutes, the sample of calibration gas was injected, at atmospheric pressure, by means of a six-port injection

valve. The temperature program and data acquisition were then activated simultaneously. After the calibration run was completed the response factors were generated or updated (8).

TABLE I

| Compound                | Mol. Wt | B. P. (°C) | Retention Time, min. |
|-------------------------|---------|------------|----------------------|
| Hydrogen sulfide        | 34.08   | -60.7      | 0.71                 |
| Methyl mercaptan        | 48.11   | 6.2        | 1.99                 |
| Ethyl mercaptan         | 62.13   | 35.0       | 3.38                 |
| Dimethyl sulfide        | 62.13   | 37.3       | 4.98                 |
| Methyl ethyl sulfide    | 76.16   | 66.6       | 9.05                 |
| Dimethyl disulfide      | 94.20   | 109.7      | 9.63                 |
| Methyl propyl sulfide   | 90.19   | 95.5       | 14.79                |
| Diethyl sulfide         | 90.19   | 92.1       | 16.90                |
| Methyl isobutyl sulfide | 104.22  | 112.5      | 21.88                |
| Diethyl disulfide       | 122.25  | 154.0      | 30.89                |
| Dipropyl sulfide        | 118.24  | 142.4      | 46.62                |

Providing that the flow rates of the fuel gases to the flame photometric detector have not changed, there should be no need for frequent recalibration. However, the calibration blend is analyzed daily to assure optimal performance of the system. Following calibration, a hydrocarbon sample from a high pressure gas cylinder is purged through the sample loop and injected in the same manner. Figure 1 presents a typical chromatogram for sulfur analysis in a hydrocarbon matrix.

Precision data for 10 replicate runs of the two calibration blends is presented in Table II.

TABLE II

| Compound             | Level (ppm) | Std. Dev. | Retention Time (min.) | Std. Dev. |
|----------------------|-------------|-----------|-----------------------|-----------|
| Hydrogen sulfide     | 15.4        | 0.2       | 0.71                  | 0.03      |
| Methyl mercaptan     | 16.2        | 0.1       | 2.00                  | 0.04      |
| Ethyl mercaptan      | 15.9        | 0.1       | 3.38                  | 0.03      |
| Dimethyl sulfide     | 15.7        | 0.1       | 4.99                  | 0.03      |
| Dimethyl disulfide   | 15.9        | 0.3       | 9.63                  | 0.04      |
| TOTAL                | 79.1        | 0.7       |                       |           |
| Dimethyl sulfide     | 16.3        | 0.1       | 4.99                  | 0.03      |
| Methyl ethyl sulfide | 16.1        | 0.1       | 9.05                  | 0.04      |
| Diethyl sulfide      | 15.9        | 0.1       | 16.90                 | 0.04      |
| Diethyl disulfide    | 15.3        | 0.4       | 30.89                 | 0.04      |
| TOTAL                | 63.6        | 0.7       |                       |           |

### Sampling

During the course of the quantitative GC analysis of sulfur compounds in gaseous hydrocarbon streams it was observed that the light sulfur compounds (namely hydrogen sulfide and methyl mercaptan) were being depleted in the standard high pressure sampling cylinders.

Figure 2 presents the rate of H<sub>2</sub>S depletion in standard 2250-ml stainless steel sampling cylinders (Cyls. No. 1 to 3). The cylinders were filled with Matheson certified standard containing 230 ppm H<sub>2</sub>S in nitrogen. Within four minutes, 70% of the sulfur content was lost (cylinder No. 1). After 20 minutes no H<sub>2</sub>S could be detected in the sample cylinder. Cylinder No. 1A is actually cylinder No. 1 that was steam cleaned, dried under house vacuum and refilled with the Matheson standard. A similar sulfur loss was confirmed by the Dohrman Sulfur Analyzer.

In another experiment, a clean sampling cylinder was filled with 290 ppm of H<sub>2</sub>S in ethylene to determine if the hydrocarbon matrix affects the rate of sulfur loss. As illustrated in Figure 3 (curve I), the concentration of H<sub>2</sub>S decreased 50% in less than 10 minutes. The same cylinder was flushed with helium, evacuated on a high vacuum line and refilled with the same amount of H<sub>2</sub>S in ethylene. Although the number of active sites on the inner walls had been reduced, the passivation in this manner did not eliminate the problem entirely (curve II). After the initial drop in sulfur concentration, the rate of loss had reduced. Eventually, sulfur was lost completely overnight.

The same cylinder used in the above experiment was emptied but not cleaned and again refilled with 290 ppm H<sub>2</sub>S in ethylene (Figure 4).

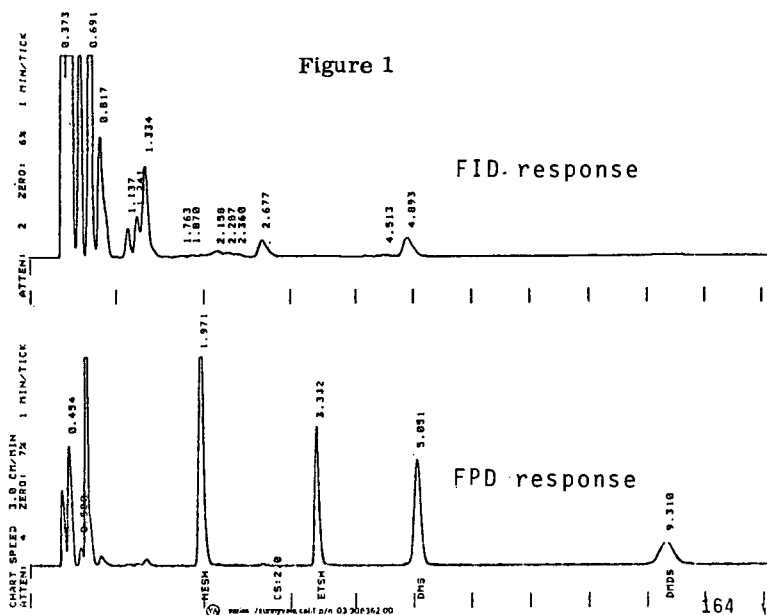


Figure 2. HYDROGEN SULFIDE IN NITROGEN MATRIX

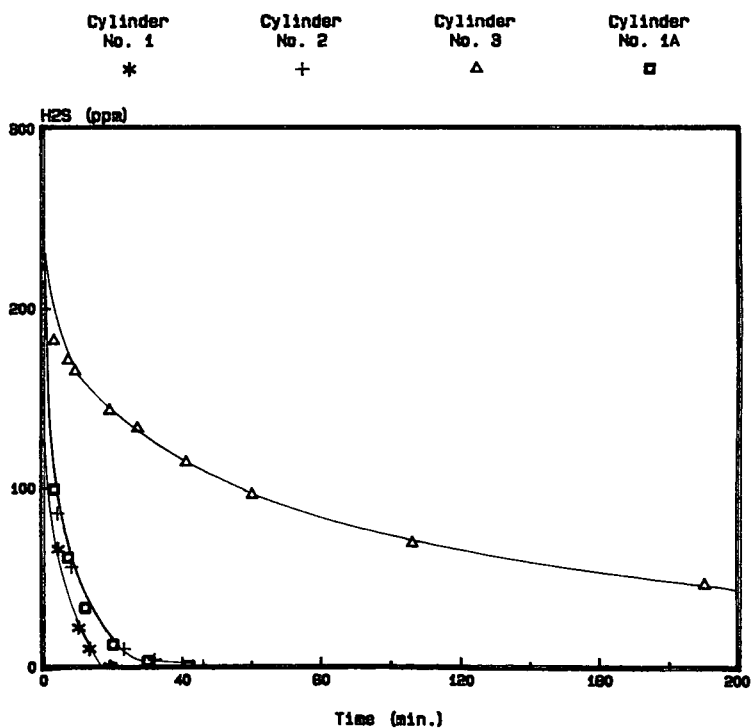


Figure 3. HYDROGEN SULFIDE IN HYDROCARBON MATRIX

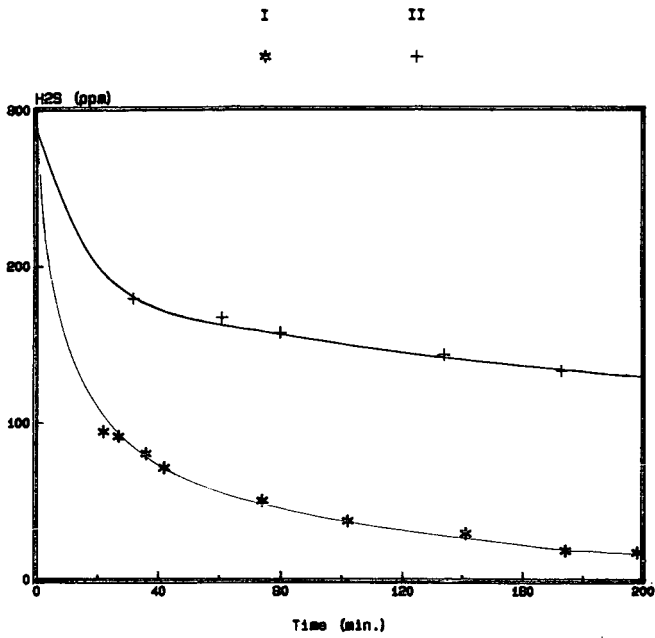


Figure 4. EFFECT OF MOISTURE

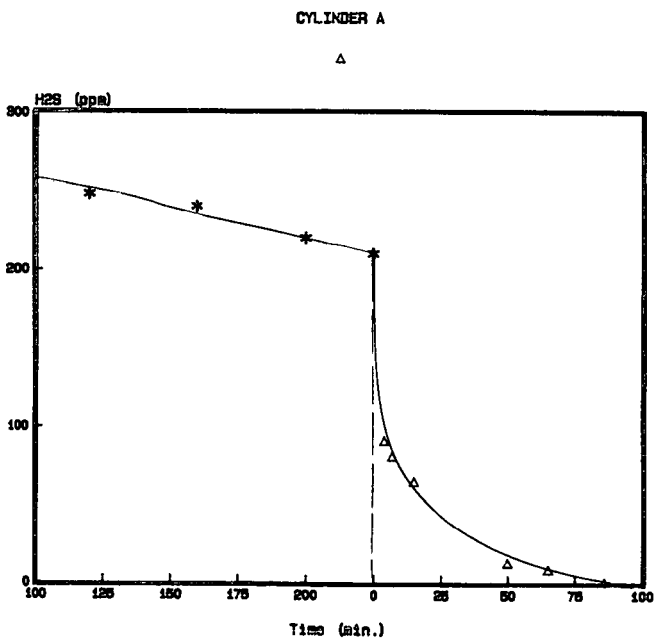


Figure 5. TEFLON-GRAPHITE COATING

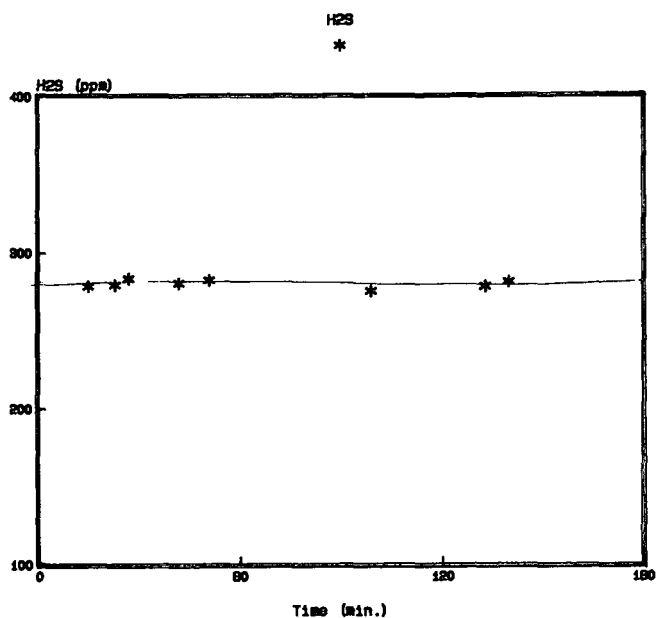
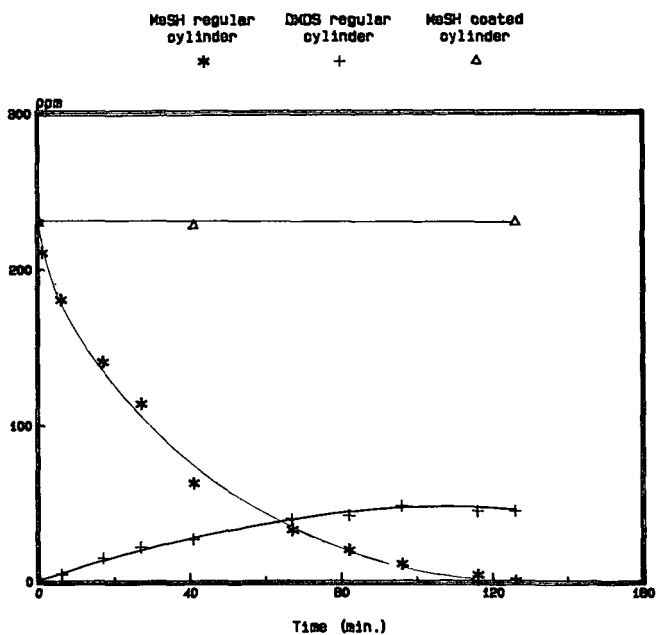
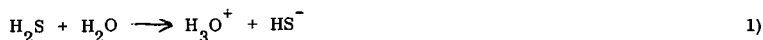


Figure 6. METHYL MERCAPTAN IN HYDROCARBON MATRIX



Presumably, the walls of the sample cylinder were further passivated, and the sulfur depletion rate was very low. After about 4 hours at a sulfur concentration of 210 ppm, the sample was transferred to a cylinder (passivated in the same manner) that contained 0.2 ml of water. A sudden drop in sulfur content (curve A) illustrates the high solubility of  $H_2S$  in water according to the reaction:



Provided a moisture-free environment is assured, adsorption on the metal walls appears to be the predominant cause for the decrease in sulfur concentration.

In an attempt to contain light sulfur compounds, a 2250 ml gas sample cylinder was lined with 0.0005 inch of teflon-graphite where the coating was baked onto the metal surface. The cylinder was tested with the same  $H_2S$  in ethylene mixture as in previous experiments (Figure 5). There was no apparent decrease in  $H_2S$  concentration over a period of 48 hours.

Figure 6 presents the comparative study of the two types of sample cylinders, i.e., teflon-graphite coated and regular (stainless steel) when methyl mercaptan is present in the hydrocarbon environment (ethylene matrix). Rapid oxidation of methyl mercaptan to dimethyl disulfide, reaction probably being catalyzed by the metal surface, as well as depletion on the walls is evident in the "regular" cylinder. However, in the teflon-graphite coated cylinder, the reaction did not take place and mercaptan content was unchanged over the time period indicated.

#### DISCUSSION

The unique and reactive properties associated with sulfur gases have presented difficult obstacles in attempts to contain low levels of these gases in high pressure cylinders (9, 10). Many factors are responsible for the apparent loss of sulfur content in the standard sample cylinders, such as, among others:

- Chemical reaction with, or promoted by, water molecules.
- Adsorption and/or reaction on the walls of the sampling cylinders.
- Oxidation of mercaptans to disulfides.

The results of this study indicate that gas mixtures containing low concentrations of sulfur compounds can exhibit stability if proper cylinder material and cylinder treatment techniques are used. Further evaluation of the teflon-graphite coated cylinders for their suitability in sampling of sulfur containing gases in various plant streams is under way. In addition, long term experience is being gathered.

#### LITERATURE CITED

- (1) Ferguson, D. A. and Luke, L. A., *Chromatographia*, 12, 197 (1979).
- (2) Patterson, P. L., *Anal. Chem.*, 50, 345 (1978).
- (3) Feeney, M., DeGood, J. and Warren, E., *Pittsburgh Conf., Abstracts*, No. 350 (1982).
- (4) McGaughey, J. F. and Gangwal, S. K., *Anal. Chem.*, 52, 2079 (1980).
- (5) Farwell, S. O. and Gluck, S. J., *Anal. Chem.*, 51, 609 (1979).
- (6) Pearson, C. D. and Hines, W. J., *Anal. Chem.*, 49, 123 (1977).
- (7) Fredriksson, S. A. and Cedergren, A., *Anal. Chem.*, 53, 614 (1981).
- (8) *Vista 401 Chromatography Data System Operators Manual*, Varian (1980).
- (9) Kramer, F. J. and Wechter, S. G., *J. Chrom. Sci.*, 18, 674 (1980).
- (10) Shultz, J. F., Karn, F. S. and Anderson, R. B., *Ind. Eng. Chem.*, 54, 44 (1972).

AN ANALYTICAL MODEL OF COMBUSTION OF SPENT OIL SHALE BLOCKS:  
THE MODEL AND EXPERIMENTS

By

M-D. Ho, E. M. Suuberg<sup>a</sup> and H. L. Toor

Department of Chemical Engineering, Carnegie-Mellon University, Pittsburgh, Pennsylvania 15213

INTRODUCTION

Oil shale, a potential source of liquid fuel, is a fine-grained, sedimentary rock composed of both organic and inorganic solid compounds. The production of liquid fuel from oil shale requires the retorting of the shale, in which oil and gas are destructively distilled from the shale rock, leaving behind a highly carbonaceous char within the spent shale matrix. The amount of char left depends on the richness of the raw shale. Typically, 23% by weight of the organic material originally present in the shale is left as char (1).

Combustion of this char could potentially provide all or part of the heat requirement for retorting of the shale (2). There have recently been several studies dealing with the combustion behavior of spent shale (2-8). Although char in shale is not pure carbon, most studies have treated it as carbon with reasonable success.

In the combustion of spent oil shale in an environment of air with other inert gases, there are three active components to be considered, O<sub>2</sub>, CO<sub>2</sub> and CO and four major chemical reactions (9, 10), namely:

• Direct oxidation of the residual char, a process which is limited by the diffusion of oxygen and which creates an "unburned core".



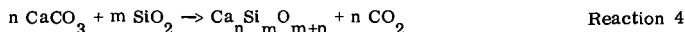
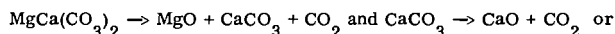
• Oxidation of CO



• CO<sub>2</sub>-C gasification reaction



• Carbonate decomposition reactions<sup>b</sup>



Therefore, the combustion of spent shale consists of two competing schemes: one is the direct oxidation of char; the other is the gasification of the char by CO<sub>2</sub> released from the carbonate decomposition reactions.

There have been several modeling studies of the combustion of spent shale in the presence of oxygen and nitrogen (2-7) which used the classical shrinking core model. This model assumes that the reaction rate is limited only by the internal diffusion of oxygen; hence, it neglects the other reactions (2, 3 and 4) which may play a major role at elevated temperature (above 875°K).

Mallon and Braun (7, 11) have included the decomposition and gasification reactions (3 and 4) in their model, but they treated the gasification reaction and the direct oxidation reaction independently and then superposed the two results. This approximation was inaccurate. Braun et al.

a. Present address: Division of Engineering, Brown University, Providence, Rhode Island 02912.

b. For the detail and kinetics of this reaction, see Manor et al (8).

(2) modeled gasification of spent oil shale blocks by steam and  $\text{CO}_2$  but did not consider oxidation reactions. Their solution scheme involved solving differential equations numerically.

Our previous publication (Manor et al. (8)) offered a model which successfully predicted the combustion behavior of shale in nitrogen diluted air, but that model also required the numerical solution of differential equations.

The model that we present here is an improvement over the model of Manor et al. The major advantage of the new model lies in the simplicity of the closed form result which eliminates the necessity of cumbersome numerical solution of the differential equations. Our new model thus allows more convenient use of the single particle (or block) combustion model in the modeling of packed bed retorts. Experiments similar to those carried out earlier were used to extend the data.

## DEVELOPMENT OF THE MODEL

Consider the burning sample shown schematically in Figure 1. We will use the assumptions that were employed by Manor et al. (8).

1. Mass transfer processes may be treated as pseudo-steady.
2. Only radial transport in a cylinder is considered.
3. Temperature is spatially uniform.
4. No significant pressure gradient exists within the shale.
5. The reaction of char with oxygen is fast enough to be lumped at the surface of the unburned core.
6. The gasification Reaction 3 occurs uniformly within the unburned core.
7. Carbonates decompose uniformly throughout the shale.
8. The bulk flow of all species out of the shale is dominated by the release of carbon dioxide from the decomposition of carbonates.
9. Fick's law holds for each component and all effective diffusivities are equal.

An additional assumption that allows the model to be treated analytically is that the oxidation reaction of carbon monoxide is instantaneous<sup>a</sup>.

### Transport Model

The formal statement of assumption 8 is:

$$N_t = R_4 \left( \pi r^2 / 2 \pi r \right) = R_4 r / 2 = G L y \quad (1)$$

where

$$L = C D_e / r_s$$

$$G = R_4 r_s^2 / (2 D_e C)$$

$$y = r / r_s$$

and where  $r_s$  is the radius of the cylinder. Other symbols are defined in the table of nomenclature.

The formal statement of assumption 9 is:

$$N_i = -C D_e dX_i / dr + X_i N_t \text{ or } N_i = -L dX_i / dy + X_i G L y, \quad i = \text{CO}, \text{CO}_2, \text{O}_2 \quad (2)$$

The species conservation equation for each component can be written as:

$$1/r \, d/dr (r N_i) = \sum_j \nu_{ij} R_j \quad (3)$$

where  $\nu_{ij}$  is the stoichiometric coefficient of component  $i$  with respect to  $R_j$ . At the surface of the cylindrical sample ( $r=r_s$  or  $y=1$ ), external mass transfer resistance is taken into account by specifying:

$$N_{i,s} = (K_x + N_t) [2 Q / (K_x + 2Q)] X_{i,s} - K_x [2 Q / (K_x + 2Q)] S_{i,f} \quad (4)$$

- a. The measured  $\text{CO}/\text{CO}_2$  ratio at the surface of the shale never exceeded 20% in the ignition stage and then declined very rapidly to a negligible value, therefore, we assume all  $\text{CO}$  is burned to  $\text{CO}_2$  very quickly in the presence of oxygen. See also Manor et al. (8) for more detail.



where  $Q$  is the molar flow rate of sweeping gas per unit surface area of the sample. The new correction term,  $[2Q/(K_x + 2Q)]$ , is used to take into account the change in sweeping gas compositions due to the mass transfer to and from the sample. When the gas flow rate is very large, the correction term reduces to unity and is not required.

Define a pseudo-component concentration:

$$X_1 \equiv 1/2 X_{CO} + X_{CO_2} + X_{O_2}, \quad N_{x_1} \equiv 1/2 N_{CO} + N_{CO_2} + N_{O_2}$$

It follows from Equation 3 and the stoichiometry of the reactions that

$$1/r \, d/dr (r N_{x_1}) = R_4 \quad (5)$$

The substitution of Equation 2 into Equation 5 yields:

$$1/y \, d/dy (-y (dX_1/dy) + X_1 G y^2) = G \quad (6)$$

subject to the boundary conditions that, at the center of the sample, the flux is zero and at the surface of the sample, Equation 4 holds for pseudo-component 1.

Thus, Equation 6 can be solved to give:

$$X_1 = 1 + Kx/(Kx + G L) (X_{1,f} - 1) \exp((y^2 - 1) G/2) \quad (7)$$

which eliminates one unknown.

For the sake of convenience, we shall first consider the two regions of shale separately: the unburned core region and the product of shell layer.

#### Core Reaction Model

The core reaction model is similar to the one in Manor et al. (8), it is rederived here for the convenience of the reader. Within the unburned core section, the conservation equation for CO can be written as:

$$1/r \, d/dr (r N_{CO}) = 2 R_3 \quad (8)$$

with boundary conditions:

$$r = 0, \quad dX_{CO}/dr = 0; \quad r = r_c, \quad X_{CO} = X_{CO,c}$$

where  $r_c$  is the radius of the edge of the unburned core. Assumption 6 allows  $R_3$  to be treated as position independent. Its value is evaluated at the average concentrations of reactants within the core. Therefore, Equation 8 can be integrated to give:

$$X_{CO} = (X_{CO,c} - B) \exp[(y_c^2 - y^2) G/2] + B$$

where

$$B = 2 R_3 / R_4 = R_3 (4GL/r_s)$$

Note that  $X_{CO_2} = X_1 - 1/2 X_{CO}$  in the core region, since  $X_{O_2} = 0$  and the average mole fractions are:

$$\langle X_{CO} \rangle = (X_{CO,c} - B) \left[ \frac{1 - \exp(-G y_c^2/2)}{G y_c^2/2} \right] + B \quad (9)$$

$$\langle X_{CO_2} \rangle = (X_{CO_2,c} - 1 + B/2) \left[ \frac{1 - \exp(-G y_c^2/2)}{G y_c^2/2} \right] + 1 - B/2 \quad (10)$$

where

$$X_{CO_2,c} = X_{1,c} - 1/2 X_{CO,c}$$

It is assumed that  $C_2O-C$  gasification proceeds at a rate given by the equation suggested by Ergun (13)

$$R_3 = \frac{K_a G_c}{1 + \langle X_{CO} \rangle / K_{ex} \langle X_{CO_2} \rangle} \quad (\text{gmole/cm}^3 \text{sec}) \quad (11)$$

where  $K_a = 4.5 \times 10^7 \exp(-24,500/T) + 3.75 \times 10^2 \exp(-16,000/T) \text{ sec}^{-1}$  (as suggested by Campbell and Burnham (9)).  $C_c$  is the molar concentration of char (gmole/cm<sup>3</sup>) and  $K_{ex} = 138 \exp(-7,500/T)$  (from Ergun and Menster (14)).

#### Shell Transport and Reaction Model

In order to eliminate reaction terms in the conservation equation, let us again create a pseudo-component  $X_2$ , where

$$X_2 \equiv X_{O_2} - 1/2 X_{CO}, \quad N_{x_2} \equiv N_{O_2} - 1/2 N_{CO}$$

If follows that in the shell region,

$$1/r \, d/dr (r N_{x_2}) = 0 \quad (12)$$

and with Equation 2 and dimensionless variables,

$$1/y \, d/dy [-y (dX_2/dy) + X_2 G y^2] = 0 \quad (13)$$

Equations 12 and 13 can be integrated to give

$$y N_{x_2} = M \quad (14)$$

and

$$X_2 = M/L \, F(y, y_c) \exp(G y^2/2) + X_{2,c} \exp[G/2(y_c^2 - y^2)] \quad (15)$$

where:

$$X_{2,c} = X_{O_2,c} - 1/2 X_{CO,c}, \quad F(y, y_c) = \int_{y_c}^y \frac{\exp(-G \tau^2/2)}{\tau} \, d\tau$$

and  $M$  is an integration constant. At  $y=1$ , Equation 4 is used as the other boundary condition.

Since we have assumed that the oxidation reaction of carbon monoxide is instantaneous, it follows that the coexistence of carbon monoxide and oxygen is not allowed and the flame front at which all the oxidation reactions occur is assumed to be infinitely thin.

The flame front occurs either at the core surface, case 1, or out of the core surface (i.e., at  $r > r_c$ ), i.e., case 2.

#### Case 1: Flame Front at the Core Surface

In this case, oxygen flux to the core surface will be consumed both by the reaction with carbon monoxide produced in the core and by the direct oxidation of char, i.e.,

$$-N_{O_2,c} = (R_1 + R_3) r_c / 2$$

where

$$R_1 = K_1 C_c X_{O_2,c}$$

and the value of  $K_1$  is provided by Sohn and Kim (10) as  $1.503 \times 10^7 \exp(-11102/T) \text{ sec}^{-1}$ . (In Manor et al. (8),  $K_1$  was assumed to be infinitely large.)

Since oxygen is present at the core surface in this case, we can assume  $X_{CO,c}$  and  $N_{CO,c}$  to be zero, which requires

$$X_{2,c} = X_{O_2,c} \text{ and } M = y_c N_{O_2,c}.$$

Therefore, we can calculate the oxygen flux by solving Equation 15 to get:

$$N_{O_2,s} = N_{X_2,s} = \frac{K_x X_{O_2,f}^{-(K_x+G/L)} X_{O_2,c} \exp((1-y_c^2)G/2)}{(K_x+2Q)/2Q + (G + K_x/L) F(1, y_c) \exp(G/2)} \quad (16)$$

where

$$X_{O_2,c} = \frac{K_x X_{O_2,f} - R_3 r_s y_c^2 / 2 [(K_x+2Q)/2Q + (G + K_x/L) F(1, y_c) \exp(G/2)]}{K_1 C_c r_s y_c^2 [(K_x+2Q)/2Q + (G + K_x/L) F(1, y_c) \exp(G/2)] + (K_x+GL) \exp((1-y_c^2)G/2)}$$

#### Case 2: Flame Front Out of Core Surface

In case 2, the flame front is being pushed outward by carbon monoxide, so oxygen cannot reach the core surface and  $X_{2,c}$  must be less than zero, since  $X_{2,c} = 1/2 S_{CO,c}$

Note that since

$$N_{O_2,c} = 0, N_{X_2,c} = -1/2 N_{CO,c},$$

a mass balance around the core surface gives:

$$N_{CO,c} = R_3 r_c \quad (17)$$

Using Equations 14 and 17, we can get

$$M = -R_3 r_s y_c^2 / 2 \quad (18)$$

Equations 15 and 18 allow us to compute the value of  $X_{2,c}$  as:

$$X_{CO,c} = -2X_{2,c} = \frac{-2K_x X_{O_2,f}^{-(K_x+G/L)} + r_s y_c^2 R_3 ((K_x+2Q)/2Q + (G + K_x/L) F(1, y_c) \exp(G/2))}{(G/L + K_x) \exp(G/2 (1-y_c^2))} \quad (19)$$

#### Model Solution

Note that in the core region, if we substitute Equations 9 and 10 into Equation 11,  $R_3$  can be solved as a function of  $X_{CO,c}$ , while in the reacted shell region  $X_{CO,c}$  is either zero in case 1, or can be obtained from Equation 19 as a function of  $R_3$  in case 2. Simultaneous solution of these two regions gives the following equation:

$$R_3 = \sqrt{\frac{(K_3 K_5 K_{ex}^2 - 2K_3 K_4 K_5 K_{ex}^2 + (K_4 K_{ex})^2 - 2K_2 K_{ex} (K_3 K_5 + K_4) + 4K_1 K_4 K_5 K_{ex} + K_2^2) + K_2 - K_3 K_5 K_{ex} - K_4 K_{ex}}{(4K_1 - 4K_3 K_{ex})}} \quad (20)$$

where

$$K_1 = C_4 - 2 C_4 C_5 + 2 C_1 C_5$$

$$K_2 = 2 C_2 C_5$$

$$K_3 = C_1 C_5 + 1/2 C_4 - C_4 C_5$$

$$K_4 = 1 + 2 C_3 C_5 - 2 C_5$$

$$K_5 = 2 K_{ab} \rho_c / MW_c$$

and

$$C_1 = 0 \quad (\text{Case 1})$$

or

$$r_s y_c^2 \exp(G y_c^2) [F(1, y_c)/L + \exp(-G/2)(kx + 2Q)/2Q/(k_x + GL)] \quad (\text{Case 2})$$

$$C_2 = 0 \quad (\text{Case 1})$$

or

$$2X_{O_2, f} \exp(G/2(y_c^2 - 1)) [k_x / (GL + k_x)] \quad (\text{Case 2})$$

$$C_3 = 1 + \exp(G/2(y_c^2 - 1)) [k_x / (GL + k_x)] (X_{O_2, f} + X_{CO_2, f} - 1) \quad (\text{Case 1})$$

or

$$1 + \exp(G/2(y_c^2 - 1)) [k_x / (GL + k_x)] (2X_{O_2, f} + S_{CO_2, f} - 1) \quad (\text{Case 2})$$

$$C_4 = r_s / 2GL$$

$$C_5 = \left[ \frac{1 - \exp(-G y_c^2 / 2)}{G y_c} \right]$$

Thus,  $R_3$  can be obtained from Equation 20 and all the other quantities desired, such as

$$N_{O_2, s}$$

(the oxygen consumption rate) and  $dy_c/dt$  (the rate of shrinkage of the core) can be calculated in a straightforward fashion. A trial and error calculation procedure is used to determine whether case 1 or case 2 is true. This model is then integrated numerically only over time, with the reaction rates and temperature recalculated at each time step.

## PHYSICAL PROPERTIES

In the model calculation, the temperature is calculated from

$$\rho_s C_p (dT_s/dt) = h S \Delta T + \sum R_i \Delta H_i$$

where the heat capacity is:

$$C_p = 0.72 + 7.7 \times 10^{-4} T_s^2 / (T_s + 300) \text{ J/gm-K}$$

and the heat transfer coefficient<sup>a</sup> is:

$$h = 9.76 \times 10^{-4} + 2.48 \times 10^{-6} (T_s - 755) \text{ W/cm}^2\text{K}$$

The temperature difference  $\Delta T$  in the heat loss term is actually measured in our experiments, it usually maintains a constant value throughout an experiment due to the configuration of the reactor.

A general correlation based on a random pore model (15) allows us to estimate the effective diffusivity of spent oil shale as:

$$D_e = \epsilon^2 D_{O_2, \text{air}}$$

where  $\epsilon$  is the porosity and

$$D_{O_2, \text{air}}$$

is the bulk binary diffusivity of oxygen in air. Note that there are no adjustable parameters in the above equation. This approach is a modification of that used by Manor et al.

For the purpose of prediction, porosity, char concentration and shale grade can be conveniently estimated from shale density using correlations in the literature (16, 17).

Smith provided a theoretical relationship between density and oil yield for oil shale (17) and he supported his prediction with experimental results. The correlation was found to be very good in our experiments.

The data on the carbonaceous char contents of spent shales was gathered by Stanfield et al. (1) and his result can be correlated as follows:

$$W_c = 1.903 \times 10^{-3} + 2.283 \times 10^{-4} A$$

where  $W_c$  is the char density as percentage of the raw shale density (not weight fraction of the spent shale, as Dockter and Turner stated) and  $A$  is the shale grade in liters of oil per ton. The initial porosity of the spent shale retorted to 750°K can also be estimated with Tisot's data which is correlated by Dockter and Turner (5):

$$\epsilon = 0.111 + 1.55 \times 10^{-3} A + 1.23 \times 10^{-5} A^2$$

## EXPERIMENTAL VERIFICATION

The analytical model gives results very close to the numerical model of Manor et al., which agreed reasonably well with the experimental data reported earlier. In addition, a number of new experiments were carried out to further test the validity and applicable range of the model. The experimental conditions used were similar to the earlier one (8). Colorado oil shales were machined into cylinders and retorted in a furnace in nitrogen to a maximum temperature of 750°K. The combustion was then initiated by switching the sweep gas from nitrogen to air or nitrogen diluted air. Heat transfer to and from the furnace wall was minimized by controlling the furnace wall to within two °K of the shale surface temperature.

The effects of shale grades (from 40 to 229 liter/ton), cylinder sizes (from 1 cm to 10 cm

a. The heat transfer coefficient sometimes has been adjusted to account for non-ideal temperature distribution in the furnace during rapid temperature rise.

in diameter) and feed gas oxygen concentration (from 5% to 21%) were examined. It was found that this model adequately accounts for these effects in the testing range. Shown in Figure 2 is the comparison of experimental and model prediction of average temperatures and dimensionless reaction rates of rich shale cylinders (208 liter/ton) of two different sizes (3.5 cm, and 9.3 cm in diameter) in 13.5% oxygen plotted against dimensionless time. A 5 cm sample from the same piece of rock was also tested against the model with similar success but the result was excluded from the figure to avoid crowding. It can be seen from Figure 2 that the two different size samples give very similar curves on a dimensionless time scale (the 5 cm sample gave similar curves), but other grades of shale do not scale this way.

Various sizes (1 cm, 3.4 cm, 5.1 cm and 9.7 cm diameters) of 104 liter/ton shale have also been used and the model also predicted the combustion behavior successfully. In Table I, we compare measured and predicted total burn out times for these samples.

TABLE I

BURN OUT TIME FOR MEDIUM GRADE SHALE<sup>a</sup> (104 LITER/TON) OF FOUR DIFFERENT SIZES; EXPERIMENTS AND MODEL PREDICTION

| Expt. No. | Shale Diameter | O <sub>2</sub> % | Burn Out Time |          |
|-----------|----------------|------------------|---------------|----------|
|           |                |                  | Expt.         | Model    |
| 55        | 9.7 cm         | 21%              | 660 min.      | 670 min. |
| 65        | 5.1 cm         | 15%              | 340 min.      | 330 min. |
| 67        | 3.4 cm         | 15%              | 160 min.      | 163 min. |
| 69        | 1.0 cm         | 15%              | 20 min.       | 22 min.  |

- a. Important parameters used are: Initial porosity = 30%, carbon density = 0.06 gm/cm<sup>3</sup>, spent shale density = 1.87 gm/cm<sup>3</sup>.

#### CONCLUSION

An analytical model satisfactorily predicts the combustion behavior of spent oil shale blocks. The only additional assumption besides those employed by Manor et al. (8) is that the oxidation reaction of carbon monoxide is instantaneous.

#### ACKNOWLEDGMENTS

We wish to thank Occidental Petroleum Corporation and Rio Blanco Oil Shale Company for supplying the oil shale used in this work.

#### NOMENCLATURE

|                |  |
|----------------|--|
| A              | shale grade, liter/ton   |
| B              | constant defined as $2R_3/R_4$ , dimensionless                       |
| C              | molar concentration in gas phase, gmole/cm <sup>3</sup>              |
| C <sub>c</sub> | molar concentration of char in shale, gmole/cm <sup>3</sup>          |
| C <sub>i</sub> | constants, defined below Equation 20                                 |
| C <sub>p</sub> | heat capacity of the shale, J/gm-K                                   |
| D <sub>e</sub> | effective diffusivity of gases in the shale, cm <sup>2</sup> /sec    |
| G              | constant = $R_4 r_s^2 / 2CD_e$ , dimensionless                       |
| h              | heat transfer coefficient, W/cm <sup>2</sup> K                       |
| K <sub>i</sub> | constants, defined below Equation 20                                 |
| K <sub>x</sub> | mass transfer coefficient, gmole/sec-cm <sup>2</sup>                 |
| L              | constant = $CD_e / r_s$ , gmole/sec-cm <sup>2</sup>                  |
| N <sub>t</sub> | net molar flux anywhere within the sample, gmole/sec-cm <sup>2</sup> |

|                       |  |
|-----------------------|--|
| $N_i$                 | molar flux of any species $i$ , gmole/sec-cm <sup>2</sup>  |
| $Q$                   | the molar feed rate of gas per unit surface area of the sample   |
| $R_1$                 | molar rate of the direct oxidation of char, gmole/sec-cm <sup>3</sup>                                      |
| $R_2$                 | molar rate of the oxidation reaction of CO, gmole/sec-cm <sup>3</sup>                                      |
| $R_3$                 | molar rate of CO <sub>2</sub> -C gasification reaction, gmole/sec-cm <sup>3</sup>                          |
| $R_4$                 | molar rate of release of CO <sub>2</sub> from carbonate decomposition reactions, gmole/sec-cm <sup>3</sup> |
| $r$                   | radial position within shale sample, cm  |
| $r_s$                 | the radius of the shale sample, cm   |
| $S$                   | surface area of sample per unit volume, cm <sup>-1</sup>   |
| $T_s$                 | shale temperature, K   |
| $\Delta T$            | temperature difference between the shale and the sweeping gas  |
| $\Delta H_j$          | heat of reaction $j$ , J/gm-K  |
| $W_c$                 | weight fraction of carbonaceous char in raw shale, dimensionless   |
| $x_i$                 | mole fraction of any species $i$ , $i$ =CO, O <sub>2</sub> , CO <sub>2</sub> , dimensionless               |
| $\langle x_i \rangle$ | average mole fraction of species $i$ in the core region, $i$ =CO <sub>2</sub> , CO, dimensionless          |
| $y$                   | $=r/r_s$ , normalized radial position within sample, dimensionless   |
| $\epsilon$            | porosity, dimensionless  |

#### SUBSCRIPTS

|     |                                       |
|-----|---------------------------------------|
| $c$ | value at the core edge                |
| $f$ | value in the feed stream              |
| $i$ | CO, O <sub>2</sub> or CO <sub>2</sub> |
| $s$ | value at the shale surface            |

Figure 1: Reaction scheme. This diagram indicates the locations at which the four main reactions occur, and indicates the sources and sinks of the three key reactant species.

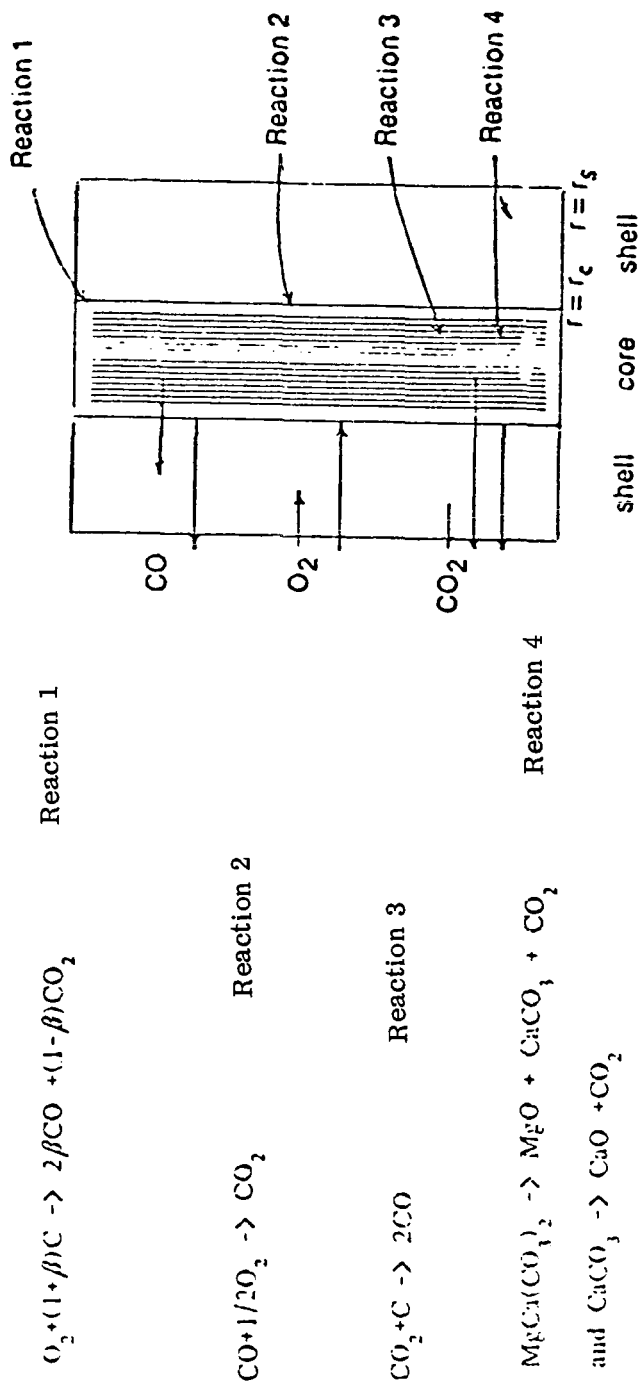
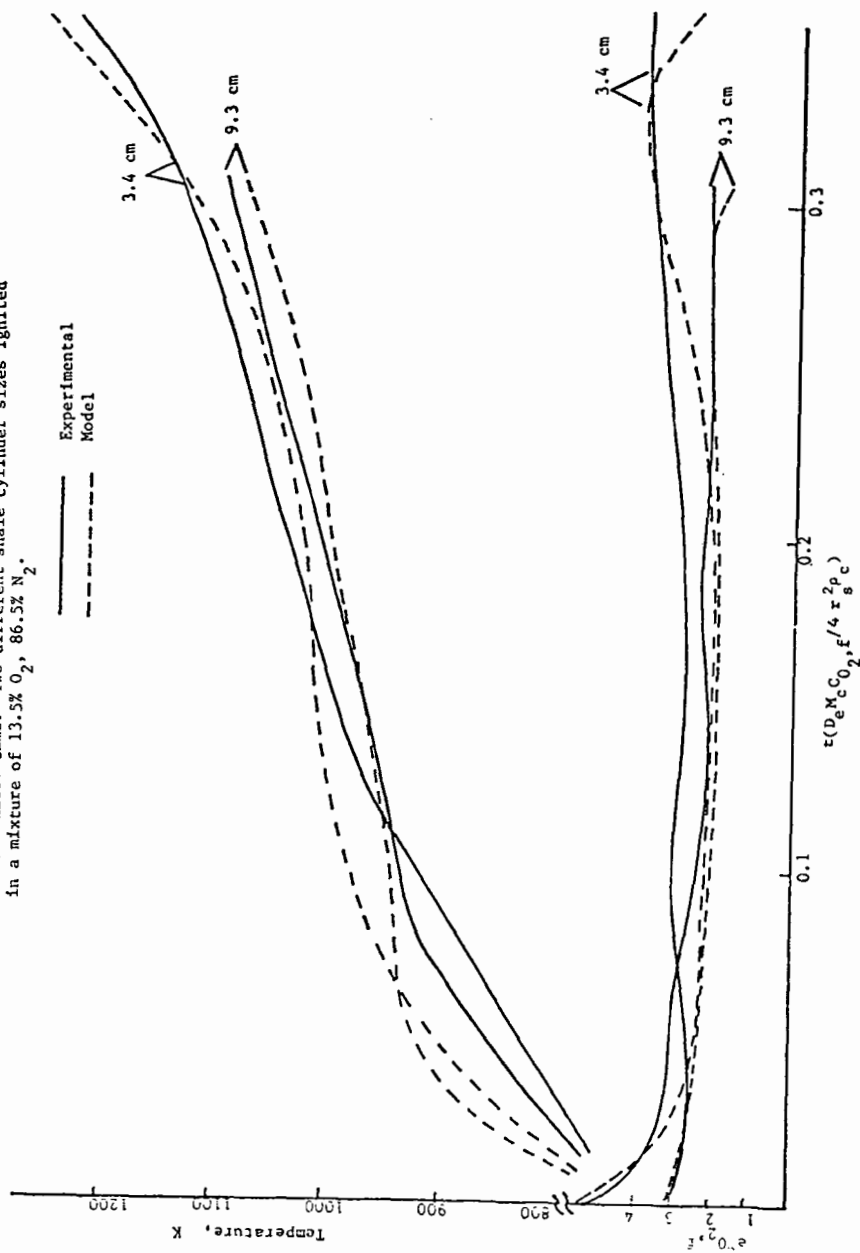




Figure 2: Comparisons of experimental results and model predictions. Average temperatures and dimensionless reaction rates vs. dimensionless time. Two different shale cylinder sizes ignited in a mixture of 13.5% O<sub>2</sub>, 86.5% N<sub>2</sub>.



# LITERATURE CITED

- (1) Stanfield, K. E. , Frost, I. E. , Mcauley, W. S. and Smith, W. S. , "Properties of Colorado Oil Shale", U. S. Bureau of Mines, RI 4825 (1951).
- (2) Dockter, L. , "Combustion of Oil-Shale Carbon Residue", AICHE Symp. Series, Vol. 72, No. 155 , p. 24 (1975).
- (3) Huang, E. T. S. , "Retorting of Single Oil-Shale Blocks with Nitrogen and Air", SPE Journal, p. 331 (October 1977).
- (4) Thomson, W. J. and Soni, Y. , "Oxidation of Oil Shale Char", In Situ, Vol. 4, No. 1, p. 61 (1980).
- (5) Dockter, L. and Turner, T. F. , "Combustion Rates for Oil Shale Carbonaceous Residue", In Situ, Vol. 2, No. 3, p. 197 (1978).
- (6) Duvall, J. J. and Tyner, C. E. , "Laboratory and Modeling Studies of the Combustion Retorting of Large Blocks of Oil Shale", Tech. report, Sandia Laboratories (1979).
- (7) Mallon, R. and Braun, R. , "Reactivity of Oil Shale Carbonaceous Residue with Oxygen and Carbon Dioxide", Quarterly of the Colorado School of Mines, Vol. 71, No. 4, Proceedings of the 9th Oil Shale Symp. (1976).
- (8) Manor, Y. , Suuberg, E. M. , Ho, M. and Toor, H. L. , "The Ignition and Combustion Behavior of Spent Shale Particles", in 19th Interntl. Symp. on Combustion, The Combustion Institute, Pittsburgh, PA, p. 1093 (1982).
- (9) Campbell, J. H. and Brunham, A. K. , "Reaction Kinetics for Modeling Oil Shale Retorting", In Situ, Vol. 4, No. 1 (1980).
- (10) Sohn, H. Y. and Kim, S. K. , "Intrinsic Kinetics of the Reaction between Oxygen and Carbonaceous Residue in Retorted Oil Shale", Ind. Eng. Chem., Process Design and Development, Vol. 19, No. 4, p. 550 (1980).
- (11) Braun, R. L. , "Mathematical Modeling of Modified In-Situ and Aboveground Oil Shale Retorting", Tech. report UCRL-53119, Lawrence Livermore Laboratory (1981).
- (12) Braun, R. L. , Mallon, R. G. and Sohn, H. Y. , "Analysis of Multiple Gas-Solid Reactions during the Gasification of Char in Oil Shale Blocks", Tech. report UCRL-85279, Lawrence Livermore Laboratory (April 1981).
- (13) Ergun, S. , "Kinetics of Reaction of Carbon Oxidide with Carbon", Journal of Physical Chem. , Vol. 60, p. 480 (1956).
- (14) Ergun, S. and Menster, M. , "Reaction of Carbon with CO<sub>2</sub> and Steam", in Chem. and Physics of Carbon, P. L. Walker, ed. , p. 203 (1965).
- (15) Smith, J. M. , Chem. Engineering Kinetics, McGraw-Hill Co. , p. 466 , 3rd ed. (1981).
- (16) Tisot, R. , "Alterations in Structure and Physical Properties of Green River Oil Shale by Thermal Treatment", J. Chem. Eng. Ref. Data, Vol. 12, p. 405 (1967).
- (17) Smith, J. W. , "Theoretical Relationship Between Density and Oil Yield for Oil Shales", Tech. report R17248, Bureau of Mines (April 1969).

THE EFFECT OF CRYOGRINDING ON THE MOLECULAR WEIGHT OF  
SAMPLES OF POLYISOBUTYLENE

By

P. F. Waters

The American University, Washington, D. C. 20016  
and

A. F. Hadermann and J. C. Trippe

General Technology Applications, Inc., Arlington, Virginia 22209

INTRODUCTION

A significant recent development in polymer technology is the discovery that megadalton-molecular-weight macromolecules can be dissolved instantaneously in liquids which are normally solvents for the materials. This finding portends increasing development and use of ultra high molecular weight macromolecules deriving from the superior effects they exhibit in a variety of applications. Past studies have demonstrated that macromolecules, added in small quantities, (1) enhance the flow of liquids through pipelines; (2) impart high extensional viscosities to and (3) impede the aerosolization of liquids in which they are dissolved. The latter is a property of antimisting fuels.

In the event that antimisting fuels gain wide use, a not inconsiderable facilitation of the feasibility might well be the on-site dissolution of the macromolecules in the fuels. This requirement is occasioned by the high susceptibility of some dissolved macromolecules to shear degradation; a concomitant of fuel transportation and transfer by pumping. The cryogenic comminution and subsequent blending of macromolecules with the fuels offers a direct route to instantaneous dissolution. The process is described elsewhere (3-5).

The antimisting effect is a strong function of the molecular weight of the additive (2, 6, 7). Consequently, an understanding of the effect of cryogrinding on the molecular weight of a potential antimisting fuel additive is required. In this study, samples of polyisobutylene of three different molecular weights were cryofractured and dissolved. Measurements of the viscosity and height-at-break in a ductless siphon (8) of the solutions were compared with those of solutions of unground samples and the comparative values were used as indicators of the extent of degradation.

EXPERIMENTAL

Samples of BASF polyisobutylene of three different molecular weights (B-100, B-200, B-200-246) were fractured in a mill, under nitrogen, at 77°K. However, they were not added immediately to the solvent as was the procedure followed in the work reported earlier. Instead, the samples were allowed to warm to room temperature under nitrogen and each was dissolved in isooctane in the usual manner, i.e., with occasional swirling in a flask over a period of several days. Simultaneously, unground samples of the same materials were similarly dissolved.

The viscosity and ductless siphon measurements were made on relatively low concentrations of the samples, because the reduced viscosities become nonlinear at concentrations near 0.1 wt % in good solvents for the molecular weights used in this study.

The data are displayed in Table I.

CONCLUSIONS

The viscosity data show that there was apparently no detectable degradation on cryogrinding the sample with the lowest molecular weight. The sample with the intermediate molecular weight suffered a molecular weight decrease of a bit above 5%. It was reported earlier that cryogrinding reduced the molecular weight of a sample of B-200 by about 6% (5). In that instance,  $\bar{M}_v$  was determined in cyclohexane at 30°C, with the material cryoground directly into the solvent and the concentration measured by weight after precipitation of the macromolecules from solution with acetone. The molecular weight of the sample with the highest molecular weight decreased by about 9%. The relative decrease in the molecular weight on cryogrinding,

$$\frac{\Delta \bar{M}_v \%}{\bar{M}_v}$$

approaches a limiting value of 1.5.

TABLE I

VISCOSITY AVERAGE MOLECULAR WEIGHT<sup>a</sup> AND REDUCED HEIGHT-AT-BREAK OF SOLUTIONS OF POLYISOBUTYLENE IN ISOCTANE AT 20°C

| Sample                 | $\bar{M}_v \times 10^{-6}$<br>(g/mol) | $C \times 10^{-2}$<br>(g/dl) | $\frac{h}{C}$<br>$\frac{cm}{(g/dl)}$ |
|------------------------|---------------------------------------|------------------------------|--------------------------------------|
| B-100 (unground)       | 1.00                                  | 1.91                         | 0                                    |
|                        |                                       | 3.76                         | 0                                    |
|                        |                                       | 7.74                         | 0                                    |
| B-100 (cryoground)     | 1.00                                  | 3.83                         | 0                                    |
|                        |                                       | 5.94                         | 0                                    |
|                        |                                       | 7.72                         | 0                                    |
| B-200 (unground)       | 3.59                                  | 3.84                         | 11.9                                 |
|                        |                                       | 5.70                         | 12.9                                 |
|                        |                                       | 7.69                         | 13.8                                 |
| B-200 (cryoground)     | 3.40                                  | 4.03                         | 14.2                                 |
|                        |                                       | 5.15                         | 14.6                                 |
|                        |                                       | 8.07                         | 16.3                                 |
| B-200-246 (unground)   | 5.96                                  | 3.89                         | 53.8                                 |
|                        |                                       | 5.91                         | 54.7                                 |
|                        |                                       | 7.85                         | 56.8                                 |
| B-200-246 (cryoground) | 5.42                                  | 3.85                         | 43.7                                 |
|                        |                                       | 5.82                         | 48.0                                 |
|                        |                                       | 7.76                         | 49.3                                 |

a.  $[\eta] = 3.06 \times 10^{-4} M^{0.65}$  (9)

The reduced height-at-break data reveal a strong molecular weight dependency. Whereas the cryogrinding appears to have improved the viscoelastic properties of the sample with intermediate molecular weight, it causes a decided decrease in the effect in the sample with the highest molecular weight. The latter change is in the expected direction, commensurate with the degradation revealed by the viscosity measurements. In the cryogrinding process free radicals are generated (5) and while the viscosity average molecular weight decreases by about 5% for the B-200 sample, the alteration of the molecular weight distribution due to post-grinding free radical coupling might conceivably lead to an increase in the reduced ductless siphon height-at-break because in the polyisobutylene/isooctane system, the intrinsic viscosity is related to

$$\bar{M}_v^{0.65}$$

whereas the height-at-break is proportional to

$$\bar{M}_v^{2.3}$$

A relatively few such coupled molecules would contribute far less to the shear viscosity than to the extensional viscosity. Indeed, it may well be that only the very largest molecules in a sample contribute to the antimisting effect.

# LITERATURE CITED

- (1) Proceedings of the IUTAM Symp. on Structure of Turbulance and Drag Reduction, F. Frenkel, M. Landahl and J. Tumley, eds., Phys. Fluids 20, No. 10, Part II (1977).
- (2) Chao, K. C., Child, C. A., Grens, E. A. and Williams, M. S., Am. Inst. Ch. Eng. J., in press.
- (3) Waters, P. F., Trippe, J. C. and Hadermann, A. F., Proceeding of the Aircraft Research and Technology for Antimisting Kerosene Conf., p. 5-1 ff, Atlantic City, NJ, February 18-19, 1981. Report No. FAA-CT-81-181, U. S. Dept. of Trans., June, 1981.
- (4) Trippe, J. C., Waters, P. F. and Hadermann, A. F., Application of GTA Blending Process to Antimisting Fuel Additives, Report No. FAA-CT-81-51, U. S. Dept. of Trans., May, 1981.
- (5) Waters, P. F., Hadermann, A. F., Weitzen, W. and Trippe, J. C., IUPAC 28th Macromolecular Symp. Proceedings, p.679, July 12-16, 1982.
- (6) Hadermann, A. F., Waters, P. F., Trippe, J. C. and Weitzen, W., Contract No. DAAK-70-81-C-0134, U. S. Army Mobility Equip. Res. and Dev. Com., Fort Belvoir, VA, January 15, 1982.
- (7) Waters, P. F., Hadermann, A. F. and Trippe, J. C., Proceedings of the 2nd Interntl. Conf. on Reactive Processing of Polymers, pp. 11-22, J. T. Lindt, ed., University of Pittsburgh, November 2-4, 1982.
- (8) Chao, K. K. and Williams, M. C., J. Rheology, in press.
- (9) BASF Tech. Leaflet No. M 2353 E/81538; May, 1978.

CHEMICAL COAL BENEFICIATION WITH AQUEOUS HYDROGEN  
 PEROXIDE/SULFURIC ACID SOLUTIONS

By

N. P. Vasilakos and C. S. Clinton  
 Department of Chemical Engineering, University of Texas, Austin, Texas 78712

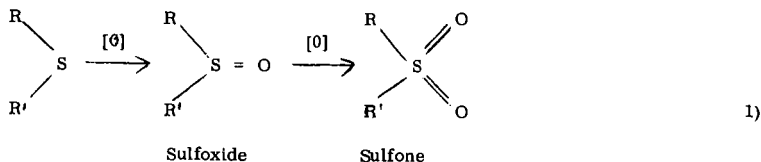
INTRODUCTION

There is a pressing need for significant improvement in the effectiveness and the economics of coal desulfurization, especially in the light of the latest, strict air-quality standards set by EPA for coal-fired power plants. The challenge is particularly crucial for the future of chemical (or precombustion) desulfurization of coal, where specific reagents are used to attack selectively and to remove both the inorganic and the organic sulfur from coal before combustion. Current chemical desulfurization processes are faced with a serious dilemma: either operate under severe process conditions (high temperatures and pressures, strong- and thus nonselective- desulfurizing media) promoting high sulfur removal from coal but at the expense of higher capital and operating costs and/or severe degradation of the coal material, or utilize mild reaction schemes not affecting the integrity of the coal matrix during processing but displaying low efficiency of sulfur-reduction (especially organic-sulfur reduction) in coal. A low-cost, technically simple, coal-treatment process that removes the organic as well as inorganic sulfur in coal effectively without having to destroy the carbon matrix would be a major breakthrough in coal utilization.

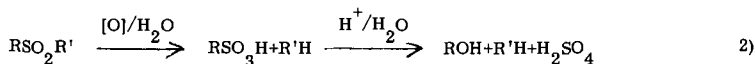
All the chemical desulfurization processes that are presently in an advanced development stage (TRW Meyers, Battelli Hydrothermal, KVB, DOE Oxydesulfurization, and JPL Chlorinolysis processes) employ either oxidizing reagents or basic media to reduce the sulfur content in coal. Oddly enough, little consideration has been given so far in the coal desulfurization literature to the potential benefits from acid systems. Inherent advantages exist in coal treatment by acid systems over alkaline ones, namely:

- Acid systems can extract sodium from the organic phase of the coal, thereby improving the slagging characteristics of the coal during combustion; alkaline systems add alkali.
- Acid systems can attack apatite/phosphorite in the coal as well as pyrite (1) and, thus, can free ash and trace elements (including radioactives) from their original association; alkaline systems do not attack the phosphate minerals and tend to immobilize trace elements in the form of hydroxides, etc.
- Acid systems have a potential for extracting nitrogeenous substances such as aniline and pyridine from the coal; alkaline systems can only extract phenols and organic acids, thus, removing fuel value without improving NO<sub>x</sub> emissions.

Oxidizing systems, on the other hand, can in principle remove both the pyritic and organic sulfur from coal in the form of sulfates, but oxidizing systems suffer from the serious drawback of being unselective, resulting in large losses in heating value of the treated coal. The high cost and scarcity of feed stock the severe conditions required and the lack of effectiveness on organic sulfur of current chemical desulfurization processes has stimulated renewed interest in selective oxidation under mild conditions as a method for removing sulfur from coal and residual oil. The basic scheme consists of selectively oxidizing the organosulfur compounds to the corresponding sulfones, thus destabilizing the carbon-sulfur bond (2):



The sulfones are then oxidized further to sulfonic acids which can, in turn, be hydrolyzed to yield sulfuric acid and completely desulfurized hydrocarbon products (3):



The first step in the sequence, i. e. the oxidation of sulfur compounds to sulfones, is extensively documented in the literature. Numerous oxidants have been reported which can effect the conversion of even the most stable organosulfur compounds (thiophenes) to the corresponding sulfones, including  $\text{NO}_2$  (4),  $\text{Cl}_2/\text{H}_2\text{O}$  (5),  $\text{H}_2\text{O}_2$ /acetic acid and hydroperoxides (6).

The oxidation of sulfur beyond the sulfone stage (Reaction 2) has not been studied to any significant extent and there are very few references in the literature on the desulfurizing effects of extended oxidation of organosulfur compounds. Vasilakos (7) has reported the complete desulfurization of aliphatic sulfides by oxidative chlorination in aqueous systems at low temperatures ( $60^\circ\text{C}$ ) and atmospheric pressure.

The key to an economically feasible desulfurization process based on oxidation is, of course, selectivity. Concurrent oxidation of the remainder of the coal matrix by the sulfur-oxidizing agent should be minimized to prevent excessive loss of the heat content of the coal. A comparison of half-wave potentials for oxidation of organic substrates of the type found in coal (8) shows that organosulfur compounds as well as alcohols and amines are vastly more susceptible to oxidation than are ether and benzene derivatives. Thus, given a mild oxidizing agent, it may be possible to oxidize the organic sulfur compounds, amines and alcohols without destroying the hydrocarbon portion of the coal molecule.

One of the most promising oxidants in this direction is hydrogen peroxide, particularly in acid solutions, where it has a standard oxidation potential approximately 1.4 V more positive than that of pyrite and about 1.6 V more positive than the  $\text{SO}_2/\text{S}$  couple (9). Thus,  $\text{H}_2\text{O}_2$  is an oxidizing agent capable of oxidizing effectively the pyritic sulfur to the sulfate form.

Mukai et al. (10) studied the treatment of several Japanese bituminous coals with 3 wt % aqueous hydrogen peroxide. This treatment was claimed to give nearly quantitative removal of pyritic sulfur without changing the caking properties of the coal. No data on organic-sulfur reduction were given. Nalwalk and coworkers (11) also reported that decomposition of coal with 30 wt %  $\text{H}_2\text{O}_2$  slowly oxidized pyrite to sulfate.

Smith (12) investigated the desulfurization of U. S. coals with 10-15 wt %  $\text{H}_2\text{O}_2$ , 0.1-0.3 N  $\text{H}_2\text{SO}_4$ , aqueous solutions. Treatment of several coals at ambient temperature with  $\text{H}_2\text{O}_2$  alone had a noticeable effect in removing pyritic sulfur, but the reaction was significantly enhanced when a small amount of sulfuric acid was added to the peroxide solutions. Although pyritic sulfur and ash were effectively removed in this way, organic sulfur remained unaffected. Minimal attack on the organic constituents of the coal matrix was observed. The reaction mechanism was postulated to involve the intermediate formation of peroxysulfuric acid,  $\text{H}_2\text{SO}_5$  (catalyzed by metal ions and sulfates present in coal), followed by oxidation of the pyrite, with competing peroxide decomposition by metal ions.

The apparent resistance of the organic sulfur in coal to oxidative desulfurization in this case does not necessarily imply that organic sulfur functionalities are not affected by the  $\text{H}_2\text{O}_2/\text{H}_2\text{SO}_4$  treatment. As we will show in the section on model compounds, all the basic organosulfur structures present in coal can be readily converted to the sulfone form under the conditions of the  $\text{H}_2\text{O}_2/\text{H}_2\text{SO}_4$  attack. In most cases, however, the oxidation does not proceed beyond the sulfone stage, and the additional desulfurization steps necessary to free the organic sulfur from the coal matrix (Equation 2) do not take place.

In a recent study (13), Kralik has reported that a hot aq.  $\text{Na}_2\text{CO}_3$  wash of coal pretreated with a mild oxidizing agent results in significant organic-sulfur reduction, mainly by splitting off relatively low-molecular-weight, oxidized sulfur compounds from the hydrocarbon matrix. It is feasible that the high selectivity of the peroxide treatment of coal towards sulfur oxidation could be combined with a subsequent alkaline hydrolysis step to leach out a significant portion of the oxidized organosulfur compounds, thus affecting not only pyritic, but also organic-sulfur removal from coal.

## EXPERIMENTAL

Chemical beneficiation experiments were carried out in batch mode at ambient temperature and pressure with a Redstone high-volatile A, bituminous coal. The ultimate analysis and sulfur forms for this coal, designated as PSOC-715, are included in Table I. In each run, approximately 20 grams of the dried and sized (200x325 mesh) coal was slurried in a 500-ml Pyrex Erlenmeyer flask with 300 ml of a 15 wt %  $\text{H}_2\text{O}_2$  solution of the desired  $\text{H}_2\text{SO}_4$  concentration. At the end of the reaction period the slurry was vacuum-filtered through a fine-porosity fritted glass funnel and the coal was washed several times with water for analytical purposes. Treated coal samples were dried for 24 hours under vacuum at  $110^\circ\text{C}$  and then analyzed for proximate and ultimate composition and heating value. A portion of the  $\text{H}_2\text{O}_2/\text{H}_2\text{SO}_4$  treated coal was further subjected to an extended

leaching cycle with a hot (80°C) 0.1 molar  $\text{Na}_2\text{CO}_3$  solution, then washed with water and dried as before. Both the Eschka and the Fisher methods for total-sulfur content and the ASTM-D-2492 wet method for forms of sulfur were employed in the analysis of the raw and treated coals. The wet method was modified to eliminate any ash interference in the determination of the pyritic and, thus, the organic sulfur (14). In this modified method, the pyritic-sulfur content of the coal is determined by oxidation of the pyrite to ferric sulfate and subsequent gravimetric analysis of barium sulfate precipitate, rather than by atomic absorption determination of the iron as described in the ASTM method.

TABLE I

ULTIMATE ANALYSES AND SULFUR FORMS OF COAL SAMPLES TREATED WITH A  
15 WT %  $\text{H}_2\text{O}_2$ , 1N  $\text{H}_2\text{SO}_4$  AQUEOUS SOLUTION AT 25°C FOR VARIOUS LENGTHS OF TIME<sup>a</sup>

| Reaction<br>Time <sup>b</sup> (min) | Carbon            | Hydrogen | Oxygen            | Nitrogen                       | Ash                       | Total Sulfur |        |
|-------------------------------------|-------------------|----------|-------------------|--------------------------------|---------------------------|--------------|--------|
|                                     |                   |          |                   |                                |                           | Eschka       | Fisher |
| 0<br>(Raw Coal<br>PSOC 715)         | 73.6              | 4.73     | 11.2              | 1.08                           | 7.02                      | 2.46         | -      |
| 15                                  | 78.0              | 5.50     | 8.24              | 1.16                           | 5.14                      | 2.04         | -      |
|                                     | 77.7              | 5.45     | 8.78              | 1.18                           | 5.00                      | 1.85         | 1.94   |
| 30                                  | 78.6              | 5.20     | 7.99              | 1.15                           | 5.07                      | 2.01         | -      |
|                                     | 78.3              | 5.47     | 8.47              | 1.18                           | 4.76                      | 1.80         | 1.83   |
| 60                                  | 74.4              | 4.98     | 13.3              | 1.17                           | 4.41                      | 1.71         | -      |
|                                     | 74.5              | 4.84     | 13.5              | 1.19                           | 4.44                      | 1.55         | 1.37   |
| 90                                  | 74.6              | 4.90     | 13.6              | 1.10                           | 4.18                      | 1.58         | -      |
|                                     | 74.9              | 4.91     | 13.3              | 1.18                           | 4.26                      | 1.47         | 1.29   |
| 120                                 | 78.2              | 5.27     | 9.46              | 1.15                           | 4.38                      | 1.57         | -      |
|                                     | 78.2              | 5.35     | 8.75              | 1.24                           | 5.08                      | 1.38         | 1.48   |
| 180                                 | 77.4              | 5.21     | 10.8              | 1.06                           | 4.16                      | 1.35         | -      |
|                                     | 77.5              | 5.22     | 10.8              | 1.24                           | 3.96                      | 1.26         | 1.23   |
| 240                                 | 77.5              | 4.99     | 11.4              | 1.14                           | 3.76                      | 1.23         | -      |
|                                     | 77.2              | 5.21     | 11.7              | 1.03                           | 3.72                      | 1.12         | 1.17   |
| Reaction<br>Time <sup>b</sup> (min) | Sulfate<br>Sulfur |          | Pyritic<br>Sulfur | Organic<br>Sulfur <sup>c</sup> | Heating Value<br>(Btu/lb) |              |        |
| 0<br>(Raw Coal<br>PSOC 715)         | 0.39              |          | 1.31              | 0.76                           | 12869                     |              |        |
| 15                                  | <0.05             |          | 1.11              | 0.93                           | 13805                     |              |        |
|                                     | <0.05             |          | 0.96              | 0.89                           | 13811                     |              |        |
| 30                                  | <0.05             |          | 1.04              | 0.97                           | 13877                     |              |        |
|                                     | <0.05             |          | 0.91              | 0.89                           | 13693                     |              |        |
| 60                                  | <0.05             |          | 0.89              | 0.82                           | 12915                     |              |        |
|                                     | <0.05             |          | 0.80              | 0.75                           | 12969                     |              |        |
| 90                                  | <0.05             |          | 0.70              | 0.88                           | 12921                     |              |        |
|                                     | <0.05             |          | 0.60              | 0.87                           | 12885                     |              |        |
| 120                                 | 0.07              |          | 0.65              | 0.86                           | 13743                     |              |        |
|                                     | <0.05             |          | 0.47              | 0.91                           | 13895                     |              |        |
| 180                                 | <0.05             |          | 0.50              | 0.85                           | 13587                     |              |        |
|                                     | <0.05             |          | 0.37              | 0.89                           | 13592                     |              |        |
| 240                                 | 0.09              |          | 0.35              | 0.79                           | 13530                     |              |        |
|                                     | <0.05             |          | 0.20              | 0.92                           | 13526                     |              |        |

a. All reported values are wt % (on a dry basis), unless otherwise noted.

b. For each reaction time, the first row of data corresponds to a single-step,  $\text{H}_2\text{O}_2/\text{H}_2\text{SO}_4$  treatment. The second row of data corresponds to the same  $\text{H}_2\text{O}_2/\text{H}_2\text{SO}_4$  treatment followed by an aqueous wash of the treated coal with a hot (80°C) 0.1M  $\text{Na}_2\text{CO}_3$  solution.

c. Determined by difference using the Eschka total-sulfur value.



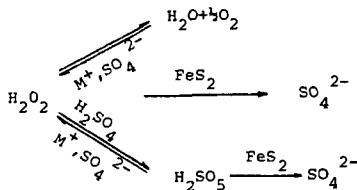
## RESULTS AND DISCUSSION

Tables I and II summarize our data on the treatment of the PSOC-715 coal with a 15 wt % aqueous  $\text{H}_2\text{O}_2$  solution of various  $\text{H}_2\text{SO}_4$  concentrations, at  $25^\circ\text{C}$  and for various lengths of time. Total sulfur and pyrite and ash removal from coal are depicted in Figures 1 and 2, respectively, as functions of the reaction time. Figure 3 shows the effect of the  $\text{H}_2\text{SO}_4$  concentration of the peroxide solution on pyritic sulfur removal.

The results indicate that there is a very significant reduction in total sulfur content for the  $\text{H}_2\text{O}_2/\text{H}_2\text{SO}_4$  treated coal under the given experimental conditions. This reduction ( $\sim 55\%$  in 4 hours) comes entirely from the almost complete elimination of pyrite and sulfates from coal. While sulfate sulfur (and ash) is leached out at the very early stages of the peroxide treatment, pyritic sulfur removal continues at a reasonable rate even after 4 hours of reaction. The results confirm earlier observations about the high selectivity of the peroxide reactions towards sulfur, the rest of the organic coal matrix being affected to a minimal extent. Carbon, hydrogen, nitrogen and oxygen contents of the treated coal remain at approximately the raw coal levels. No organic sulfur is removed in these room temperature experiments. On the other hand, pyritic sulfur reduction is accompanied by a significant reduction in the ash content of the coal ( $\sim 47\%$  in 4 hours), and by a slight but noticeable increase in its heating value. This increase of about 5% is most probably due to the removal of low-heat-content inorganic matter from coal.

Subsequent wash of the  $\text{H}_2\text{O}_2/\text{H}_2\text{SO}_4$  treated coal with a sodium carbonate solution does not result in additional ash reduction, or, as was expected, in any organic sulfur removal. However, a small but consistent decrease in the total sulfur content is observed in all cases, due to further removal of pyritic sulfur from the coal. The exact mechanism of this alkaline pyrite desulfurization is not clear at this point.

Pyritic sulfur removal also displays an interesting dependence on the  $\text{H}_2\text{SO}_4$  concentration of the peroxide solution. The data in Table II show that aqueous hydrogen peroxide alone is quite efficient in removing a substantial portion of the pyrite and the ash from coal. At the other extreme, treatment of the coal with a 1N sulfuric acid solution has absolutely no effect on pyritic sulfur, although some ash is actually removed. The combination of  $\text{H}_2\text{O}_2$  and  $\text{H}_2\text{SO}_4$  in aqueous solution results in a synergistic effect, where pyrite and ash reduction in coal significantly exceed the corresponding reduction brought about by each reagent alone. The effect is pronounced at low acid concentrations, but above a concentration of approximately 0.2N  $\text{H}_2\text{SO}_4$  the trend is reversed. Concentrated sulfuric acid seems to have an adverse effect on the oxidation of pyrite by hydrogen peroxide, so that, for example, the level of pyritic sulfur removal for a 2N  $\text{H}_2\text{SO}_4$  peroxide solution falls below even that for pure hydrogen peroxide. As Smith (12) has pointed out, the  $\text{H}_2\text{SO}_4$ -assisted oxidation of iron pyrite by hydrogen peroxide involves a complex system of parallel and consecutive reactions that may be strongly catalyzed by metal ions and sulfates present in coal. A simplified reaction mechanism can be schematically represented as follows:



The concentration of sulfuric acid in the peroxide solution may affect the kinetics and/or the equilibrium of any of these reactions (14), but the extent of the specific contribution of each step to the overall concentration effect that was observed experimentally is very difficult to estimate.

### Model Compound Studies

To investigate the effect of the  $\text{H}_2\text{O}_2/\text{H}_2\text{SO}_4$  treatment on organic sulfur under more controlled conditions, a series of kinetic experiments was carried out with three organosulfur compounds modeling possible sulfur functionalities in coal, namely dibenzothiophene, phenyl sulfide and *t*-butyl sulfide.

In each run with phenyl sulfide or dibenzothiophene, an aqueous phase consisting of 5ml 30 wt %  $\text{H}_2\text{O}_2$  and 3.3 ml 36N  $\text{H}_2\text{SO}_4$  was emulsified under intense stirring with 100 ml of a hexane phase containing 0.006 moles of the sulfide. The sulfide/peroxide-acid proportion corresponds to a 2.5 fold excess of the oxidant (assumed to be the intermediate peroxy-sulfuric acid) over the stoichiometric requirement for complete conversion (oxidation) of the sulfidic sulfur to sulfate

(Equations 1 and 2). All the reactions were carried out at 25°C. Samples of the hexane phase were withdrawn every 15 minutes and analyzed quantitatively on a Tracor 565 capillary-column gas chromatograph equipped with a Hall Electrolytic Conductivity Detector set at the sulfur detection mode. The corresponding sulfone was found to be the only final product of oxidation of phenyl sulfide and dibenzothiophene, with small amounts of the sulfoxide formed intermediately. Due to the very low solubility of the sulfoxides and the sulfones in hexane, these products were obtained mostly as solid crystals separating from the reaction mixture. The crystals were filtered, dissolved in tetrahydrofuran and analyzed on the gas chromatograph. Under the given reaction conditions, a 25% conversion of phenyl sulfide to the sulfone was obtained in 8 hours and 75% in 24 hours. For dibenzothiophene, the 24-hour conversion level was 42%. The oxidation rate was strongly dependent on the concentration of the sulfuric acid and complete conversion of the sulfide to sulfone could be achieved in a few minutes of reaction with a much higher excess of the  $\text{H}_2\text{O}_2/\text{H}_2\text{SO}_4$  oxidant.

In the t-butyl sulfide runs, 14 ml of the (liquid) sulfide was directly dispersed under intense stirring in an aqueous phase consisting of 140 ml 30 wt %  $\text{H}_2\text{O}_2$  and 96 ml 36N  $\text{H}_2\text{SO}_4$  (= 5 fold excess of oxidant). The oxidation reaction was carried out at 25°C for various lengths of time. At the end of each run, the reaction mixture was exhaustively extracted with hexane. The aqueous phase was separated and analyzed for total  $\text{SO}_4^{2-}$  content by the  $\text{BaCl}_2 \rightarrow \text{BaSO}_4$  precipitation method. The difference in sulfate contents between this phase and the initial aqueous phase (before reaction) was used to determine the  $\text{SO}_4^{2-}$  yield of the sulfide oxidation reaction. The hexane phase was analyzed for sulfur species on the gas chromatograph. After 8 hours of reaction, the t-butyl sulfide had been completely converted, t-butyl sulfone and  $\text{SO}_4^{2-}$  being the only reaction products that were detected. The sulfone yield (based on the sulfide) was approximately 20%, the remaining 80% appeared as sulfate.

The results with t-butyl sulfide are very encouraging, because they demonstrate the ability of the  $\text{H}_2\text{O}_2/\text{H}_2\text{SO}_4$  system to promote complete oxidative desulfurization of aliphatic sulfide structures under ambient reaction conditions. The fact that no organic sulfur removal was observed under similar conditions with the PSOC-715 coal may simply be an indication that most of the organic sulfur in this coal is in stable phenyl and thiophenic forms that can survive the oxidative peroxide attack. Vasilakos (7) has reported a similar case in his studies of the selective desulfurization of two bituminous coals with aqueous chlorine solutions. The coals displayed completely different organic-sulfur-reduction characteristics despite the almost identical extent and pattern of the chlorinolysis reactions.

The effect was attributed to the different distribution of the organic sulfur in the two coals in aliphatic and aromatic structures. We are currently conducting a series of  $\text{H}_2\text{O}_2/\text{H}_2\text{SO}_4$  experiments with two high organic-sulfur coals, a Texas Darco lignite and an Illinois #5 bituminous coal, to test this hypothesis and to study further the removal of sulfur functionalities from the coal matrix.

#### SUMMARY

The removal of sulfur and ash from coal treated with aqueous hydrogen peroxide/sulfuric acid solutions at ambient temperature was studied under a variety of experimental conditions. Almost complete elimination of the sulfate and the pyritic sulfur was observed in most cases, as well as substantial reduction in the ash content. The rest of the organic coal matrix was not affected to any significant extent, indicating a high selectivity of the  $\text{H}_2\text{O}_2/\text{H}_2\text{SO}_4$  system towards sulfur oxidation. An optimal  $\text{H}_2\text{SO}_4$  concentration level was established, beyond which sulfuric acid was found to have an adverse effect on the oxidation of pyrite by hydrogen peroxide. The oxidative desulfurization of model organosulfur compounds, such as t-butyl sulfide, phenyl sulfide and dibenzothiophene, by the  $\text{H}_2\text{O}_2/\text{H}_2\text{SO}_4$  system was also investigated.

#### ACKNOWLEDGMENTS

This work was supported by the Texas Energy and Natural Resources Advisory Council under Grant No. 82-UCRC-2. The support is gratefully acknowledged.

TABLE II

ULTIMATE ANALYSES AND SULFUR FORMS OF COAL SAMPLES TREATED WITH A 15 WT %  $\text{H}_2\text{O}_2$  SOLUTION (OF VARYING  $\text{H}_2\text{SO}_4$  CONCENTRATION) AT 25°C FOR TWO HOURS<sup>a</sup>

| $\text{H}_2\text{SO}_4$<br>Concentration <sup>b</sup> , (N) | Carbon | Hydrogen | Oxygen | Nitrogen | Ash  | Total Sulfur |        |
|---|--------|----------|--------|----------|------|--------------|--------|
|   |        |          |        |          |      | Eschka       | Fisher |
| Raw Coal<br>(PSOC 715)                                      | 73.6   | 4.73     | 11.2   | 1.08     | 7.02 | 2.46         | -      |
| 0   | 77.7   | 5.29     | 9.53   | 1.19     | 4.73 | 1.50         | -      |
| (H <sub>2</sub> O <sub>2</sub> only)                        |        |          |        |          |      |              |        |
| 0.1   | 80.3   | 5.63     | 7.93   | 1.22     | 3.88 | 1.08         | -      |
|   | 79.1   | 5.38     | 9.47   | 1.24     | 3.71 | 1.05         | 1.06   |
| 0.3   | 78.2   | 5.40     | 10.2   | 1.15     | 3.80 | 1.27         | -      |
|   | 78.3   | 5.36     | 9.98   | 1.25     | 3.92 | 1.18         | 1.16   |
| 0.5   | 78.0   | 5.31     | 10.1   | 1.21     | 4.04 | 1.33         | -      |
|   | 77.8   | 5.29     | 10.4   | 1.20     | 4.05 | 1.23         | 1.21   |
| 2.0   | 77.3   | 5.15     | 10.8   | 1.11     | 4.15 | 1.47         | -      |
|   | 77.5   | 5.09     | 10.8   | 1.24     | 4.02 | 1.31         | 1.35   |
| 5.0   | 78.1   | 5.26     | 9.78   | 1.10     | 4.23 | 1.48         | -      |
|   | 77.6   | 5.16     | 10.6   | 1.24     | 4.13 | 1.30         | 1.40   |
| 10.0  | 77.9   | 5.19     | 10.4   | 1.12     | 4.04 | 1.33         | -      |
|   | 77.6   | 5.19     | 10.9   | 1.15     | 3.93 | 1.25         | 1.32   |
| 1N H <sub>2</sub> SO <sub>4</sub>                           | 76.6   | 5.17     | 9.43   | 1.04     | 5.46 | 2.24         | -      |
| (No H <sub>2</sub> O <sub>2</sub> )                         | 76.0   | 4.95     | 10.6   | 1.22     | 5.13 | 2.10         | 2.19   |

| $\text{H}_2\text{SO}_4$<br>Concentration <sup>b</sup> , (N) | Sulfate<br>Sulfur | Pyritic<br>Sulfur | Organic<br>Sulfur <sup>c</sup> | Heating Value<br>(Btu/lb) |
|---|-------------------|-------------------|--------------------------------|---------------------------|
| Raw Coal<br>(PSOC 715)                                      | 0.39              | 1.31              | 0.76                           | 12869                     |
| 0   | <0.05             | 0.54              | 0.96                           | 13282                     |
| (H <sub>2</sub> O <sub>2</sub> only)                        |                   |                   |                                |                           |
| 0.1   | <0.05             | 0.13              | 0.95                           | 14064                     |
|   | <0.05             | 0.13              | 0.92                           | 14014                     |
| 0.3   | <0.05             | 0.32              | 0.95                           | 13800                     |
|   | <0.05             | 0.26              | 0.92                           | 13762                     |
| 0.5   | <0.05             | 0.47              | 0.86                           | 13735                     |
|   | <0.05             | 0.34              | 0.89                           | 13648                     |
| 2.0   | <0.05             | 0.55              | 0.92                           | 13600                     |
|   | <0.05             | 0.42              | 0.89                           | 13595                     |
| 5.0   | <0.05             | 0.54              | 0.94                           | 13568                     |
|   | <0.05             | 0.40              | 0.90                           | 13599                     |
| 10.0  | 0.11              | 0.37              | 0.85                           | 13552                     |
|   | <0.05             | 0.37              | 0.88                           | 13559                     |
| 1N H <sub>2</sub> SO <sub>4</sub>                           | <0.05             | 1.30              | 0.94                           | 13563                     |
| (No H <sub>2</sub> O <sub>2</sub> )                         | <0.05             | 1.22              | 0.88                           | 13368                     |

a. All reported values are wt % (on a dry basis), unless otherwise noted.

b. For each concentration, the first row of data corresponds to a single-step,  $\text{H}_2\text{O}_2/\text{H}_2\text{SO}_4$  treatment. The second row of data corresponds to the same  $\text{H}_2\text{O}_2/\text{H}_2\text{SO}_4$  treatment followed by an aqueous wash of the treated coal with a hot (80°C) 0.1M  $\text{Na}_2\text{CO}_3$  solution.

c. Determined by difference using the Eschka total-sulfur value.

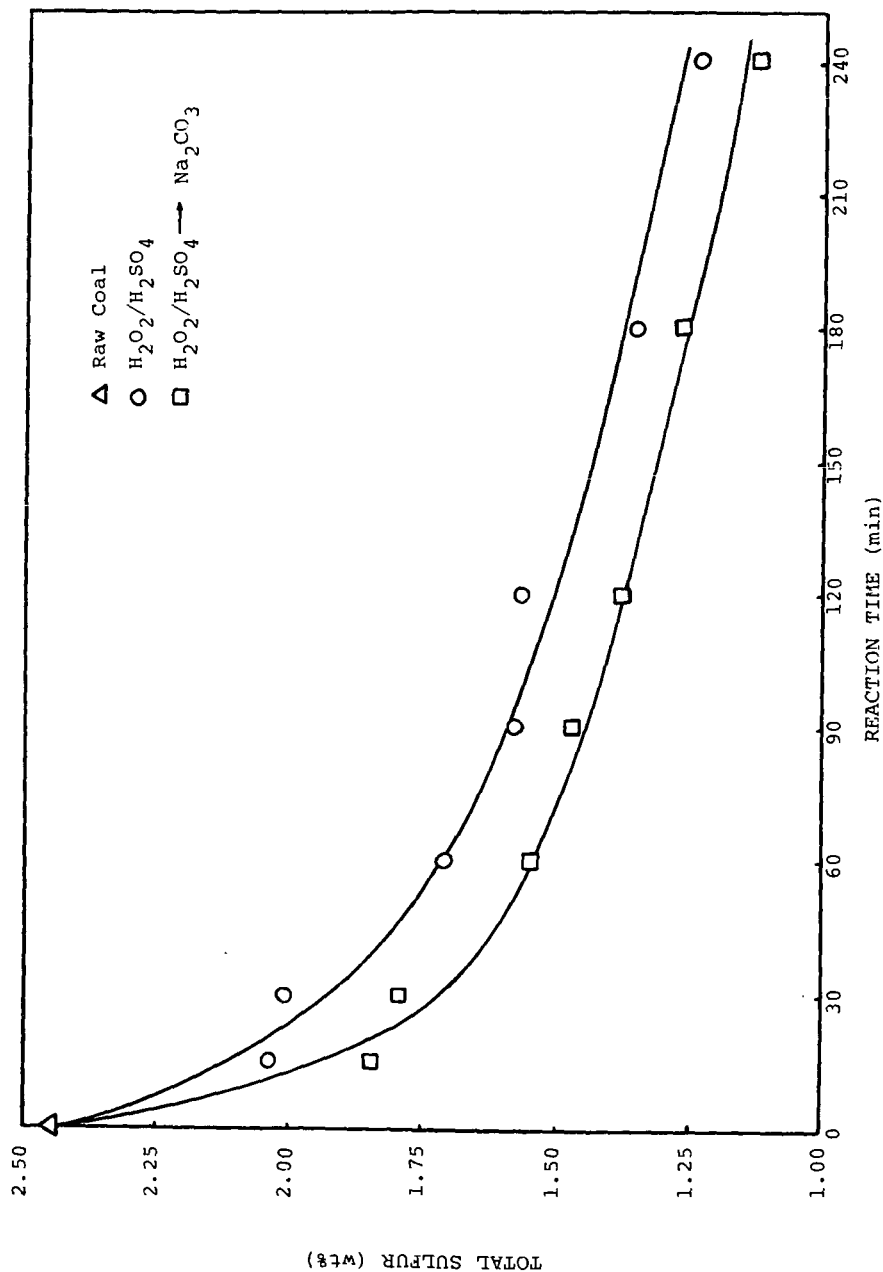


Figure 1: Total-sulfur dependence on reaction time (coal treated with a 15 wt%  $\text{H}_2\text{O}_2$ , 1N  $\text{H}_2\text{SO}_4$  aqueous solution at 25°C)

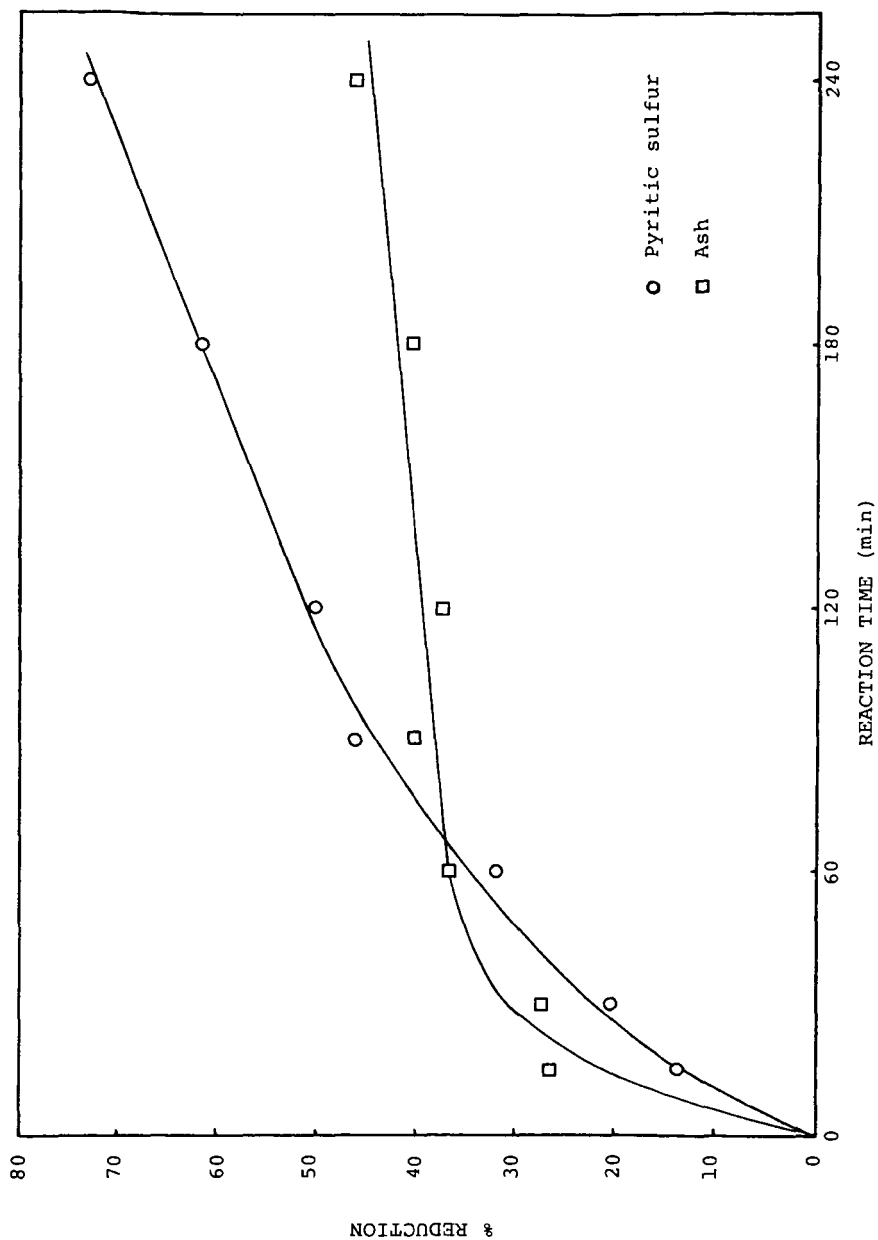


Figure 2: Pyritic-sulfur and ash reduction versus reaction time (coal treated with a 15 wt%  $\text{H}_2\text{O}_2$ , 1N  $\text{H}_2\text{SO}_4$  aqueous solution at 25°C)

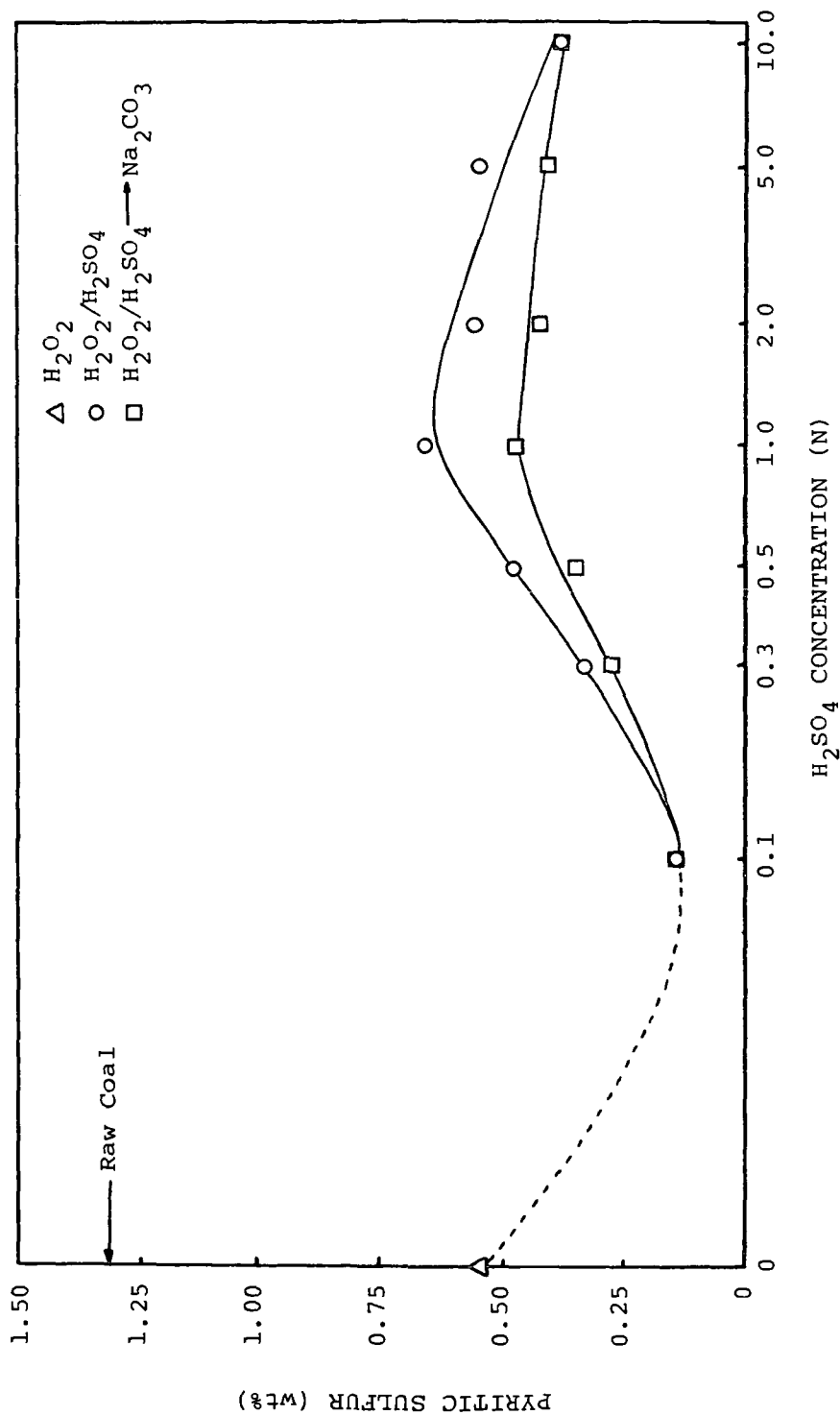


Figure 3: Effect of the acid concentration of the peroxide solution on pyritic sulfur (coal treated for 2 hours at 25°C)

# LITERATURE CITED

- (1) Du Fresne, E. R., "Coal Cleaning Versus Flue-Gas Desulfurization in Meeting New Proposed Air Pollution Standards", Assessment Report, Jet Propulsion Lab., Pasadena, CA (1979).
- (2) Attar, A. and Corcoran, W. H., *Ind. Eng. Chem. Prod. Res. Dev.*, 17, 102 (1978).
- (3) Kalvinskas, J. J., et al., "Final Report for Phase II - Coal Desulfurization by Low Temperature Chlorinolysis", Jet Propulsion Lab. Publication 80/15, Pasadena, CA (1980).
- (4) Friedman, S., Lacount, R. B. and Warzinski, R. P., "Oxidative Desulfurization of Coal", in "Coal Desulfurization", ACS Symp. Series No. 64, Washington, DC (1977).
- (5) Vasilakos, N. P., Bone, R. L. and Corcoran, W. H., *Ind. Eng. Chem. Prod. Res. Dev.*, 20, 376 (1981).
- (6) Reid, E. E., "Organic Chemistry of Bivalent Sulfur", Chemical Publishing Co., Inc., NY (1960).
- (7) Vasilakos, N. P., "Coal Desulfurization by Selective Chlorinolysis", Ph.D. Thesis, California Inst. of Tech., Pasadena, CA (1980).
- (8) Ross, S. D., Finkelstein, M. and Rudd, E. J., "Anodic Oxidation", Academic Press, Inc., NY (1975).
- (9) Meyers, R. A., "Coal Desulfurization", Marcel Dekker, Inc., NY (1977).
- (10) Mukai, S., Araki, Y., Konish, M. and Otomura, K., *Nenryo Kyoka-shi* 48, 905 (1969); *Chem. Abstr.* 72, 123720d (1970).
- (11) Nalwalk, A. J., Friedel, R. A. and Queiser, J. A., *Energy Sources* 1, 179 (1974).
- (12) Smith, E. B., "Lowering the Sulfur and Ash Contents of High-Sulfur Coals by Peroxide-Acid Treatment", ACS, Div. of Fuel Chem., Preprints, 20, 140 (1975).
- (13) Kralik, J. G., "An Investigation of the Applied Chemistry of the Reactions of Coal and Nitrogen Dioxide with Particular Emphasis on Oxidative Desulfurization", Ph.D. Thesis, California Inst. of Tech., Pasadena, CA (1982).
- (14) Monger, J. M. and Redlick, O., *J. Phys. Chem.*, 60, 797 (1956).